A Novel Antenna Architecture to Achieve Very High Bit Rates for Contactless Applications

Dipl.-Ing. Walter Kargl

Submitted as thesis to attain the academic degree ”Dr. techn.”
at

Graz University of Technology

Graz University of Technology

institut für elektronik

Institute of Electronics

Supervisor: .....
Univ.-Prof. Dipl.-Ing. Dr. techn. Wolfgang Pribyl

Co-Supervisor: .....
Ao. Univ.-Prof. Dipl.-Ing. Dr. techn. Erich Leitgeb

Graz, November 2011

EIDESSTATTLICHE ERKLÄRUNG

Ich erkläre an Eides statt, dass ich die vorliegende Arbeit selbstständig verfasst, andere als die angegebenen Quellen/Hilfsmittel nicht benutzt und die den benutzten Quellen wörtlich und inhaltlich entnommenen Stellen als solche kenntlich gemacht habe.

STATUTORY DECLARATION

I declare that I have authored this thesis independently, that I have not used other than the declared sources/resources and that I have explicitly marked all material which has been quoted either literally or by content from the used sources.

Kurzfassung

Die nachfolgende Arbeit befasst sich mit der Weiterentwicklung der kontaktlosen Smart Card Technologie, die für personenbezogene Identifikation eingesetzt wird. Bekannte Anwendungsbereiche sind kontaktlose Bezahlfunktionen, automatische Tickets für Transportmittel und der elektronische Reisepass. Der ISO/IEC 14443 Standard spezifiziert die aktuellen Verfahren für Energie- und Datentransfer basierend auf der Trägerfrequenz von 13.56MHz. Dieses Frequenzband hat sich als günstig erwiesen, um die Anforderungen kontaktloser personenbezogener Identifikation zu unterstützen. Es sind dabei gute Eigenschaften für mögliche Kommunikationsgeschwindigkeiten, Funktionsreichweite, Smart Card Prozessorleistung und kurzen Transaktionszeiten erreichbar.

Durch den technologischen Fortschritt der Halbleitertechnologien ist es möglich, immer größere Datenmengen zu günstigen Kosten und geringem Stromverbrauch auf Smart Card Prozessoren zu verarbeiten und nichtflüchtig zu speichern. Dies ermöglicht es Anwendungen, immer größere Daten zu speichern, wie zum Beispiel mehrere Fingerabdrücke zusätzlich zum heute schon abgelegten Passfoto. Eine wichtige Eigenschaft der kontaktlosen Technologie ist es, dass die Transaktionszeit kurz ist. Daher fordert ein immer größerer Datentransfer zwischen Leser und Karte eine Erhöhung der Datenrate und bessere Prozessorleistung, um die Abarbeitungszeit der Applikation konstant zu halten oder sogar zu reduzieren.

Diese Arbeit befasst sich mit neuen Methoden für die kontaktlose Datenübertragung. Dabei wird ein spezieller Fokus auf die Luftschnittstelle gelegt. Aufgrund der Tatsache, dass kontaktlose Systeme sowohl Energie als auch Daten über eine berührungslose Schnittstelle übertragen, sind die Antennensysteme so ausgelegt, dass sie eine gute Balance zwischen optimaler Energie- und Datenübertragung gewährleisten. Kapitel 2, 3 geben eine Einführung in die kontaktlos Technologie und deren Standardisierung und Regulatorien. Eine gesammelte Übersicht über die Erzeugung des magnetischen Feldes wird in Kapitel 4 zusammengefasst. In Kapitel 5 wird die Übertragungscharakteristik beschrieben. Kapitel 6 befasst sich mit dem Zeit- und Einschwingverhalten der kontaktlosen Technologie. Dabei wird im speziellen auf die Luftschnittstelle mit den Eigenschaften der Eigenresonanz und Schwingkreisgüte der individuellen Leserantennen und Kartenspulen eingegangen. In Kapitel 7 werden neue Methoden beschrieben, wie die Kommunikationslimitierungen konventioneller kontaktloser Systeme aufgehoben werden können, ohne den Energietransfer nachhaltig zu verschlechtern. Es werden Möglichkeiten aufgezeigt, die die Kommunikationsgeschwindigkeit über 13.56Mbps bis zu 54.24Mbps steigern kann. Das entspricht einer 64fachen Geschwindigkeit verglichen zum heute aktuellen ISO/IEC 14443 Standard, der bis zu einer Kommunikationsrate von 848kbps spezifiziert ist.

Abstract

This thesis is focusing on the evolution of contactless smart card technology which is widely used for personal identification nowadays. Contactless Payment Automatic Fair Collection and Electronic Passport are well known applications. The standard ISO/IEC 14443 specifies the air interface for power and communication interface at carrier frequency of 13.56MHz. This frequency band is well suited to comply with the needs of personal identification. These are reasonable communication speed, operating distance, smart card microcontroller performance and good overall transaction speed.

Technological progress in semiconductor industries makes it possible to process higher amount of data at reasonable cost and power consumption on smart card microprocessors and store these data in a non volatile memory. This enables applications to store additional information like several fingerprints together with a photo which is already flashed today into an electronic passport. An essential feature of contactless technology is a short transaction time which is a major contributor to the convenience of the technology. Therefore an increase of communication and microprocessor speed is the key to achieve the same or even reduced transaction speed by increased data volumes.

This thesis addresses new methods for contactless data communication. Special emphasis is given to the air interface. As the nature of contactless technology is transferring power and energy over one air interface typical antenna systems are designed to comply with both - data and power - needs. Chapters 2, 3 give an introduction into contactless technology, standardization and regulations. A comprehensive view on H-field properties is summarized in chapter 4. The transfer characteristics of the air interface are described in chapter 5. Chapter 6 depicts the settling and time domain characteristics of a contactless system. A detailed view is given on air interface properties like resonance frequency and quality factor of the individual reader antennas and card coils. Chapter 7 elaborates new methods to handle communication limitations of existing contactless systems without jeopardizing the power transfer properties. Methods to increase communication beyond 13.56Mbps up to 54.24Mbps are demonstrated. This represents an increase of communication speed up to a factor sixty four compared to the actual ISO/IEC 14443 standard, which specifies a maximum bit rate of 848kbps.

Acknowledgements

I like to express my thanks to Univ.-Prof. Dipl.-Ing. Dr.techn. Wolfgang Pribyl who gave me support and valuable inputs on the basis of his broad knowledge and experience.

Furthermore I would like to pronounce big thanks to the company Infineon, especially to Thomas Zollver who made it possible for me to spend two years of academic work at Graz University of Technologies, at the Institute of Electronics as a half time employee.

Special thanks go to my project team members Markus Auer, Edmund Ehrlich, Matthias Emsenhuber and Matthias Pichler. It was a great time to work with them on a challenging and interesting research topic.

It was and still is a pleasure to discuss with my Infineon colleagues Albert Missoni, Helmut Koroschetz, Thomas Leutgeb and Josef Haid.

I love my family, my wife Ulli and my three kids Lukas, Matthias and Katharina. I am glad to have them supporting me in managing my work life balance.

Walter Kargl
Graz, February 2011

Contents

List of Figures

List of Tables

Nomenclature

ADC	Analog Digital Converter
AFC	Automatic Fair Collection
ASK	Amplitude Shift Keying
BAC	Basic Access Control
BPSK	Binary Phase Shift Keying
CD	Committee Draft
CEPT	Committee on European Postal Regulation
DAC	Digital Analog Converter
DMT	Discrete Multi Tone
DSP	Digital Signal Processing
EAC	Enhanced Access Control
ECC	Electronic Communications Committee
EMC	Electromagnetic Compatibility
ERC	European Radiocommunications Committee
ETSI	European Telecommunications Standards Institute
ETU	Elementary Time Unit
FFT	Fast Fourier Transformation
HBR	High Bit Rates
HF	High Frequency
IC	Integrated Circuit
IEC	International Electrotechnical Commission
IP	Intellectual Property
ISM	Industrial, scientific and medical
ISO	International Organization for Standardization

LF Low Frequency

MASK M-ary Amplitude Shift Keying

MPSK M-ary Phase Shift Keying

NFC Near Field Communication

NRZ None Return to Zero

NRZ-L None Return to Zero Level

OFDM Orthogonal Frequency Division Multiplexing

PCD Proximity Coupling Device

PICC Proximity Integrated Circuit Card

PLL Phase Looked Loop

PSK Phase Shift Keying

QAM Quadrature Amplitude Modulation

RFID Radio Frequency Identification

RX Receive

SRD Short Range Device

TX Transmit

UHF Ultra High Frequency

VHBR Very High Bit Rates

VHDR Very High Data Rates

1 Motivation

Contactless technology became mature over the last ten years. A pressure towards increase of bit rates came up with applications like e-passport, national ID cards and many more. Requirements to store more and more data on a contacless smart card are demanding higher communication speed to transfer pictures, health care information and others in a convenient transaction time.

The funding project *ReadRF* was started in April 2008. The objective was to increase standardized bit rates by at least eight times, which is 6.78Mbps in both directions. Austrian funding organization *FFG* was the funding body. Project partners were *Infineon Technologies Austria AG* at its *Design Center in Graz* and the *Graz University of Technology* at its *Institute of Electronics*. One *Electronic Project/ Matthias Pichler* two *Master Theses/ Matthias Emsenhuber and Matthias Pichler* and three *Phd's / Markus Auer, Edmund Ehrlich and Walter Kargl* were developed. Markus Auer focused his work on card receiver circuit with special emphasis on phase demodulation. Edmund Ehrlich centered his area of research on reader transceiver architectures assessing Analog to Digital (AD) and Digital to Analog (DA) converter methods and digital signal processing. Walter Kargl did his work on contactless channel theory and introduced new methods to break limitations which are given by a conventional contactless air interface. Figure 1.1 depicts the three research areas, where the air interface part is highlighted.

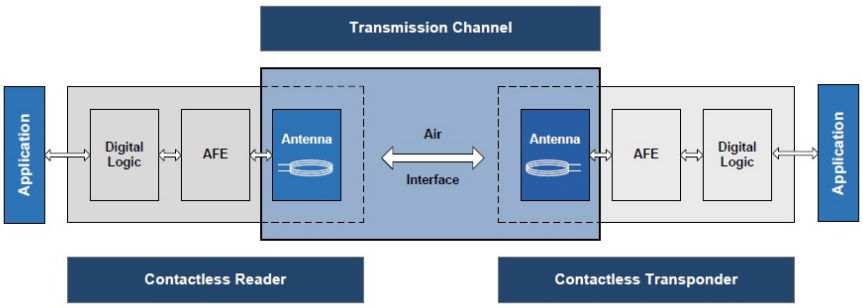

Figure 1.1: Overview Research Areas

This thesis will give a special focus on H-field properties together with transfer function characteristics and transient signal behavior. Contactless technologies of today are constraint by energy efficiency and communication speed. A high quality factor tuned resonant circuit is best for power transfer, whereas a broad band antenna circuit gives best communication speed. Standardized bit rates up to 848kbps are already challenging semiconductor vendors to develop and manufacture robust mass product contactless smart cards. This research work will come up with methods to increase contactless bit rates beyond 6.78Mbps not jeopardizing the energy path.

2 Introduction

In the mid 1980 semiconductor based RFID started to become an interesting technology for different industry applications - tagging of animals, garbage collection and many more. In the early 1990 access control for skiing areas were introduced. The typical frequency of those systems were based on 125kHz, 134kHz frequencies. Companies like Texas Instruments, Electronic Marin, Mikron - today NXP semiconductor, Nedap and many more were key players. Applications often were based on read only transponder, which did not support a change of data during life cycle of an RFID device. This was mainly driven by technological limitations and cost requirements. At this time semiconductor technologies of 1.0µm were standard, which made it almost impossible to manufacture low cost high complexity circuits. Power consumption was a further limiting factor for digital complexity. Too much logic would have limited operating range which was one key feature of applications. Data rate requirements were very low. The data transferred was typically some 64bit. Low frequency (LF) technology uses data rates of two to four kbps.

2.1 Security and Contactless Technology

In the beginning 1990 security became more and more important. The main driver was access control. It was obvious that security would became essential to further deploy RFID technology to applications like automatic fair collection, company access and many more.

Two applications were the key driver for security and RFID. One is Car Immobilizer the other Automatic Fair Collection. In 1995 a German law regulated the integration of car immobilizer for all new approved cars in Germany. Read only transponder were used at the beginning. This was changed very fast to a Challenge Response security architecture. The requirement of transponder IC individual keys made a change to Non Volatile Memory (NVM) necessary. Encryption of transferred data was not mandatory. Car Immobilizer application was well suited to 125kHz RFID technology. The rather mature technology was a further key for automotive industry, which has a focus on long time quality and reliability.

As a second and even more important step was the introduction of Automatic Fair Collection (AFC). It was the first volume project for Contactless Technology. The Sony FeliCa™ technology was selected for the Hongkong electronic ticketing system, whereas Mikron - today NXP semiconductor - could manage to deploy its Mifare™ system in the Seoul transportation project. The big difference to already existing technology was the introduction of a new *Contactless Technology*, which operated at High Frequency (HF) 13.56MHz and bit rates of 212kbps, 106kbps. The form factor *Smart Card* was used, whereas many other applications were done with *Glas Tube* or *Coin* transponder. Operating distance requirements were reduced to $<$10cm whereas transaction speed had to be less than 100ms. A mutual authentication together with data encryption was mandatory. A typical Automatic Fair Collection (AFC) application is using *value decrement*

functions which implies secure data transfer and programming to a Non Volatile Memory (NVM). Programming to a Non Volatile Memory (NVM) needed typically 4 to 5ms at this time and had to be performed several times per transaction. The increased demand on logic functions as encryption, decryption and calculation made an increase of execution speed necessary. This could be achieved by a frequency increase of 100 times compared to a 125kHz system. The increase of power consumption could be accepted as the operating distance requirement was reduced. Component cost was another driver for changing the system frequency to 13.56MHz. Resonant circuit inductor and capacitor in a 125kHz have typical values of some mH and several 100pF. At 13.56MHz these values are decreased by a factor of 1000 for the inductor and by 10 for the capacitor. A contactless card coil is typically 3µH. The resonance capacitor is several 10pF, which has to be integrated into the semiconductor device. An inductor in the mH range needs at least 50 times more turns than one with some µH. Cost is driven by silicon area on the one hand and copper and machine time on the other. The advantage of 13.56MHz card is obvious. Lamination process for smart cards can handle small copper or aluminum volumes much better than a huge amount of 200 turns in a 125kHz solution.

2.2 Standardization

This time was also the start for ISO/IEC 14443 standardization. In 1998 a first Committee Draft (CD) of ISO/IEC 14443 part two was submitted by WG8 committee for ballot. The part two specifies the air interface. A controversial discussion over years took place. Two technologies were discussed. The Mifare™ air interface was promoted by Mikron - today NXP semiconductor - and Siemens - today Infineon - who licensed Mifare™ in 1994. A new air interface technology was introduced and favored by ST-Microelectonics and Motorola Chipcard devision - today Inside Secure. It was not possible to find a common base for the two different technologies. Mifare™ convinced with a field proven mature technology. The others could argue with future proof and technology evolution from simple hardwired logic memory devices to complex CPU based smart card controller. A third party - Sony - could not manage to get its FeliCa™ technology standardized in the ISO/IEC 14443. It was decided to split part 2 and 3 into two types to solve this technology deadlock in the standardization process.

It was decided that an ISO/IEC 14443 compliant reader has to support both types, to guarantee a standardized infrastructure. In 2001 the ISO/IEC 14443 became an international standard. The bit rate was limited to 106kbps. Semiconductor supplier Infineon developed a Type A and Type B compliant card IC. NXP semiconductor - Philips at this time - focused on Type A, whereas all other vendors stuck on Type B, which is the same situation today.

2.3 Evolution of Contactless Technology

2001 was not stopping work on the ISO/IEC 14443 standard. A new standardization process was enrolled to further increase bit rate. An eight times higher bit rate for both communication directions and both types were targeted. This was achieved by amendments to the individual parts of the base standard. Major changes had to be made for the air interface part - part two - and the selection process. This enhancement was a prerequisite for the next big step in contactless technologies. Goverments all over the world, headed by USA, started to introduce an electronic

passport. Security and data rate requirements increased significantly. An electronic passport had to transfer several kByte of data from card to reader. The first implementation was based on Basic Access Control (BAC) which did not require data encryption but authentication only. As a next step the Enhanced Access Control (EAC) scheme was introduced, which included data encryption. The technology requirement increased significantly compared to applications like Automatic Fair Collection (AFC). Semiconductor technologies < 0.25 µm were able to comply with those requirements. Electronic passport application boosted contactless technology. An emerging market started to become a mature mass market.

Payment was a second volume driver. Master Card and VISA introduced an EMVCo specification for contactless payment. It requires an ISO/IEC 14443 standard compliance and additional EMVCo conformity testing. The objective was an interoperable payment infrastructure where it is guaranteed that a certified payment card can be operated by any certified reader. This was necessary to handle the interoperability of a plurality of reader and card vendors. The change from conventional magnetic stripe payment cards to contactless ones started in USA. A significant increase of security in the next years is expected to reduce fraught and increase customer convenience.

2.4 Next Generation Contactless Technology

A brief overview on state of the art RFID and contactless technologies is given in table 2.1 [23, 14]

Table 2.1 depicts state of the art standardized contactless smart card technology. A mandatory communication bit rate of 106kbps is specified. An increase of bit rate times 2, 4 and 8 is already amended in ISO/IEC 14443.

Contributions to further speed up communication by a factor of eight are available by different companies and national committees. Some are listed bellow.

- Gemalto, Leti, Resonance
- AFNOR, French national committee
- Japanese national committee
- NXP
- Infineon

RFID		Contactless Smart Card
up to 10m	**Operating Range**	$<$10cm
LF: 125kHz, 134kHz HF: 13.56MHz UHF: 868 / 900MHz $\mu Wave$: 2.45GHz	**Frequencies**	HF: 13.56MHz
ISO11784, 11785, 14223 ISO15693 ISO18000	**Standards**	ISO14443
$< 4kbps$ $< 26kbps$ $< 100kbps$	**Bit Rates**	$\leq 848kbps$
$< kByte$	**Non Volatile Memory**	$< 1MByte$
No, Low	**Security**	High
Hard Wired (HW) logic	**Processing Unit**	8 bit 16bit µController 32 bit
$< 1MHz$	**Core Frequency**	$< 100MHz$
μW	**Power Consumption**	mW

Table 2.1: RFID versus Contactless Smart Card [23, 14]

Some proposals are introducing Multi Amplitude/Multi Phase Shift Keying (MASK, MPSK) symbol modulation. Others are increasing speed by bit time reduction. Two modulation methods - Amplitude Shift Keying (ASK) and Phase Shift Keying (PSK) - are discussed. Almost all contributions are focusing on bit rates up to 6.8Mbps.

A committee draft (CD) is already available for ballot, where two proposals - Amplitude Shift Keying (ASK) and Phase Shift Keying (PSK) - are specified. One - contributed by Infineon Technologies - is enhancing ISO/IEC 14443 Type B layer 2 and layer 3 up to 6.8Mbps. A second solution - contributed by NXP semiconductor - defines a new PSK scheme with up to sixteen symbols and a maximum phase excursion of 0° to 60°. A special run in pattern is specified to have a learning phase to handle signal distortion and inter symbol interference (ISI).

Proximity Integrated Circuit Card (PICC) to Proximity Coupling Device (PCD) communication is proposed by enhancing the existing standard to 6.8Mbps by increasing subcarrier frequency to 6.8MHz. Bit time is decreased according to bit rate increase. Bit, byte and frame coding are adjusted as it was done for High Bit Rates (HBR).

2.5 Contribution to Novel Methods, Equations and Communication Concepts

This thesis contributes to increase bit rates in a contactless system up to and beyond 13.56Mbps.

- A comprehensive set of equations for contactless air interface and components is presented in chapter 4.
- Chapter 5 describes transfer functions for energy transfer and data communication in a contactless system.
- Novel equations denoting dynamic behavior of a contactless communication system are developed in chapter 6.
- Bit rates up to 13.56Mbps and higher can be achieved by a novel dual antenna architecture. Different concepts and modulation techniques are presented in chapter 7

3 Regulation and Standards

Regulation and standards are essential for high volume mass markets. Compatibility of different Proximity Integrated Circuit Card (PICC) vendors is a prerequisit for proper field operation.

3.1 ISO/IEC 14443 Standard

The standard ISO/IEC 14443 specifies the contactless technology for smart cards of ID1 size. The power interface is defined to be operational from 1.5A/m up to 7.5A/m. Communication and protocol layers are described in parts 2, 3 and 4. Part two specifies coding and bit rates.

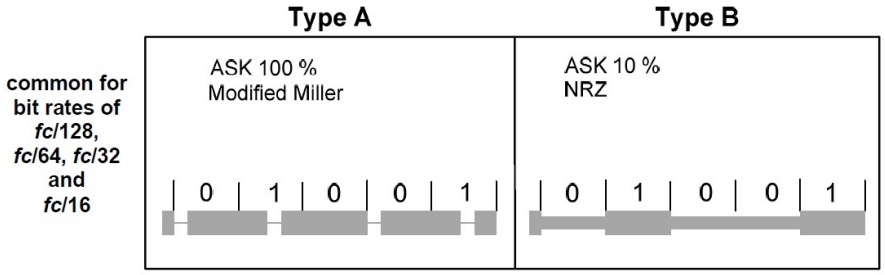

Figure 3.1: ISO/IEC 14443 A/B downlink coding [12]

The mandatory bit rate to be compliant to the standard is 106kbps in both directions. High Bit Rates (HBR) up to 848kbps are optional but widely used in industry applications - e.g. ePassport. Figure 3.2 depicts uplink signals.

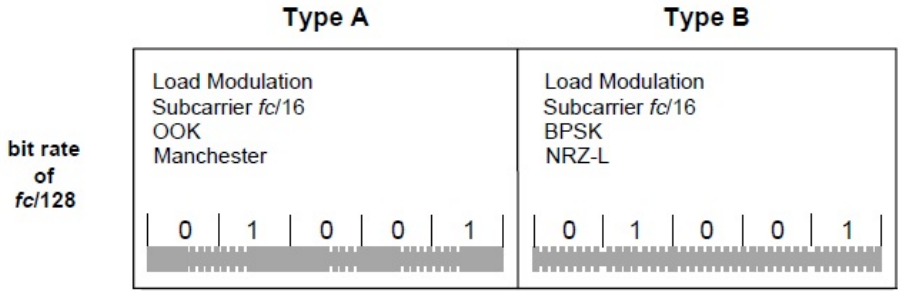

Figure 3.2: ISO/IEC 14443 A/B uplink coding [12]

Uplink coding is done by load modulation, which changes the impedance of the Proximity Integrated Circuit Card (PICC). This change of impedance can be detected by a reader receiver circuit.

A subcarrier frequency of 848kHz is defined to shift the sidebands of communication signals by 13.56MHz±848kHz. This shift makes it easier to notch the carrier signal, which has high power compared to the data signal. A Binary Phase Shift Keying (BPSK) modulated subcarrier is shown in figure 3.3. Data coding is None Return to Zero (NRZ) as specified in ISO/IEC 14443 Type B. The spectrum plot denotes a power to data signal difference of about -80dB.

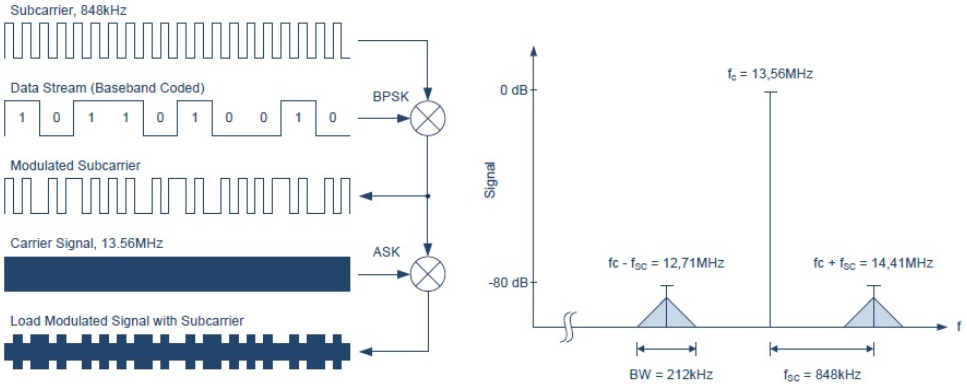

Figure 3.3: ISO/IEC 14443 NRZ BPSK encoded subcarrier [9]

High Bit Rates (HBR) are defined to linearly shrink the equivalent timing unit (ETU). ISO/IEC 14443 Type A additionally changes modulation and coding from Manchester coded Amplitude Shift Keying (ASK) signals to None Return to Zero (NRZ) Binary Phase Shift Keying (BPSK). Byte and block framing stay type individual and identical to bit rate of 106kbps. Field modulation is specified in a wider range for Type A as it cannot be guaranteed, that a 100% modulation reaches its settled condition.

3.2 Regulations and Emission Limits

International regulation authorities are defining power levels at different frequency bands which have to be fulfilled by a device manufacturer. This is necessary to prevent interference of different technologies and groups. Military applications, firefighters, medical, industry, science and many more has to coexist. Dedicated Industry Scientific Medical (ISM) frequency bands are defined to operate a variety of applications. The Industrial Scientific Medical (ISM) frequency band at 13.56MHz is used by RFID and contactless technology. Power limits for this band is specified in the standard TR 70-03 (CEPT/ERC REC) [4].

The EN 300 330 norm (ETSI) [8] specifies test methods how a device can be tested to fulfill the norm. Figure 3.4 presents the H-field characteristic of a Proximity Coupling Device (PCD). Two areas can be discriminated. Near field is the range where inductive coupling dominates and far field where radiation is performed. Far field decreases by 20dB per decade, wheras near field characteristic is shaped by the law Biot Savart which is explained in detail in chapter 4. The shape depends on the antenna radiant. A small antenna gives a higher H-field at distance 0m compared to a large one. The 60dB decay starts at distance equal to the antenna radiant, which results in a lower H-field at test position in 10m distance.

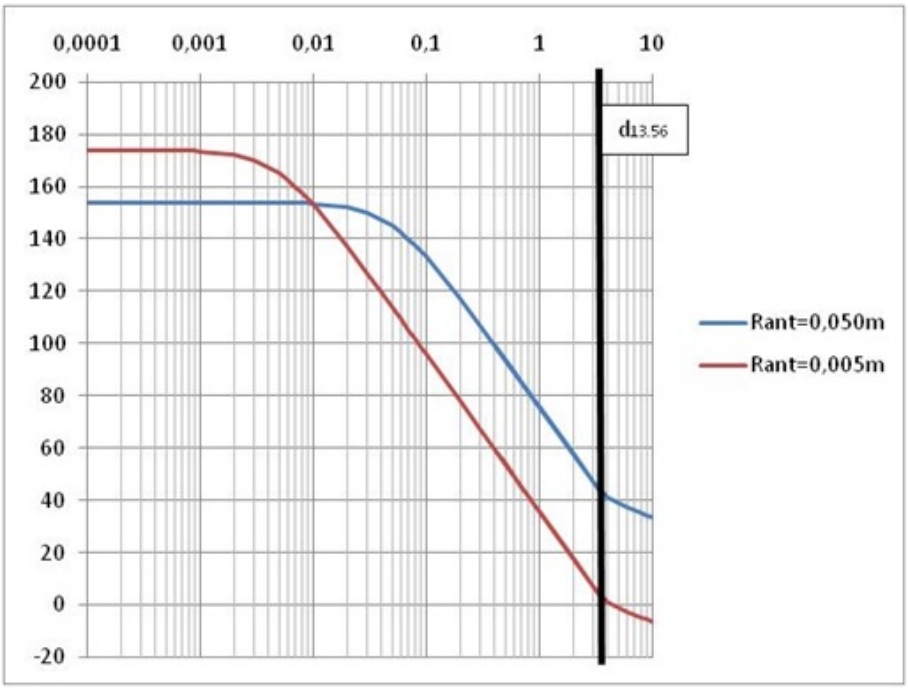

Figure 3.4: PCD H-field characteristic over distance[9, 24]

Transition position near to far field is at 3.521m for contactless technology, which is marked in figure 3.4 and denoted in equation (3.1)[9, 24].

$$d = \frac{\lambda}{2 \cdot \pi} = \frac{c}{2 \cdot \pi \cdot f} \qquad d_{13.56} = \frac{300\,000 \frac{km}{s}}{2 \cdot \pi \cdot 13.56 MHz} \approx 3.521m \tag{3.1}$$

H-field at distance 0m is proportional to $1/R_{ant}$. The cut off distance is at position R_{ant}. Increasing antenna diameter by a factor of 10 reduces field strength at antenna plane by 10 respectively -20dB, whereas cut off distance is shifted by a factor of 10. The field characteristic decreases by 60dB beyond the cut off distance. In the range where both antennas are at their -60dB branch the larger antenna is 40dB above the small one.

Not only the power limit at 13.56MHz is relevant. Side band levels, which are in the surrounding of the carrier, has to be respected too. In a contactless system reader antenna are small compared to RFID long range systems. This is because of different requirements on operating distance and power dissipation as listed in table 2.1. The communication speed is much higher in contactless systems than in RFID applications. Therefore side band limits are more important for contactless technology than others. Figure 3.5 depicts the emission limits of the HF field at 13.56 MHz.
The maximum H-field radiation, which is allowed to be emitted at 13.56MHz, is 60dB µA/m measured at a distance of 10 meters. The frequency mask limits side band levels, which are generated by a Proximity Coupling Device (PCD) when it is modulating data to a Proximity Integrated Circuit Card (PICC). Side bands are defined by modulation strength and bit rate. Higher modula-

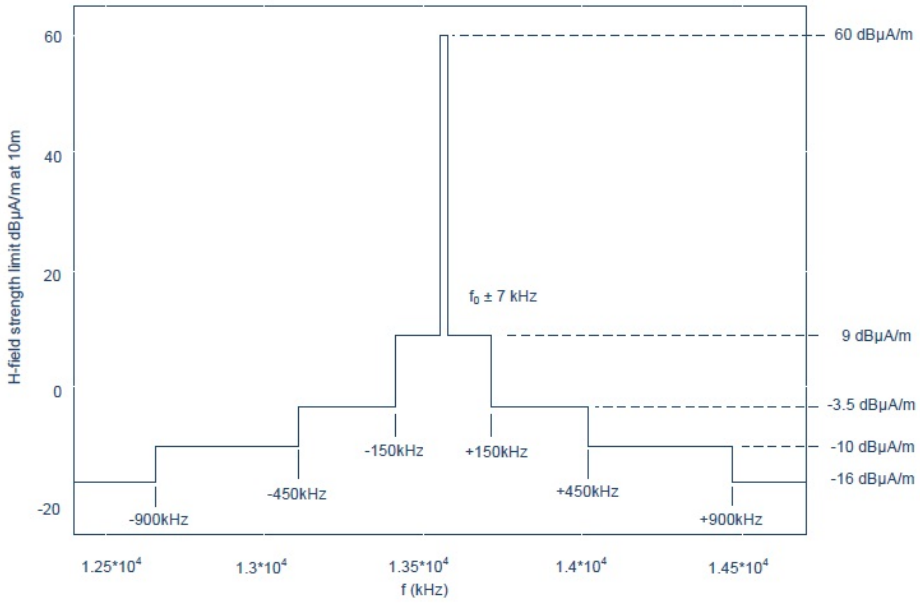

Figure 3.5: Emission Limits for ISM band at 13.56MHz[9], [11]

tion and higher bit rate are increasing side band levels. This is important to know for increasing data rates. The emission is limited to -16dB µA/m at frequencies beyond ±900kHz.

4 Contactless Technology Air Interface

This chapter discusses the channel properties in a contactless system. The international standard ISO/IEC 14443 specifies the H-field as test environment for a Proximity Integrated Circuit Card (PICC) as well as for a Proximity Coupling Device (PCD). A method will be presented how to calculate H-field properties based on antenna geometries. Furthermore a contactless system comprising a reader antenna and card coil with mutual interaction will be analyzed and described in detail. It is the objective of this chapter to give a comprehensive overview of H-field properties, inductances and coupling factors.

4.1 Equivalent Circuit

A contactless air interface channel can be described mathematically by using an appropriate equivalent circuit. Figure 4.1 depicts the mutual coupling of two inductances.

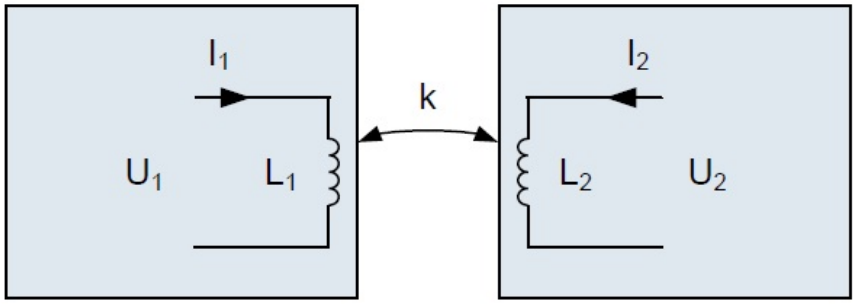

Figure 4.1: Components of an RFID System [10]

The inductance L_1 denotes the reader antenna whereas L_2 is defined by the transponder coil. The mutual interaction between those two inductances is described by the coupling coefficient *k*, which is proportional to the equation defined by the law of Biot Savart.

Basic equations are described to couple energy between two antennas. The objective is to get familiar with mutual inductances, H-field and coupling coefficients. Methods to calculate inductances, mutual inductances and coupling coefficients over distance are presented. It is possible to simulate the characteristics of a contactless system based on geometric parameters. The air interface is mostly defined by geometric properties as 'Maximum reader antenna size', 'card form factor' and required operating volume. In the international standard ISO/IEC 14443 the parameter set is reduced to a homogeneous operational H-field and minimum Load Modulation Amplitude (LMA) levels for different card sizes - e.g. ID1, ID1/2, and smaller.

4.2 Law of Biot Savart

A contactless system is built with a reader terminal, which is the power generator. A power amplifier is typically driving current into the reader antenna which is matched to the driver's output resistor. This section describes how the H-field is generated in a reader's antenna. Furthermore H-field characteristics and properties are presented. Parts of this section are already presented in [20]. The 'Law of Biot Savart' defines the transformation of current into magnetic field. It describes that a wire element which is driven by an AC current I generates an H-field at point P. This is denoted by equation (4.1).

$$H(P) = \frac{I}{4\pi} \oint \frac{d\vec{s} \times \overrightarrow{QP}}{|\overrightarrow{QP}|^3} \tag{4.1}$$

where

H	is the magnetic field
I	is the current through the wire element
$d\vec{s}$	is a vector of infinitesimal length
Q	is the source point
P	is the point where the magnetic field is calculated, and
$\overrightarrow{QP}$	is the vector from Q to P

The path integral of a wire segment of length l can be used to interpolate any closed loop antenna type - e.g. a circular or rectangular antenna. The geometric representation is shown in figure 4.2.

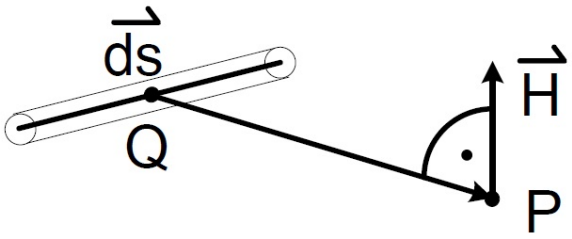

Figure 4.2: H-field generated by a current in a wire segment of length *l*

Antennas in contactless systems are typically built such that all turns are in one plane. This is valid for reader antennas as well as for card coils. This leads to the assumption that the wire segment is located in the xy plane. Contactless cards are often operated parallel to reader antenna. Therefore, only the z-component of the resulting H-field is calculated[20].

$$\vec{s} = \begin{pmatrix} u \\ v \\ 0 \end{pmatrix}$$

$$\overrightarrow{QP} = \begin{pmatrix} x-u \\ y-v \\ z \end{pmatrix}$$

$$d\vec{s} \times \overrightarrow{QP} = \begin{pmatrix} dv \cdot z \\ -du \cdot z \\ du \cdot (y-v) - dv \cdot (x-u) \end{pmatrix}$$

Equation (4.1) gives:

$$H_z(P) = \frac{I}{4\pi} \int \frac{(y-v) \cdot du - (x-u) \cdot dv}{\sqrt{(x-u)^2 + (y-v)^2 + z^2}^3} \tag{4.2}$$

As a next step the wire segment is defined to be in parallel to the y-axis to further simplify the integral. This is shown in figure 4.3.

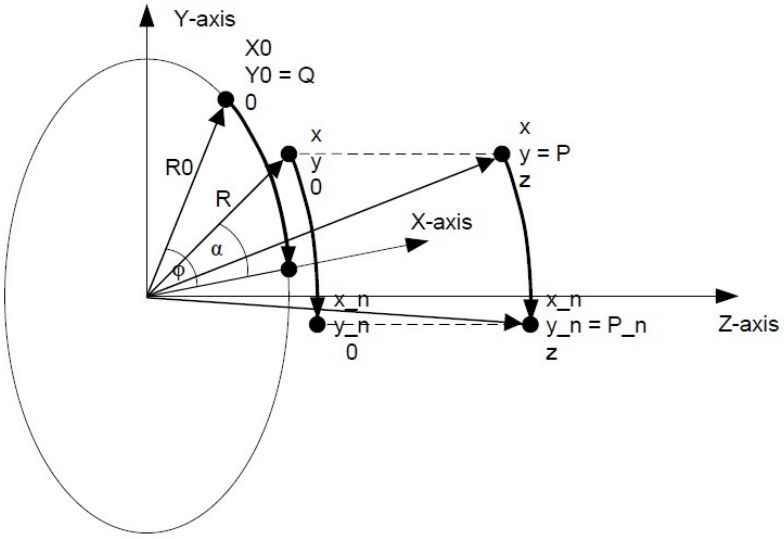

Figure 4.3: Wire segment is rotated to be parallel to y-axis

The vector $\vec{s}$ in parametric form is defined as:

$$\vec{s(t)} = \begin{pmatrix} R_0 \\ 0 \\ 0 \end{pmatrix} + t \begin{pmatrix} 0 \\ 1 \\ 0 \end{pmatrix}$$

R_0 denotes the center of the wire segment.
A rotation has to be performed to apply this definition to any wire element in the xy plane[20].

$$R_0 = \sqrt{X_0^2 + Y_0^2} \qquad \varphi = \arctan(Y_0/X_0)$$
$$R = \sqrt{x^2 + y^2} \qquad \alpha = \arctan(y/x)$$

$$P = \begin{pmatrix} R\cos(\alpha) \\ R\sin(\alpha) \\ z \end{pmatrix} \qquad P_n = \begin{pmatrix} R\cos(\alpha - \varphi) \\ R\sin(\alpha - \varphi) \\ z \end{pmatrix}$$

$$P_n = R \cdot e^{j(\alpha-\varphi)} = R \cdot e^{j\alpha} e^{-j\varphi}$$
$$x_n = x \cdot cos(\varphi) + y \cdot sin(\varphi)$$
$$y_n = y \cdot cos(\varphi) - x \cdot sin(\varphi)$$
$$z_n = z$$

P_n is the rotated H-field point at coordinates x_n, y_n and z_n. By using the transformed point P_n and the parametric form of $\vec{s(t)}$, with

$$u(t) = R_0 \qquad du = 0$$
$$v(t) = t \qquad dv = dt$$

equation (4.1) gives[20]:

$$H_z(x, y, z, \varphi, R_0, l) = \frac{I}{4\pi} \int_{-l/2}^{l/2} \frac{(x_n(x, y, \varphi) - R_0) \cdot dt}{\sqrt{(x_n(x, y, \varphi) - R_0)^2 + (y_n(x, y, \varphi) - t)^2 + z^2}^3} \quad (4.3)$$

$$H_z(x, y, z, \varphi, R_0, l) = \frac{I}{4\pi} \cdot \frac{x_n(x, y, \varphi) - R_0}{(x_n(x, y, \varphi) - R_0)^2 + z^2} \left[\frac{y_n(x, y, \varphi) - \frac{l}{2}}{\sqrt{(x_n(x, y, \varphi) - R_0)^2 + (y_n(x, y, \varphi) - \frac{l}{2})^2 + z^2}} - \frac{y_n(x, y, \varphi) + \frac{l}{2}}{\sqrt{(x_n(x, y, \varphi) - R_0)^2 + (y_n(x, y, \varphi) + \frac{l}{2})^2 + z^2}} \right] \quad (4.4)$$

Two examples - a circular and a rectangular antenna - are depicted in equations (4.5) and (4.6). For the circular antenna a diameter of $2 \cdot R$ and a wire element of length $2 \cdot R \cdot \tan(\varphi)$ is used. The circle is approximated by n segments[20].

$$H_{circular}(x, y, z, R, n) = \sum_{k=0}^{n-1} H_z(x, y, z, \frac{k \cdot \varphi}{n}, R, 2 \cdot R \cdot \tan(\frac{k \cdot \varphi}{n})) \tag{4.5}$$

where

x, y, z	are the coordinates of the point where the field is calculated
R, n	are the radiant and the number of segments of the circular antenna

Figure 4.4 illustrates the H-field distribution of a circular loop at two distances (0mm, 20mm).

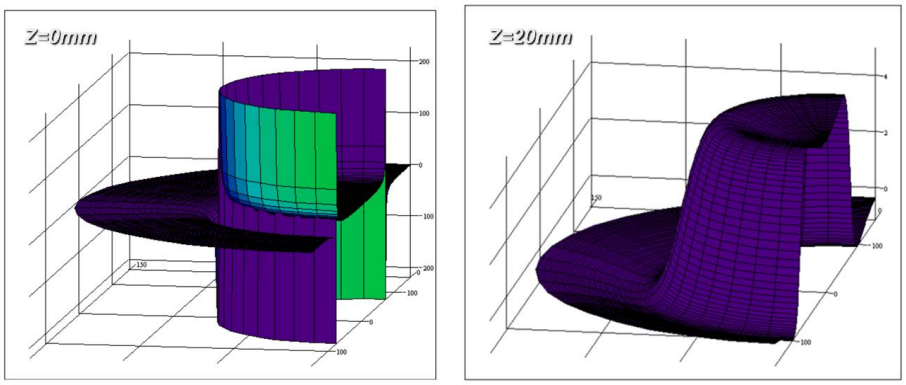

Figure 4.4: Magnetic field of a circular antenna at different distances [20]

Reader antennas are not circular only. In the past ten years more and more rectangular reader antennas were used to better utilize the given terminal dimensions. The rectangular antenna in this example is of dimension X, Y and has one turn[20].

$$\begin{aligned} H_{rectangular}(x, y, z, X, Y) = & H_z(x, y, z, 0, \frac{X}{2}, Y) + H_z(x, y, z, \frac{\pi}{2}, \frac{Y}{2}, X) + \\ & H_z(x, y, z, \pi, \frac{X}{2}, Y) + H_z(x, y, z, \frac{3 \cdot \pi}{2}, \frac{Y}{2}, X) \end{aligned} \tag{4.6}$$

where

x, y, z	are the coordinates of the point where the field is calculated
X, Y	is the dimension of the rectangular antenna

Figure 4.5 illustrates the H-field distribution of a rectangular loop at two distances (0mm, 5mm).

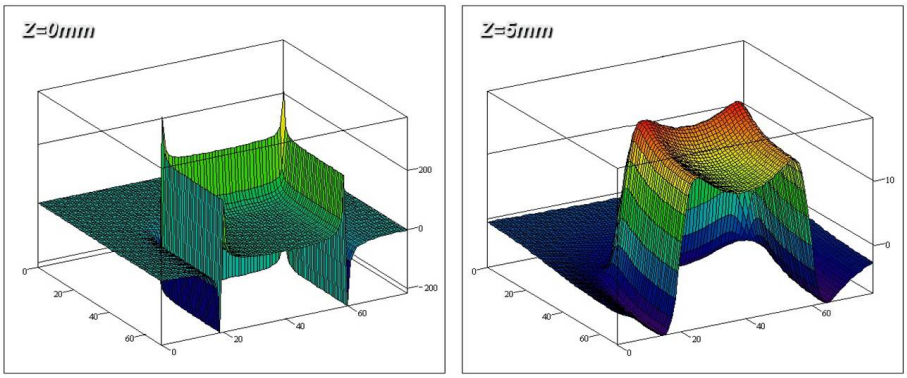

Figure 4.5: Magnetic field of a rectangular antenna at different distances [20][14]

4.3 Electromagnetic Induction

This paragraph describes the interrelationship between two loosely coupled antennas. One key element is already depicted by the law of Biot Savart - i.e. transforming current into magnetic field. As a second step the magnetic field has to be converted into a voltage. This is defined by the electromagnetic induction, which describes the transformation of a dynamic magnetic field into voltage, whereby the magnetic field is integrated over the area of a loop wire. This is shown in figure 4.6.

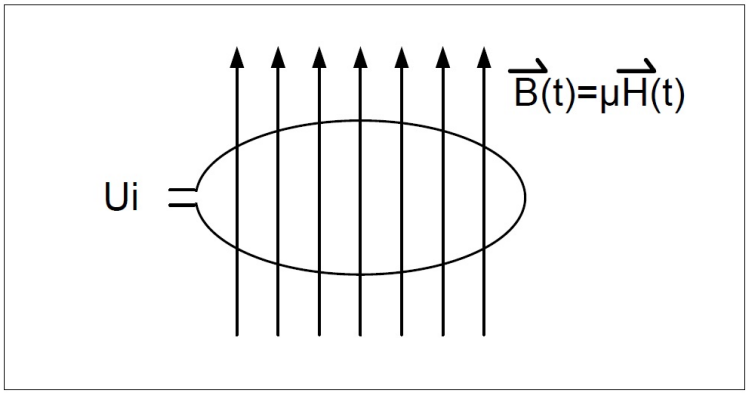

Figure 4.6: dynamic magnetic field over a wire loop [10]

Equation (4.7) denotes the electromagnetic induction [10].

$$U_i(t) = -\frac{\mathrm{d}}{\mathrm{d}t}\int_A \mu \cdot \vec{H}(t) \cdot \mathrm{d}\vec{A} \tag{4.7}$$

Contactless technology is based on carrier frequency of 13.56 MHz. Assuming that the H-field is generated by $\hat{H} \cdot \cos(\omega \cdot t)$ and the card antenna is parallel to the reader antenna, equation (4.7) gives

$$U_i(t) = -\frac{\mathrm{d}\cos(\omega \cdot \mathrm{t})}{\mathrm{d}t} \cdot \mu \int_A \hat{H} \cdot \mathrm{d}\vec{A}$$

$$U_i(t) = \omega \cdot \sin(\omega \cdot t) \cdot \mu \int_A \hat{H} \cdot \mathrm{d}\vec{A}$$

The magnitude of the induced voltage U_i is represented by equation (4.8).

$$\hat{U}_i = \omega \cdot \mu \int_A \hat{H} \cdot \mathrm{d}\vec{A} \tag{4.8}$$

Assuming a homogeneous H-field - as it is defined by the ISO/IEC 14443 standard - equation (4.8) gives

$$\hat{U}_i = \omega \cdot \mu \cdot \hat{H} \cdot A_{mean} \cdot N \tag{4.9}$$

where

ω	is the angular frequency
μ	is the magnetic permeability
$\hat{H}$	is the magnitude of the magnetic field
A_{mean}	is the mean area defined by the coil turns
N	is the number of antenna turns

The integral $\int_A \hat{H} \cdot \mathrm{d}\vec{A}$ is only definite for $z = 0$. Therefore an interpolation method is used to calculate the H-field at any position. Equation (4.10) denotes a formula which calculates an induced voltage in a rectangular pickup coil of size X, Y, which is powered by a circular antenna at distance z. Equation (4.5) is used to 'generate' the H-field which then is integrated over the pickup coil area by interpolation.

$$U_{i-pickup}(z) = \frac{X \cdot Y}{2 \cdot l \cdot 2 \cdot m} \cdot \sum_{i=-l}^{l-1} \sum_{j=-m}^{m-1} \sum_{k=0}^{n-1} H_z(i \cdot \frac{X}{2}, j \cdot \frac{Y}{2}, z, \frac{k \cdot \varphi}{n}, R, 2 \cdot R \cdot \tan(\frac{k \cdot \varphi}{n})) \tag{4.10}$$

4.4 Self and Mutual Induction

Results of the previous two sections are used in this paragraph to discuss different parameters of contactless systems. The mutual inductance of reader and card antenna is one important element, which also includes the coupling coefficient and inductances L_1 and L_2 as already mentioned in sections 4.1 and 4.3. Two basic equations - (4.4) and (4.8) - are used in this section.

$$H_z(x,y,z,\varphi,R_0,l) = \frac{I}{4\pi}\cdot\frac{x_n(x,y,\varphi)-R_0}{(x_n(x,y,\varphi)-R_0)^2+z^2}\left[\frac{y_n(x,y,\varphi)-\frac{l}{2}}{\sqrt{(x_n(x,y,\varphi)-R_0)^2+(y_n(x,y,\varphi)-\frac{l}{2})^2+z^2}}\right.$$
$$\left.-\frac{y_n(x,y,\varphi)+\frac{l}{2}}{\sqrt{(x_n(x,y,\varphi)-R_0)^2+(y_n(x,y,\varphi)+\frac{l}{2})^2+z^2}}\right]$$

$$U_i = \omega\cdot\mu\int_A \hat{H}\cdot \mathrm{d}\vec{A}$$

The impedance of an inductance is defined as

$$Z_L = \omega\cdot L = \frac{U}{I} \tag{4.11}$$

and L is given by

$$L = \frac{U}{\omega\cdot I} \tag{4.12}$$

The combination of equations (4.4) and (4.8) results in

$$U_i = \omega\cdot\mu\cdot\frac{I}{4\pi}\cdot\int_A \frac{x_n(x,y,\varphi)-R_0}{(x_n(x,y,\varphi)-R_0)^2+z^2}\left[\frac{y_n(x,y,\varphi)-\frac{l}{2}}{\sqrt{(x_n(x,y,\varphi)-R_0)^2+(y_n(x,y,\varphi)-\frac{l}{2})^2+z^2}}\right.$$
$$\left.-\frac{y_n(x,y,\varphi)+\frac{l}{2}}{\sqrt{(x_n(x,y,\varphi)-R_0)^2+(y_n(x,y,\varphi)+\frac{l}{2})^2+z^2}}\right]\cdot \mathrm{d}\vec{A} \tag{4.13}$$

Rearranging according to equation (4.12) and replacing μ by $4 \cdot \pi \cdot 10^{-7}$ gives

$$M(x,y,z) = 10^{-7} \cdot \int_A \frac{x_n(x,y,\varphi) - R_0}{(x_n(x,y,\varphi) - R_0)^2 + z^2} \left[\frac{y_n(x,y,\varphi) - \frac{l}{2}}{\sqrt{(x_n(x,y,\varphi) - R_0)^2 + (y_n(x,y,\varphi) - \frac{l}{2})^2 + z^2}} - \frac{y_n(x,y,\varphi) + \frac{l}{2}}{\sqrt{(x_n(x,y,\varphi) - R_0)^2 + (y_n(x,y,\varphi) + \frac{l}{2})^2 + z^2}} \right] \cdot \mathrm{d}\vec{A} \quad (4.14)$$

Mutual inductance $M(x,y,z)$ is used in equation (4.14) as this is the general equation for both self and mutual inductance. Self inductance is a special case of $M(x,y,z)$ where x, y, z are set to zero.

Equation (4.14) refers to one wire element. To calculate an inductance the closed loop form is necessary. The H-field of a rectangular shaped antenna - as depicted in equation (4.6) - is the base for calculating the mutual inductance of two closed loop wires.

$$M_{rect}(X_1, Y_1, z, X_2, Y_2) = 10^{-7} \cdot \int_{-\frac{Y_2}{2}}^{\frac{Y_2}{2}} \int_{-\frac{X_2}{2}}^{\frac{X_2}{2}} H_{rectangular}(x, y, z, X_1, Y_1) \cdot dx \cdot dy \quad (4.15)$$

where

X_1	is the X-dimension of loop one
Y_1	is the Y-dimension of loop one
z	is the distance between the two loops
X_2	is the X-dimension of second loop
Y_2	is the Y-dimension of second loop
$H_{rectangular}$	is the H-field generated by a rectangular antenna loop

No definite integral for equation (4.15) is possible for $z \neq 0$. Therefore the integral is interpolated by a sum of H-field points within the area of the individual coil turns, which is denoted in equation (4.16)

$$M_{rect}(X_1, Y_1, z, X_2, Y_2) = 10^{-7} \cdot \frac{X_2 \cdot Y_2}{2 \cdot l \cdot 2 \cdot m} \cdot \sum_{j=-l}^{l-1} \sum_{j=-m}^{m-1} H_{rectangular}(\frac{i}{2l} \cdot X_2, \frac{j}{2m} \cdot Y_2, z, X_1, Y_1) \quad (4.16)$$

4.4.1 Exemplary Equations for Self, Mutual Inductance and Coupling Factor

Based on equation (4.15) examples are given, how to calculate a reader antenna and a card coil inductance. Furthermore the mutual inductance and coupling factor k are derived. Many

reader are built in a rectangular shape. These reader typically are using the same shape for the antenna. Therefore a rectangular shaped antenna is used for the reader as well as the card antenna. Furthermore it is easier to follow the calculation by using the same geometric properties for both antenna types.

The mutual inductance M_{12}, which is generated by coupling between inductance L_1 and L_2, can be calculated at any distance z by equation (4.17). The two antennas are in parallel to the x, y-plane and symmetrical to the z-axis.

$$M_{12}(z) = \sum_{i=0}^{N_1-1} \sum_{j=0}^{N_2-1} M_{rect}(X_2 - \frac{\Delta w}{2} \cdot (1+2i), Y_2 - \frac{\Delta w}{2} \cdot (1+2i), z, \\ X_1 - \frac{\Delta w}{2} \cdot (1+2j), Y_1 - \frac{\Delta w}{2} \cdot (1+2j)) \tag{4.17}$$

The calculation of antenna inductance L_1 of size X_1, Y_1 and N_1 turns is denoted in equation (4.18). Gap width and wire diameter are of same dimension (Δw) in this example.

$$L_1 = \sum_{i=0}^{N_1-1} \sum_{j=0}^{N_1-1} M_{rect}(X_1 - \frac{\Delta w}{2} \cdot (1+2i), Y_1 - \frac{\Delta w}{2} \cdot (1+2i), 0, \\ X_1 - \frac{\Delta w}{2} \cdot (1+2j), Y_1 - \frac{\Delta w}{2} \cdot (1+2j)) \tag{4.18}$$

The card coil L_2 is of size X_c, Y_c and has N_2 turns. Gap width and wire diameter are of same dimension (Δw). This gives equation (4.19).

$$L_2 = \sum_{i=0}^{N_2-1} \sum_{j=0}^{N_2-1} M_{rect}(X_2 - \frac{\Delta w}{2} \cdot (1+2i), Y_2 - \frac{\Delta w}{2} \cdot (1+2i), 0, \\ X_2 - \frac{\Delta w}{2} \cdot (1+2j), Y_2 - \frac{\Delta w}{2} \cdot (1+2j)) \tag{4.19}$$

4.4.2 Calculation Variant for Self Inductance

As an alternative, self inductance L can be calculated by using the equation for M as defined in (4.17). The geometric values for the two inductances (X_1, Y_1, N_1) and (X_2, Y_2, N_2) have to be set to the same values. The distance z shall be set close to zero to have almost the same result as if using zero exactly. The advantage of this approach is, that there is no singularity as given by equation (4.4) at different positions - e.g. at point $\begin{pmatrix} X_1 \\ Y_1 \\ 0 \end{pmatrix}$.

Equation (4.20) denotes the H-field characteristic outside and inside an infinite wire [10].

$$H_{outside}(x) \propto \frac{1}{x} \qquad\qquad H_{inside}(x) \propto x \tag{4.20}$$

4.5 Coupling Coefficient

Coupling coefficient k is often used instead of mutual inductance M. Coupling coefficient k is only dependent on geometric parameters of antennas and the distance between the two. Equation (4.21) defines the relationship between mutual inductance M, inductances L_1, L_2 and coupling coefficient k.

$$M = k \cdot \sqrt{L_1 \cdot L_2} \tag{4.21}$$

Rearranging equation (4.21) and replacing M by equation (4.12) gives

$$k(x, y, z) = \frac{M(x, y, z)}{\sqrt{L_1 \cdot L_2}} \tag{4.22}$$

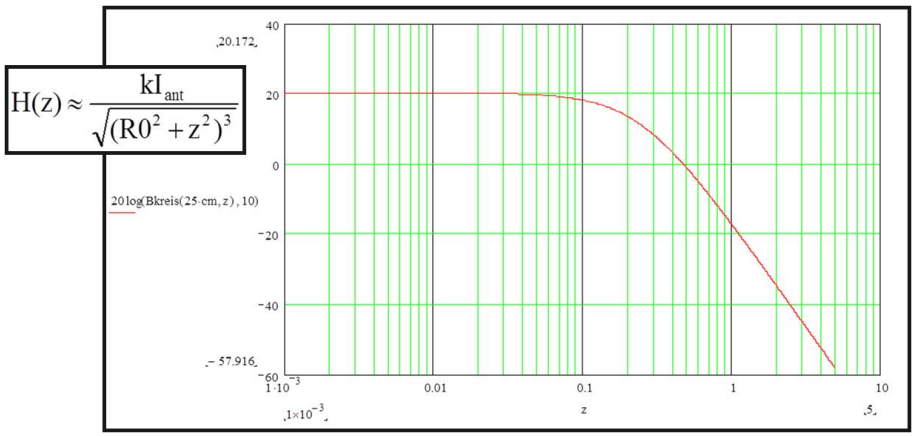

Figure 4.7: H-field over distance [14]

Coupling coefficient k is directly proportional to the H-field characteristic over distance. The factor is defined by antenna and coil geometries. The coupling characteristic reflects the behavior of a contactless system. The energy coupling is almost constant up to the radius of the antenna whereas it starts to drop by 60dB/dec at greater distances. Figure 4.7 depicts the H-field characteristic over distance of an antenna with a diameter of 50cm.

5 Transfer Functions

This chapter discusses the energy transfer in a contactless system. It is the objective of this chapter to give a comprehensive overview of energy transfer characteristics including H-field properties, mutual coupling behavior and power regulation of Proximity Integrated Circuit Cards (PICCs). Furthermore a contactless system comprising a reader antenna and card coil with mutual interaction will be analyzed and described in detail. A method of transfer functions will be introduced to describe electrical properties of a contactless system. These transfer functions will be used in following chapters to analyze energy as well as data transfer properties. Besides steady state conditions, a special focus will be set on transient behavior in chapters 6 and seven. It is the objective of this chapter to give a comprehensive overview of energy transfer characteristics including H-field properties, mutual coupling behavior and power regulation of Proximity Integrated Circuit Cards (PICCs).

5.1 Equivalent Circuit

Contactless system can be described mathematically by using an appropriate equivalent circuit. As the nature of contactless systems is expressed by inductive coupling, a transformer equation fits best. One commonly used equivalent circuit is shown in figure 5.1.

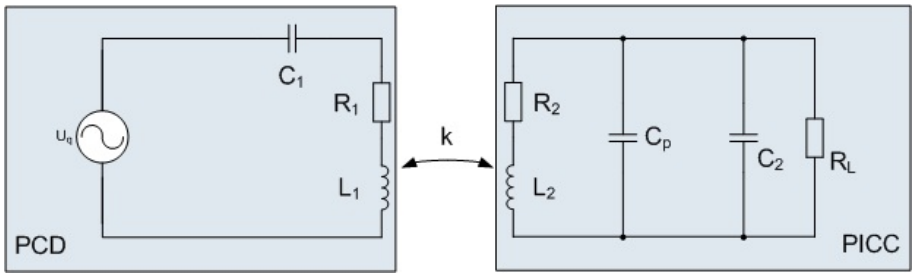

Figure 5.1: Contactless system equivalent circuit [9]

The inductance L_1 denotes the reader antenna whereas L_2 is defined by the transponder coil. The mutual interaction between those two inductances is described by the coupling coefficient *k*, which is proportional to the equation defined by the law of Biot Savart.

Following sections are analyzing energy transfer characteristics by means of transfer functions. This gives the advantage of applying methods like root locus and Laplace transformation. Objective is to describe the individual components of a contactless system - i.e. reader, card - independent of their mutual interdependency. This approach is used in the ISO standard ISO/IEC 14443. The method of the standard is, to cut a contactless system at the air interface. Instead of specifying a huge set of mutually coupled contactless systems, the ISO approach specifies H-field. The H-field is directly proportional to the induced voltage of the card. This is described in detail in section 4.3. ISO compliance tests are available for cards and reader in the ISO/IEC 10373 test specification. A card has to fulfill an operational H_{min} to H_{max} as well as a minimum Load Modulation Amplitude (LMA) test, which characterizes the signal strength of a card's modulation. A reader is checked that it generates an H-field according to the standard. The transformation from current - i.e. voltage over L - into H-field is depicted in section 4.2.

5.2 Reader Transfer Function

A contactless reader consists of a power generation circuit which runs at a frequency of 13.56MHz. Most circuits are built as single ended or differential push pull output stages. The rectangular waveform is filtered by an Electro Magnetic Compatibility (EMC) filter, which attenuates higher order harmonics to fulfill regulation requirements as specified in [9]. As first transfer function a simplified Reader circuit is characterized. The push pull driver and the Electro Magnetic Compatibility (EMC) filter is replaced by a simple sinusoidal voltage source. Antenna and output resistor of the driver are combined as one resistor. Matching circuits as presented in [11] are reduced to a series resonant circuit which is the most simple way to build a power transfer circuit for a contactless reader.

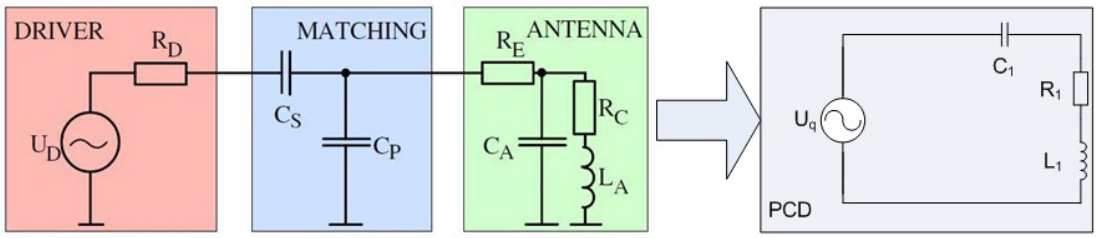

Figure 5.2: Reader equivalent circuit as presented in [11] and its reduced version

Figure 5.2 depicts the reduction of a complex reader circuit to its minimum components to describe the electrical properties of a reader power path.

The reader transfer function is calculated as U_{L1}/U_q. The source U_q represents the driver voltage. The H-field is generated over U_{L1} which is depicted in section 4.4.

$$\frac{U_{L1}}{U_q} = \frac{j\omega \cdot L_1}{j\omega \cdot L_1 + R_1 + \frac{1}{j\omega \cdot C_1}} \tag{5.1}$$

replacing $j\omega$ by s (5.1) gives

$$G_{L1}(s) = \frac{s^2 \cdot L_1 C_1}{s^2 \cdot L_1 C_1 + s \cdot C_1 R_1 + 1} \tag{5.2}$$

where

s	is the complex angular frequency
L_1	is the antenna inductance
C_1	is the tuning capacitance
R_1	is the sum of all resistances - i.e. driver, antenna and Q resistance

The transfer characteristic of $G_{L1}(s)$ is shown in figure 5.3.

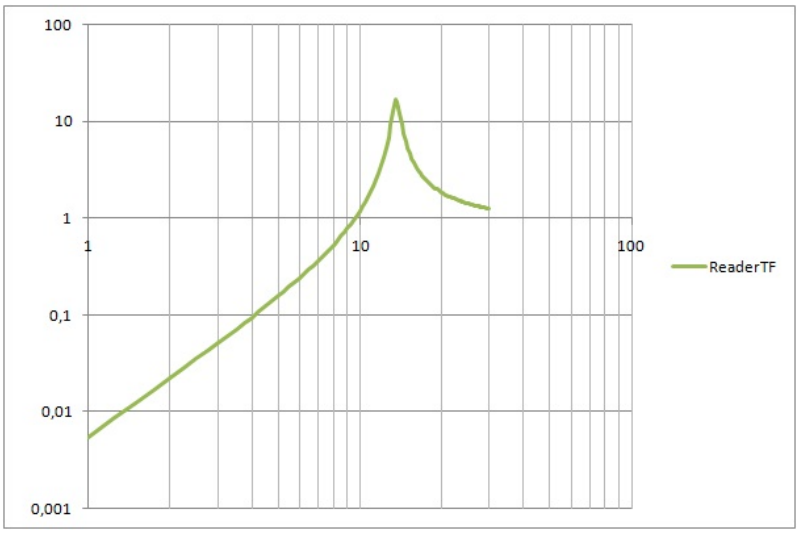

Figure 5.3: Reader transfer characteristics based on $G_{L1}(s)$

Two properties are shown in this figure. First, the transfer function is a 2nd order high pass and second, it is a resonant circuit. The resonance frequency is typically tuned to 13.56MHz, which is the operating frequency of a contactless system according to the ISO/IEC 14443 standard. The tuning is done to get best power transfer - i.e. get current into the reader antenna in a most efficient way. This current generates the H-field as described in section 4.2.

5.3 Card Transfer Function

A Proximity Integrated Circuit Card (PICC) picks up the H-field by electromagnetic induction as depicted in section 4.3. The induction generates an induced voltage U_i which is the generator voltage for the card circuit. This voltage depends on the strength of the H-field and the geometry of the card coil. Equation (4.9) denotes this characteristic.

The value *1.1* of factor $\mu \cdot \omega \cdot A_{mean} \cdot N$ is typical for an ID1 coil, which is the standard size for smart cards. In the ISO/IEC 14443 standard a minimum field strength H_{min} is specified by 1.5A/m which gives an induced voltage of $\approx 1.65V_{rms}$. State of the art card ICs need an input voltage of more than $1.65V_{rms}$. In EMVCo applications Proximity Integrated Circuit Cards (PICC) are often built with smaller size antennas because credit cards have areas where antenna turns are not allowed to be located. This further reduces the induced voltage by a significant factor. Therefore induced voltage U_i is transformed by a resonant circuit to gain the necessary voltage to operate the Proximity Integrated Circuit Card (PICC).

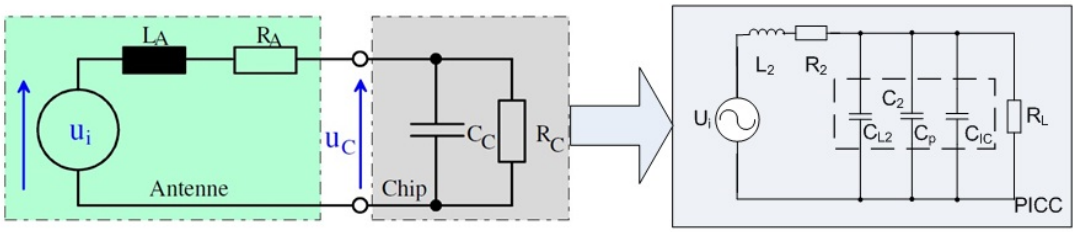

Figure 5.4: Card equivalent circuit as presented in [11] and the version used in this section

The card transfer function is calculated as U_L/U_i. The source U_i represents the induced voltage. U_i is generated by electromagnetic induction as depicted in section 4.3. Equation (5.3) denotes the card transfer function.

$$\frac{U_L}{U_i} = \frac{\frac{1}{j\omega \cdot C_2 + \frac{1}{R_L}}}{j\omega \cdot L_2 + R_2 + \frac{1}{j\omega \cdot C_2 + \frac{1}{R_L}}} \tag{5.3}$$

Replacing $j\omega$ by s and rearranging (5.3) gives

$$G_L(s) = \frac{1}{s^2 \cdot L_2C_2 + s \cdot C_2R_2 + s \cdot \frac{L_2}{R_L} + \frac{R_2}{R_L} + 1} \tag{5.4}$$

where

s	is the complex angular frequency
L_2	is the card coil inductance
C_2	is the sum of all tuning capacitances - i.e. IC input, coil and package capacitances
R_2	is the card coil resistance
R_L	is the card IC equivalent load resistance

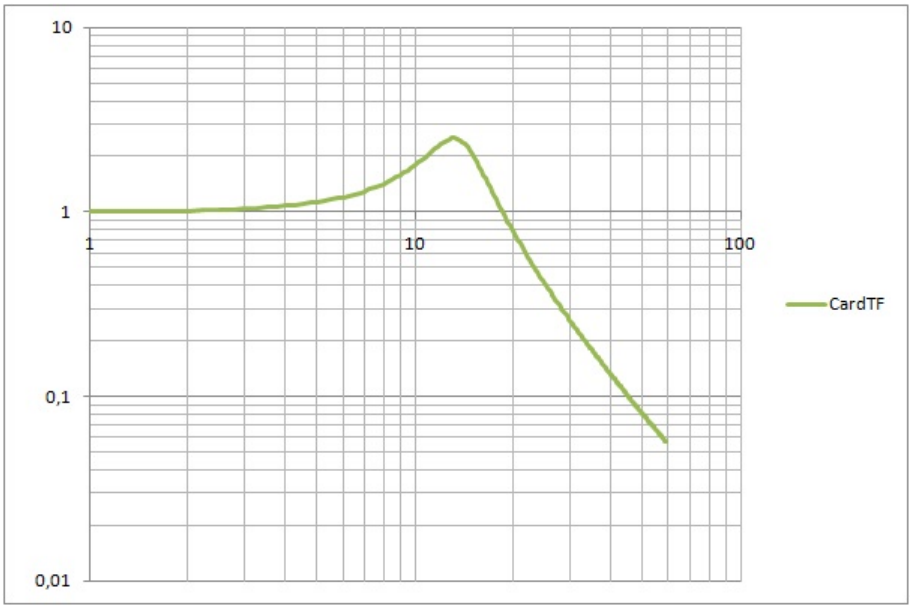

Figure 5.5: Card transfer characteristics based on transfer function $G_L(s)$

As mentioned before, figure 5.5 shows the resonant circuit characteristics [9]. It transforms the induced voltage to an appropriate IC input voltage. The circuit represents a 2nd order low pass which becomes dominant at frequencies higher than the resonance frequency. This property leads to a tuning strategy which always tends to tune a card at a higher resonance frequency than the system frequency. Component tolerances as well as multiple stacked cards are the root for that strategy. If the resonance frequency is shifted down below 13.56MHz the gain of the resonant circuit starts to become a loss factor caused by the attenuation of the low pass filter.

5.4 Load Modulation Amplitude (LMA) Transfer Function

A second transfer function is important for a Proximity Integrated Circuit Card (PICC). It is the characteristic of sourcing an H-field by the card impedance. In the standards ISO/IEC 14443 and ISO/IEC 10373 this property is named LMA as it is the way how a card is generating its modulation data. A card generates an H-field H_2 by loading the induced voltage U_i by the card IC impedance. This is depicted in figure 5.6. U_{L2} is the voltage at the card inductance which is generated by the current I_2. This current is the source for H_2 as denoted in section 4.2.

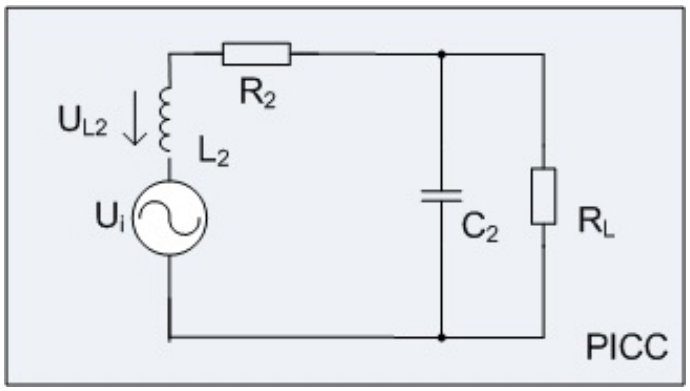

Figure 5.6: Voltage over card coil

This behavior is general for a Proximity Integrated Circuit Card (PICC). Modulation is a special operating condition where the card IC impedance is changed to modify the H_2 field. This change in impedance can be detected by the reader receiver circuit. The Load Modulation Amplitude (LMA) is measured with a sense coil specified in ISO/IEC 10373 at a defined distance. The transfer function G_{L2} is defined by equations (5.5) and (5.6)

$$\frac{U_{L2}}{U_i} = -\frac{j\omega \cdot L_2}{j\omega \cdot L_2 + R_2 + \frac{1}{j\omega \cdot C_2 + \frac{1}{R_L}}} \tag{5.5}$$

Replacing $j\omega$ by s and rearranging (5.5) gives

$$G_{L2}(s) = -\frac{s^2 \cdot C_2 L_2 + s \cdot \frac{L_2}{R_L}}{s^2 \cdot C_2 L_2 + s \cdot C_2 R_2 + s \cdot \frac{L_2}{R_L} + \frac{R_2}{R_L} + 1} \tag{5.6}$$

where

s	is the complex angular frequency
L_2	is the card coil inductance
C_2	is the sum of all tuning capacitances - i.e. IC input, coil and package capacitances
R_2	is the card coil resistance
R_L	is the card IC equivalent load resistance

An independent view on transfer characteristics - i.e. without mutual interdependency - was described in the previous sections. The mutual influence of the loosely coupled system was omitted for simplicity. The following section starts to describe a first method to incorporate the behavior of mutual inductances in a contactless system. Changes in distance between card and reader are changing the input impedance of the card. This reflects the regulation behavior of a contactless card to prevent overvoltage and to derive best power and communication performance [14]. The mean to transfer data from card to reader is to change the card impedance. A card IC typically modulates its input voltage. Although this is - in most cases - implemented as amplitude modulation at the card IC terminals, a receiver has to cope with amplitude and phase modulation signals. This will be analyzed in detail within this chapter.

5.5 Air Interface Transfer Function

The energy transfer from reader source voltage U_q to the card IC input U_L is denoted by equations (5.2) and (5.4). The missing component is the transfer function of the air interface. The electrical properties - H-field, inductance, coupling coefficient - are described in detail in section 5.5. The air interface transfer function is derived from equations presented in sections 4.2 and 4.3. The H-field is generated by current I_1 which is powering the reader antenna L_1. Current I_1 has to be transformed to a voltage to be able to be used in a voltage transfer function.

$$I_1 = \frac{U_{L1}}{j\omega \cdot L_1} \tag{5.7}$$

$$U_{i_2} = j\omega \cdot M(x,y,z) \cdot I_1 \tag{5.8}$$

Rearranging to U_{i_2}/U_{L1} gives

$$G_{AIF_1}(s) = \frac{M(x,y,z)}{L_1} \tag{5.9}$$

Using coupling coefficient k equation (5.9) results in

$$G_{AIF_1}(s) = k(x,y,z)\frac{\sqrt{L_1 \cdot L_2}}{L_1} = k(x,y,z)\sqrt{\frac{L_2}{L_1}} \tag{5.10}$$

The mutual interdependence of antenna L_1 and coil L_2 leads to a second transfer function of the air interface which is representing H-field H_2 generated by the current I_2 through coil L_2. The same method as used for antenna L_1 applies to the second air interface transfer function $G_{AIF_2}(s)$.

$$I_2 = \frac{U_{L2}}{j\omega \cdot L_2} \tag{5.11}$$

$$U_{i_1} = j\omega \cdot M(x,y,z) \cdot I_2 \tag{5.12}$$

Rearranging to U_{i_1}/U_{L2} gives

$$G_{AIF_2}(s) = \frac{M(x,y,z)}{L_2} \tag{5.13}$$

Using coupling coefficient k equation (5.13) results in

$$G_{AIF_2}(s) = k(x,y,z)\frac{\sqrt{L_1 \cdot L_2}}{L_2} = k(x,y,z)\sqrt{\frac{L_1}{L_2}} \tag{5.14}$$

Equations $G_{AIF_1}(s)$ and $G_{AIF_2}(s)$ are denoting the air interface transfer functions. The terms $k \cdot \sqrt{\frac{L_2}{L_1}}$ and $k \cdot \sqrt{\frac{L_1}{L_2}}$ are representing the well known factors N_2/N_1 and N_1/N_2 which are valid for an ideal transformer without losses. An inductance is proportional to $A_L N^2$ [10, 20]. This property can be derived from equation (4.18). An ideal transformer has a coupling factor k of approximately one and its effective area A_L is identical for both inductors, L_1 and L_2. This results in

$$1 \cdot \sqrt{\frac{A_L \cdot N_2^2}{A_L \cdot N_1^2}} = \frac{N_2}{N_1}$$
$$1 \cdot \sqrt{\frac{A_L \cdot N_1^2}{A_L \cdot N_2^2}} = \frac{N_1}{N_2}$$

5.6 Energy Transfer to the Card IC

Combining transfer functions of reader $G_{L1}(s)$, card $G_{L2}(s)$, $G_L(s)$ and air interface functions $G_{AIF_1}(s)$, $G_{AIF_2}(s)$ are giving the energy transfer function $G_e(s)$. The feed forward branch is built by $G_{L1}(s)$ and $G_{AIF_1}(s)$. The feedback loop is depicted by $G_{L2}(s)$ and $G_{AIF_2}(s)$. $G_L(s)$ is transforming the induced voltage at card coil L_2 to the input terminals of the card IC.

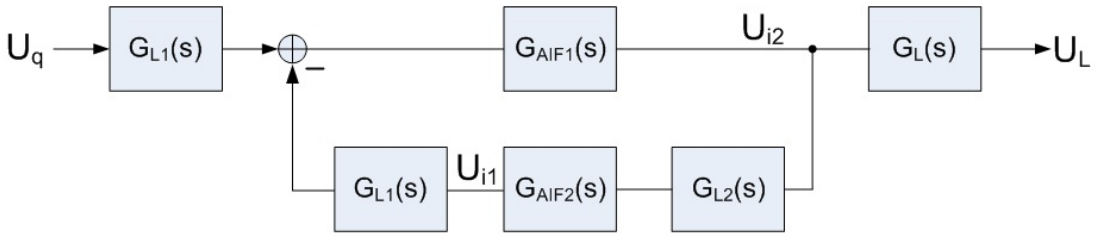

Figure 5.7: Energy Transfer Function

Figure 5.7 represents the block diagram of energy transfer function $G_e(s)$. The induced voltages - which are generated by the air interface properties - are denoted as U_{i_2} and U_{i_1}. Generator voltage U_q is the reader output driver. U_L represents the card IC input.

Equation (5.15) is derived from figure 5.7

$$G_e(s) = G_{L1}(s) \cdot \frac{G_{AIF_1}(s)}{1 + G_{L1}(s) \cdot G_{AIF_1}(s) \cdot G_{L2}(s) \cdot G_{AIF_2}(s)} \cdot G_L(s) \tag{5.15}$$

where

G_e	is the energy transfer function
G_{L1}	is the reader power generation circuit
G_{AIF_1}	is the feed forward function - antenna voltage to induced card voltage
G_{L2}	is generating the coil voltage over L_2
G_{AIF_2}	is the feedback from card coil to reader antenna
G_L	is transforming the card's induced voltage to the IC input terminal
U_q	is the reader's power generator voltage
U_{i_1}	is the induced voltage at the reader antenna
U_{i_2}	is the induced voltage at the card coil
U_L	is the card IC input voltage

As a next step, the air interface functions $G_{AIF_1}(s)$ and $G_{AIF_2}(s)$ are replaced by its parametric values $k(x,y,z) \cdot \sqrt{\frac{L_2}{L_1}}$ and $k(x,y,z) \cdot \sqrt{\frac{L_1}{L_2}}$. This leads to equation (5.16).

$$G_e(s) = G_{L1}(s) \cdot \frac{k(x,y,z) \cdot \sqrt{\frac{L_2}{L_1}}}{1 + k(x,y,z)^2 \cdot G_{L1}(s) \cdot G_{L2}(s)} \cdot G_L(s) \tag{5.16}$$

Equations (5.15) and (5.16) are denoting the air interface transfer function more detailed. It is not only characterized by equations depicted in section 5.5. The main difference is the feedback loop of the induced voltage U_{i_2} over coil L_2 which is generating an induced voltage U_{i_1} at reader antenna L_1. Voltage U_{i_1} is multiplied by the reader transfer function $G_{L1}(s)$ before being fed into the feed forward branch. This characteristic is essential for data transfer analysis. It is obvious that data, which is modulated by a Proximity Integrated Circuit Card (PICC), is shaped by the resonant circuit of the reader. The properties of a typical reader are depicted in section 5.2.

The transfer function $G_{AIF}(s)$ can be derived from equation (5.16). Figure 5.8 highlights the blocks of the complex air interface transfer function which is denoted in equation (5.17).

$$G_{AIF}(s) = \frac{k(x,y,z) \cdot \sqrt{\frac{L_2}{L_1}}}{1 + k(x,y,z)^2 \cdot G_{L1}(s) \cdot G_{L2}(s)} \tag{5.17}$$

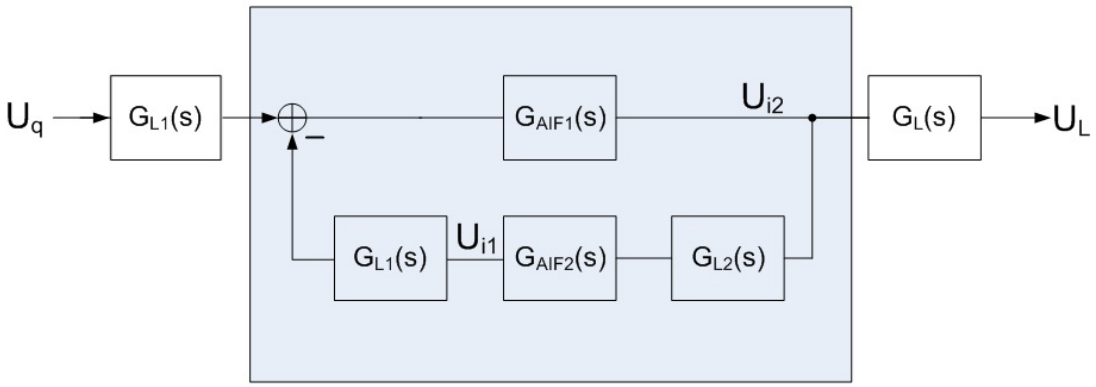

Figure 5.8: Air Interface Transfer Function

5.7 Card Feedback

In previous sections, a focus is given on energy transfer from reader to card. The change in characteristics based on mutual interaction between reader antenna and card coil is depicted. The objective of section 5.7 is to discuss the loading behavior of a Proximity Integrated Circuit Card (PICC) and its impact on reader circuits. The load modulation of a Proximity Integrated Circuit Card (PICC) and its electrical appearance at the reader receiver is explained. Figure 5.9 is a transfer function block diagram, which depicts the influence of mutual coupling. The output voltage U_{L1} is used as this is one option to sense the load changes of a card.

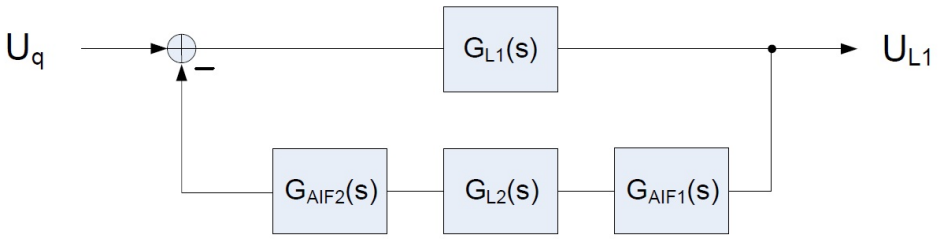

Figure 5.9: Feedback Transfer Function

If the feedback loop is omitted, the transfer function just gives the reader transfer function as used in equation (5.2). This is the system state, where no card is inserted into the reader field and therefore no feedback is possible.

By inserting a card into the system this characteristic changes to equation (5.18), where the feedback loop starts to influence the reader transfer function. The feedback depends on the

coupling coefficient k and the electrical properties of the Proximity Integrated Circuit Card (PICC).

$$G_{L1_{coupled}}(s) = \frac{G_{L_1}(s)}{1 + k(x,y,z)^2 \cdot G_{L1}(s) \cdot G_{L2}(s)} \tag{5.18}$$

5.7.1 Calculation of transformed Card Impedance

Analysis of the individual parameters of a Proximity Integrated Circuit Card (PICC) on the reader can be done more efficient using electrical components instead of Laplace representations. This is already used in previous sections to derive the proper transfer functions. Equations (5.1) and (5.5) are used in the next steps.

$$\frac{U_{L1}}{U_q} = \frac{j\omega \cdot L_1}{j\omega \cdot L_1 + R_1 + \frac{1}{j\omega \cdot C_1}}$$

$$\frac{U_{L2}}{U_i} = -\frac{j\omega \cdot L_2}{j\omega \cdot L_2 + R_2 + \frac{1}{j\omega \cdot C_2 + \frac{1}{R_L}}}$$

Replacing the nominators by impedance Z_1 and Z_2 these equations are giving

$$\frac{U_{L1}}{U_q} = \frac{j\omega \cdot L_1}{Z_1} \tag{5.19}$$

$$\frac{U_{L2}}{U_i} = -\frac{j\omega \cdot L_2}{Z_2} \tag{5.20}$$

The transfer functions $G_{L1}(s)$ and $G_{L2}(s)$ are replaced by its voltage divider representation. Equation (5.21) can be derived from equation (5.18).

$$\frac{U_{L1}}{U_q} = \frac{j\omega \cdot L_1}{Z_1} \cdot \frac{1}{1 + k(x,y,z)^2 \cdot \frac{\omega \cdot L_1}{Z_1} \cdot \frac{\omega \cdot L_2}{Z_2}} \tag{5.21}$$

Expanding equation (5.21) gives

$$\frac{U_{L1}}{U_q} = \frac{j\omega \cdot L_1}{Z_1 + \frac{k(x,y,z)^2 \omega^2 \cdot L_1 L_2}{Z_2}} \tag{5.22}$$

Based on equation (5.22) an equivalent circuit can be derived for reader and inserted card. The left hand part of figure 5.10 is representing the reader circuit without an inserted card - already

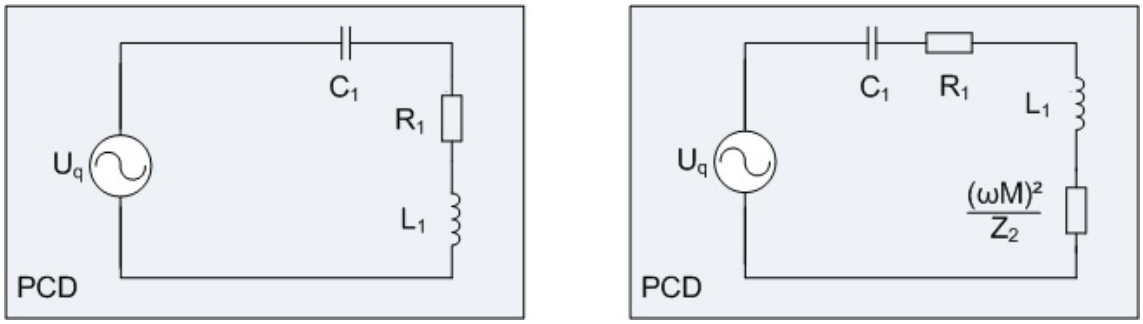

Figure 5.10: Equivalent circuit with and without transferred card impedance

depicted in section 5.2. In this case coupling coefficient k(x,y,z) - i.e. mutual inductance M(x,y,z) - is set to zero. An inserted card is changing the circuit by its transformed impedance [14, 20]. Equation (5.23) denotes the property of the transformed impedance.

$$Z_{TF_{21}} = k(x,y,z)^2 \cdot \frac{\omega^2 \cdot L_1 L_2}{Z_2} = \frac{\omega^2 \cdot M^2(x,y,z)}{Z_2} \tag{5.23}$$

How does the card impedance influence the reader circuit?

The load of the card is regulated and modulated by the card IC, which is an active load. A detailed analysis of active load regulation will be given in section 5.9. The reader resonant circuit is modified by the card impedance and mutual coupling. Assuming Z_2 to be tuned to resonance at 13.56MHz, equation (5.23) gives

$$Z_{TF_{21tuned}} = k(x,y,z)^2 \cdot \frac{\omega^2 \cdot L_1 L_2}{R_{total}} \tag{5.24}$$

where

ω	is the angular frequency
$k(x,y,z)^2 \cdot L_1 L_2$	is the mutual inductance squared
R_{total}	is the total series resistance of coil L_2 and card IC resistor

In the special case of a tuned impedance at the secondary side - i.e. Proximity Integrated Circuit Card (PICC) - the transformed impedance is ohmic only. The resistance is therefore only modifying the quality factor of the reader resonant circuit but does not change the resonance frequency of the primary side. The impact on current I_1, which generates the H-field is strongly dependent on R_{total}. In the case of a low ohmic impedance the current in antenna L_1 is reduced. On the other hand the current increases, if there is a high ohmic loading. Latter case represents the modulated case. When modulating, a card IC is typically clamping its input voltage to a lower level than in normal mode. This leads to a higher series resistance.

5.7.2 Influence of Card Impedance on Reader Resonant Circuit

The card impedance and it's transformed value is analyzed. The card IC active load is the main focus as these values can be influenced by a semiconductor circuit. The card impedance Z_2 takes a major role as depicted in equation (5.23).

$$Z_2 = j\omega \cdot L_2 + R_2 + \frac{1}{j\omega \cdot C_2 + \frac{1}{R_L}} \tag{5.25}$$

Rearranging (5.25) to $Z_2 = \Re\{Z_2\} + j\Im\{Z_2\}$ gives

$$Z_2 = R_2 + \frac{R_L}{1 + (\omega \cdot C_2 R_L)^2} + j\left(\omega \cdot L_2 - \frac{1}{\omega \cdot C_2} \cdot \frac{(\omega \cdot C_2 R_L)^2}{1 + (\omega \cdot C_2 R_L)^2}\right) \tag{5.26}$$

Using the definition of the quality factor $Q_p = \frac{Y_0}{G}$ [10], (5.26) can be written as

$$Z_2 = R_2 + \frac{R_L}{1 + Q_p^2} + j\left(\omega \cdot L_2 - \frac{1}{\omega \cdot C_2} \cdot \frac{Q_p^2}{1 + Q_p^2}\right) \tag{5.27}$$

where

R_2	is the card coil resistance
R_L	is the card IC load
L_2	is the card coil inductance
C_2	is the card resonance capacitance
Q_p	is the quality factor of the parallel circuit $R_L \| C_2$
R_s	is $R_L \cdot \frac{1}{1 + Q_p^2}$
C_s	is $C_2 \cdot \left(1 + \frac{1}{Q_p^2}\right)$

If $Q_p >> 1$ the parallel to series transformed components are

$$R_s \approx \frac{R_L}{Q_p^2}$$
$$C_s \approx C_2$$

This operating condition is typical when a card is in weak field. In this case the card IC can consume only little current which results in a high impedance R_L. It can be seen that $\Im\{Z_2\}$ is kept almost unchanged and the resistance $R_{total}=R_2+R_s$ is rather low ohmic.

Nevertheless, the card IC input voltage is almost short cut during modulation. This results in a low ohmic resistance R_L. In this case Q_p becomes less or equal one, which gives the following series equivalents.

$$R_s \geq \frac{R_L}{2}$$
$$C_s \geq 2 \cdot C_2$$

Modulation state is changing relevant the resonance frequency. Doubling C_s results into a shift of resonance frequency down by 30%.
Figure 5.11 denotes a R(R_L), X(R_L) plot of impedance Z_2. The influence of resonance tuning is depicted in different curves - from tuned to detuned. All plots are circles with different centers and individual diameters.

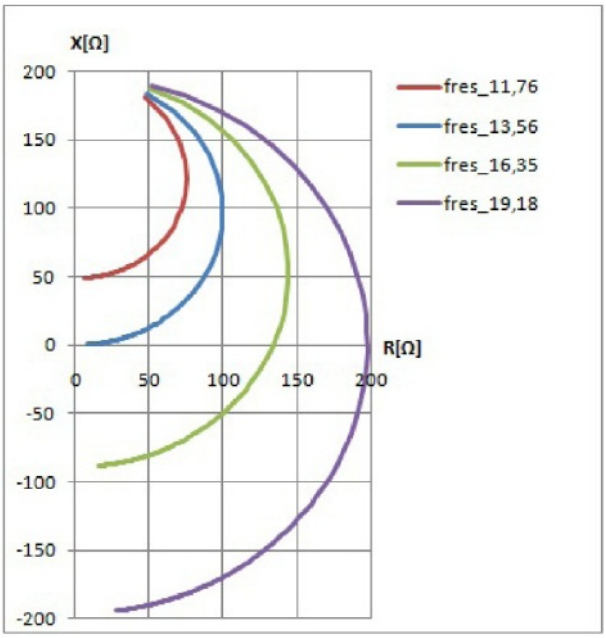

Figure 5.11: R, X plot of Z_2 over R_L

A special tuning case is $\approx$ 19.20MHz, which is 13.56MHz $\cdot\sqrt{2}$. It can be seen in the graph, that the (R, X) plot gives a circle with center at (0,0). Calculating the magnitude of the resulting impedance gives a constant value over R_L.

$$|Z_2(f_{res} = 19.20)| = \sqrt{(R(R_L))^2 + (X(R_L))^2} = const \tag{5.28}$$

This results in a constant transfer characteristic for G_{L2}(s) which is representing the load modulation signal of a card. Modulating between two different resistors R_L is not changing the magnitude

of the signal. The information is not amplitude but phase modulated. In most, cases the data is phase and amplitude modulated. The test standard ISO/IEC 10373-6 considers this property for Load Modulation Amplitude (LMA) Testing. Although the test is called Load Modulation Amplitude it considers phase modulation as well. A Fast Fourier Transformation (FFT) is used to calculate modulation sidebands, which implicitly includes amplitude and phase information.
The characteristic depicted in figure 5.11 changes, if the mutual interaction is considered. ISO/IEC 10373 specifies Load Modulation Amplitude (LMA) measurements by sensing H-field H_2 as denoted in (5.5), by sensing H_2 with a standardized sense coil. The result is proportional to [13]

$$U_{LMA} = k_{sense} \cdot \sqrt{\frac{L_{sense}}{L_2}} \cdot U_{L2}$$

The ISO concept is omitting the mutual interaction, whereas a reader has to cope with coupling of both antennas - L_1 and L_2 and therefore a reader has to handle changes of the transferred card impedance. The transferred impedance is denoted in (5.23)

$$Z_{TF_{21}} = \frac{\omega^2 \cdot M(x,y,z)}{Z_2}$$

The transformation from Z_2(R, X) plot to $Z_{TF_{21}}$(R, X) is shown in figure 5.12.

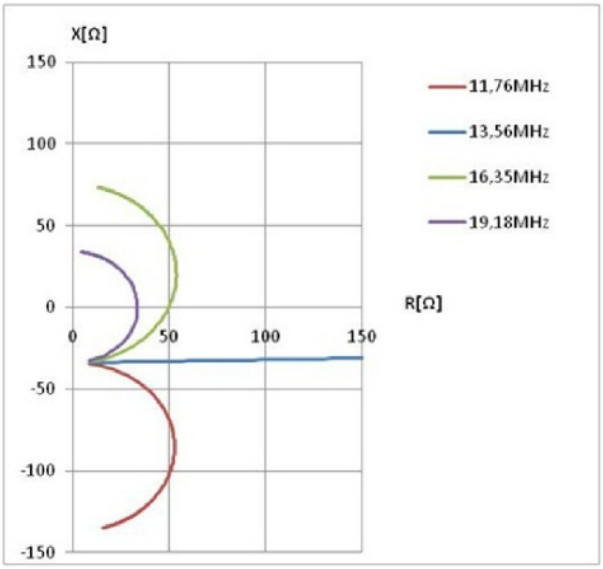

Figure 5.12: R, X plot of transferred card impedance over R_L

Looking at special resonance frequency 19.20MHz it can be seen, that the characteristic over R_L is a circle with center at (0,0). This condition gives the same magnitude for $Z_{TF_{21}}$ independent of load resistor R_L. Another special case can be seen at 13.56MHz, where the plot gives a line parallel to the R-axis. Case 19.20MHz is only changing phase over R_L whereas the tuned case is changing amplitude.

5.8 Reader Receiver Architectures

A reader has to cope with phase and amplitude signals as well. It even becomes more sophisticated as both resonant circuits - reader and card - are involved including mutual coupling. Old reader architectures used envelope detectors. The choice was made because of its simple and cheap implementation. The main drawback of peak detectors is their sensitivity to amplitude changes only. Applications with small number of reader and cards can handle the tuning impact by special manufacturing strategies. An alternative is to spent effort in filter and matching circuits, which leads to higher component cost and a more complex foot print.

5.8.1 IQ Demodulator

A more comprehensive approach is the use of an IQ receiver which is able to detect both phase and amplitude information. A novel architecture based on an Analog to Digital Converter (ADC) IQ receiver is presented in patent application [17]. An Advantageous almost all digital approach is used. The objective is, to convert analog signals as soon as possible into the digital domain. Filtering and data processing is done by digital logic. Conventional IQ demodulators are typically using a mixer circuit to get rid of the carrier signal. An analog multiplier is often used to multiply the incoming antenna signal with a local oscillator. In a contactless system the local oscillator is the frequency reference which is necessary to generate the 13.56MHz system frequency. Figure 5.13 is a block diagram of a conventional - state of the art - IQ demodulator.

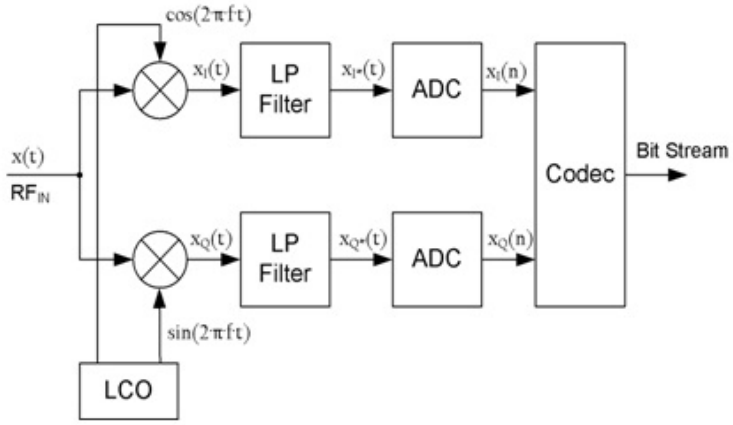

Figure 5.13: Conventional IQ Demodulator [17]

The incoming signal x(t) is multiplied by $\cos(\omega_1 \cdot t)$ for the I-channel $x_i(t)$ and by $\sin(\omega_1 \cdot t)$ for the Q-channel $x_q(t)$ [5]. The analog IQ-channel signals are low pass filtered and then analog to digital converted. The necessity of a low pass filter is linked to the nature of analog mixing denoted in

equation (5.29).

$$x_i(t) = \frac{1}{2} \cdot \cos((\omega_1 + \omega_2)) \cdot t) + \frac{1}{2} \cdot \cos((\omega_1 - \omega_2) \cdot t) \tag{5.29}$$

where

ω_1	is the angular frequency of the local oscillator
ω_2	is the angular frequency of the antenna input signal

Signal components at $\omega_1 + \omega_2$ are generated caused by the mixing process, which is a convolution in frequency domain. These tones are disturbing the signal detection and therefore have to be attenuated by a low pass filter. The order of the filter has to be defined according to the needs of Signal to Noise Ratio (SNR) and depends strongly on the highest available baseband signal frequency. The Standard bit rate of a contactless proximity system based on ISO/IEC 14443 is 106kbps. A subcarrier at 848kHz is used for Proximity Integrated Circuit Card (PICC) to Proximity Coupling Device (PCD) data transfer. The high frequency mixing component is at $\approx$ 27MHz - the doubled system frequency. State of the art technologies are already using the optional eight times higher High Bit Rate (HBR) amendments of ISO/IEC 14443, which do not change the subcarrier frequency as the highest bit rate is 848kbps. A 1st order low pass with cut off frequency of 1MHz is already attenuating $\approx$ 30dB of higher order mixing components. The next technology step is a further increase of bit rate by at least a factor of eight. This leads to a signal frequency of $\approx$ 7MHz. A much more complex filter is necessary to handle the higher order harmonics.

A new IQ receiver concept is depicted in *US Patent application, 12755094* [17]. Instead of using an analog mixer with disadvantages mentioned before, a direct sampling method is introduced. The nature of analog to digital conversion is, that frequency tones are available at all multiples of the sampling frequency.

$$f_s(t) = \sum_{k=-\infty}^{+\infty} \delta(t - k \cdot T_s)$$

$$F_s(f) = \frac{1}{T_s} \sum_{k=-\infty}^{+\infty} \delta(f - \frac{k}{T_s})$$

where

$f_s(t)$	is the time domain ADC sampling function
$F_s(f)$	is the frequency domain correspondence
T_s	is the sampling period
δ	is the Dirac impulse function
k	is $\in Z$

A subset of k (-1, 1) is representing the corresponding frequencies of an analog mixer as depicted before. All other frequency bins are generating mirrors at frequency positions higher than $f_s/2$. According to *Nyquist-Shannon Theorem* the sampling frequency has to be at least two times higher than the highest signal frequency. All higher frequencies are mirrored into other frequency bands, which is known as aliasing. Figure 5.14 depicts the frequency domain representation of an Analog to Digital Converter (ADC) sampled antenna input signal.

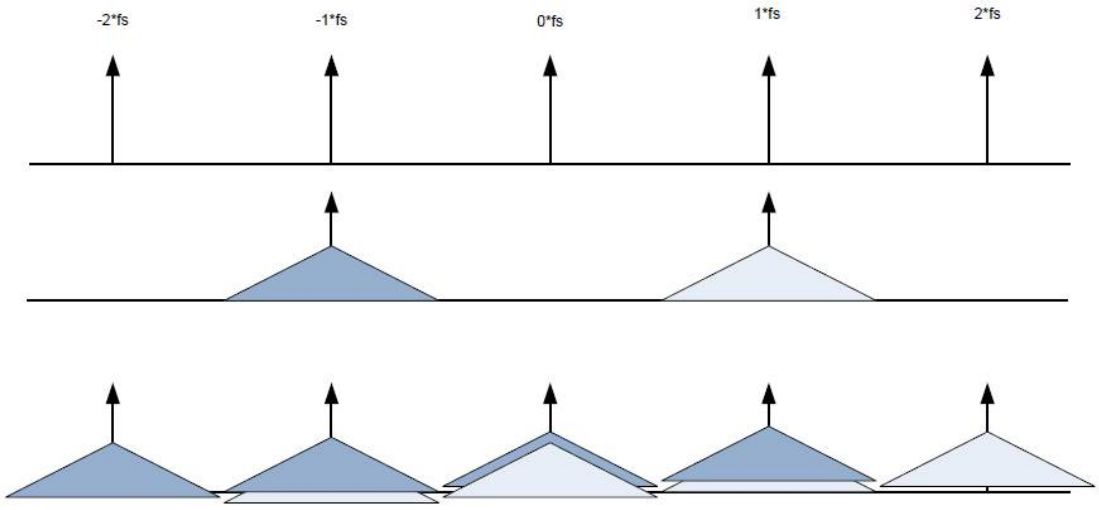

Figure 5.14: ADC sampling spectrum

The respective spectrum of a state of the art analog mixer is shown in figure 5.15. A comparison of the two figures shows that the baseband information is same for both approaches. The mixing components are apparent at every sampling frequency of the Analog to Digital Converter (ADC), whereas an analog mixer generates these signals at the doubled LCO frequency.

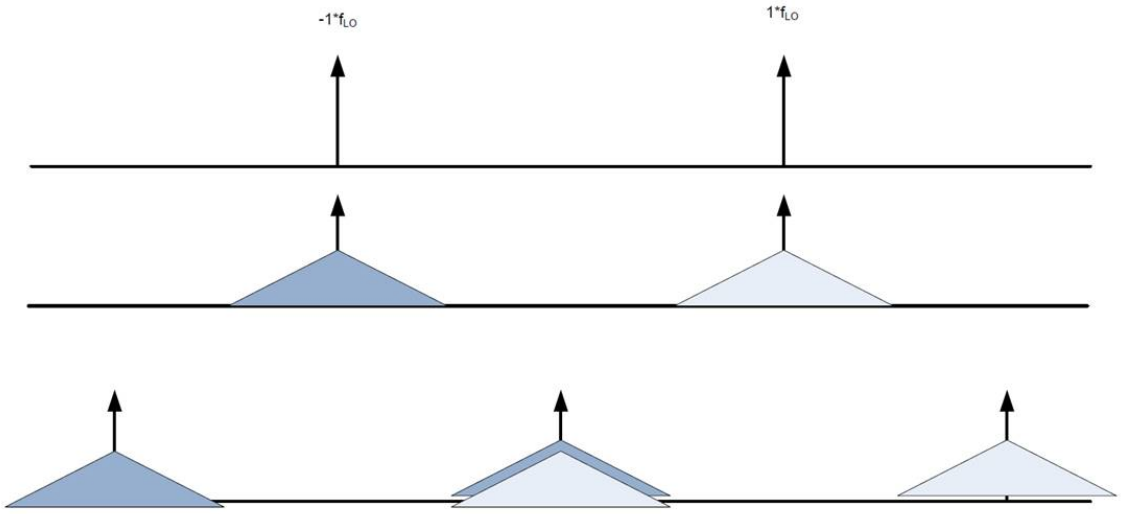

Figure 5.15: Conventional mixer spectrum without low pass filter

No signals higher than $f_s/2$ are possible at the output of an Analog to Digital Converter (ADC) by construction, which represents an ideal low pass filter.

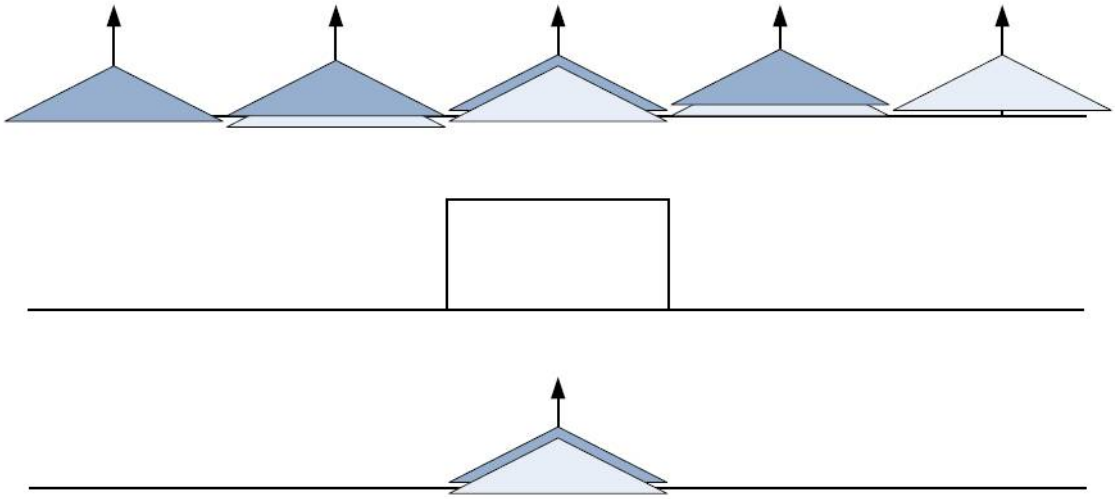

Figure 5.16: ADC sampled spectrum including inherent low pass filter

The *Nyquist-Shannon Theorem* has to be fulfilled for the Analog to Digital Converter (ADC) sampling. The signal frequency may not exceed $f_s/2$ otherwise aliasing frequencies are mixed into the base band. To prevent aliasing a filter can be used at the Analog to Digital Converter (ADC) input stage. As the air interface is inherently a band filter no extra external components are necessary. Figure 5.17 is depicting the sample spectrum in case of aliasing.

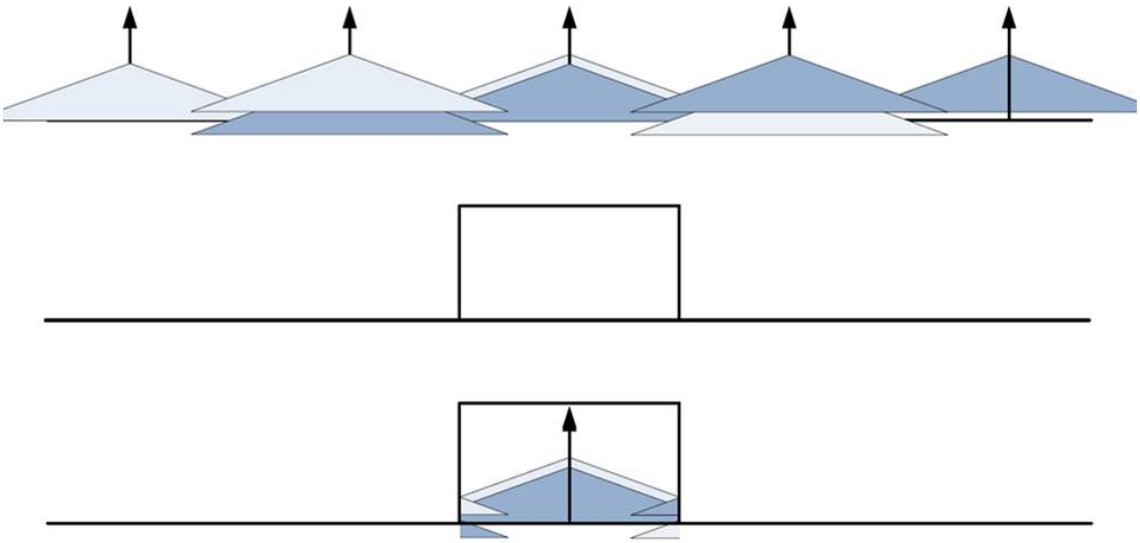

Figure 5.17: ADC aliasing at too high input signals

The use of an Analog to Digital Converter (ADC) as a mixer structure is depicted in figures 5.14 and 5.16. An Analog to Digital Converter (ADC) mixing IQ demodulator is presented in *US Patent application, 12755094* [15]. The generation of an I and Q channel needs a mixing with a cosine and sine reference signal. This can be obtained by two Analog to Digital Converters (ADC) which are sampling the input signal by a 90° phase difference, which represents the phase shift between cosine and sine. The sampling frequnency of both converters is 13.56MHz, which represents the mixing. Alternatively one Analog to Digital Converter (ADC) with a four times higher sample rate can be used, where the first sample represents the I channel the second the Q Channel and the third and fourth is omitted.

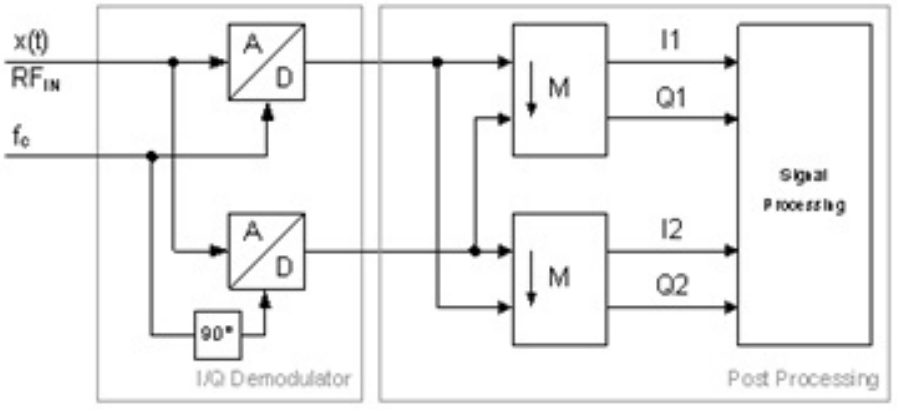

Figure 5.18: IQ ADC sampler, disclosed in [15]

Analog to Digital Converter (ADC) option one and a special post processing structure is shown in figure 5.18. Post processing will not be further analyzed in this thesis. A comprehensive research summary on this topic is given in the thesis of Edmund Ehrlich [6].

5.8.2 Results

A comprehensive reader receiver for contactless technology is presented. The structure is able to handle signal frequencies up to 6.78MHz which is corresponding to a bit rate of 13.56Mbps. This high bit rate can be obtained by a special coding scheme disclosed in *Invention Disclosure, 2009. Reference No.: 2009E51126 AT* [16]. The Analog to Digital Converter (ADC) based structure is well suited for semiconductor integration. In new short channel technologies - e.g. a 90nm or 65nm process - high resolution 54Msample converters are available at reasonable cost and quality.

5.9 Card Impedance Regulation and Load Modulation

In previous sections card impedance R_L, C_2 is used to calculate transfer characteristics and transformed impedances. The components are treated to be passive. Figure 5.11 depicts the property of card impedance at different resonance frequencies over R_L. The influence on card

impedance for different values of R_L is clear. A card IC typically changes its load R_L and keeps the resonance capacitor C_2 almost constant. The load regulation of a card IC is necessary to handle the dynamic in a contactless environment. The ISO/IEC 14443 standard specifies an operating H-field range from 1.5A/m up to 7.5A/m. Absolute maximum ratings are even defined at 12.0A/m. As discussed in section 5.5 this field strength leads to induced voltages up to 12V. Assuming a card transfer function as depicted in 5.4 this gives an IC input voltage of 50V[14]. This rough hand calculation makes it clear that a card IC has to regulate its input to prevent destruction by overvoltage. The most common regulation strategy of regulation is to limit the input voltage to a predefined level. This property of a card IC makes a passive load element R_L to an active regulated one. This section discusses a method how to handle the dynamic behavior of R_L in a transfer function. Equation (5.3) is used to derive R_L for a dedicated card IC input voltage U_L and induced voltage U_i. The corresponding H-field is proportional to U_i as denoted in equation (4.9). An alternative approach is described in [9] which does not elaborate an equation to calculate the load resistor for a given induced voltage and a maximum card-IC voltage. The calculation of load resistor is necessary for a typical card IC, as the modulated and unmodulated states are defined by card input voltage regulation at two different values. Unmodulated input voltage is typical $5V_p$ whereas modulated voltage level is regulated down to $1.5V_p$. The modulated state can increase over H-field depending on regulation circuit implementation, whereas the unmodulated state typically stays almost constant. This behavior is not modeled in this section.

Equation (5.3) is used to derive a Proximity Integrated Circuit Card (PICC) load resistor.

$$\frac{U_L}{U_i} = \frac{\frac{1}{j\omega \cdot C_2 + \frac{1}{R_L}}}{j\omega \cdot L_2 + R_2 + \frac{1}{j\omega \cdot C_2 + \frac{1}{R_L}}}$$

As mentioned before the regulation is done by keeping the IC input voltage constant. Equation (5.30) is depicting the magnitude of U_L.

$$\left|\frac{U_L}{U_i}\right| = \frac{\left|\frac{1}{j\omega \cdot C_2 + \frac{1}{R_L}}\right|}{\left|j\omega \cdot L_2 + R_2 + \frac{1}{j\omega \cdot C_2 + \frac{1}{R_L}}\right|} \tag{5.30}$$

Using definitions [10, 20]

$$\lambda^2 = \omega^2 \cdot L_2C_2 = \frac{\omega^2}{\omega_{res}^2} \qquad Q_{L_2} = \frac{\omega \cdot L_2}{R_2}$$
$$\omega \cdot C_2 = \frac{\lambda^2}{\omega \cdot L_2} \qquad \omega \cdot L_2 = \frac{\lambda^2}{\omega \cdot C_2}$$

equation (5.30) gives

$$\left|\frac{U_i}{U_L}\right|^2 = \left[(1-\lambda^2) + \frac{R_2}{R_L}\right]^2 + \left[\frac{\omega \cdot L_2}{R_L} + \lambda^2 \frac{R_2}{\omega \cdot L_2}\right]^2$$
$$R_L^2 \cdot \left|\frac{U_i}{U_L}\right|^2 = \left[R_L \cdot (1-\lambda^2) + R_2\right]^2 + \left[R_2 \cdot Q_{L_2} + R_L \cdot \lambda^2 \frac{1}{Q_{L_2}}\right]^2$$

Rearranging to RL=0 results in

$$\left[\left|\frac{U_i}{U_L}\right|^2 - (1-\lambda^2)^2 - \lambda^4 \frac{1}{Q_{L_2}^2}\right] \cdot R_L^2 - 2 \cdot R_2 \cdot R_L - R_2^2 \cdot (1+Q_{L_2}^2) = 0$$

Solving the quadratic equation gives

$$R_{L_{1,2}} = R_2 \cdot \frac{1 \pm \sqrt{1 + \left[\left|\frac{U_i}{U_L}\right|^2 - (1-\lambda^2)^2 - \lambda^4 \frac{1}{Q_{L_2}^2}\right] \cdot (1+Q_{L_2}^2)}}{\left|\frac{U_i}{U_L}\right|^2 - (1-\lambda^2)^2 - \lambda^4 \frac{1}{Q_{L_2}^2}} \tag{5.31}$$

with $Q_{L_2} >> 1$ equation (5.31)results in

$$R_{L_{1,2}} = \frac{R_2 \pm \omega \cdot L_2 \sqrt{\left|\frac{U_i}{U_L}\right|^2 - (1-\lambda^2)^2}}{\left|\frac{U_i}{U_L}\right|^2 - (1-\lambda^2)^2} \tag{5.32}$$

Figures 5.19, 5.20 are depicting card impedances Z_2 and transferred card impedances $Z_{TF_{21}}$.

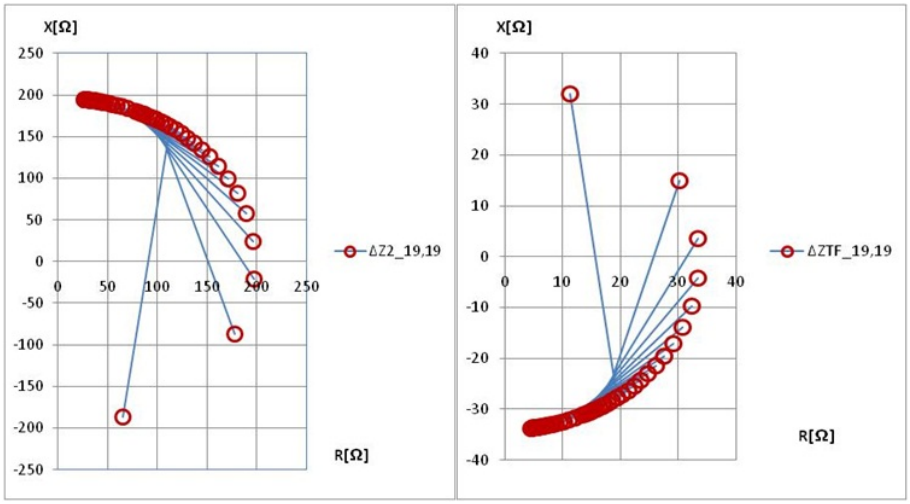

Figure 5.19: R, X plot of load modulation at $f_{res} = 19.2MHz$

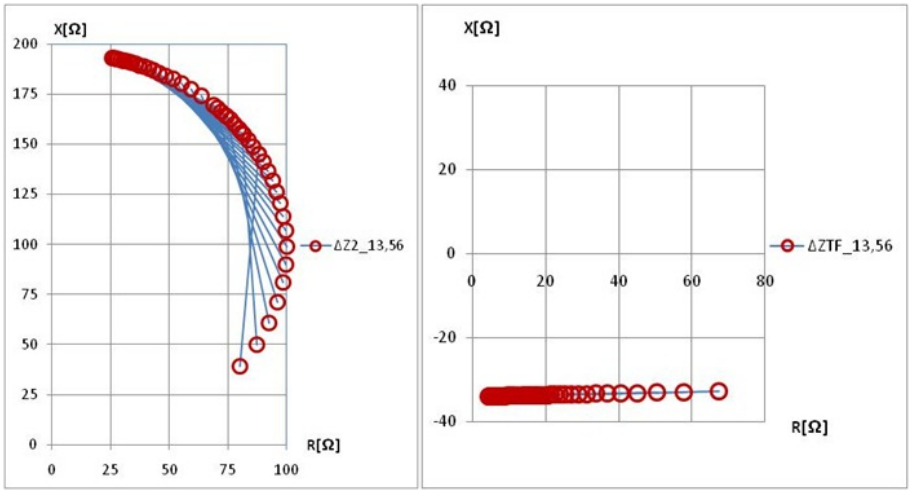

Figure 5.20: R, X plot of load modulation at $f_{res} = 13.56MHz$

In case of tuning at f_{res}=19.2MHz it can be seen, that the magnitude of the individual loading states (unmodulated, modulated) is constant. Whereas the Delta of modulated and unmodulated state is giving a signal which can be demodulated by an appropriate receiver concept as described is section 5.8. An envelope detector is clearly not sufficient and becomes even more critical when incorporating the system transfer function with both resonant circuits - reader and card - influencing each other.

6 Time Domain Analysis and Transient Settling

In chapter 5 frequency domain methods are used to characterize a communication system. Dynamic system behavior - like signal settling, over-/ undershoots and Inter Symbol Interference (ISI) - cannot be analyzed in frequency spectrum. Therefore frequency domain signals are transferred to time domain functions. A special focus is set to communication limitations based on contactless channel properties.

Laplace and Inverse Laplace transformation is chosen to derive both - settled and transient - signals. Amplitude and Phase Shift Keying (ASK, PSK) are step response time signals which can be derived from Laplace operation.

6.1 ISO/IEC 14443 Modulation principle

Amplitude Shift Keying (ASK) modulation is standardized. Two types - Type A and Type B - are specified in ISO/IEC 14443 part two. Figures 6.1, 6.2 are depicting wave shapes of these types at 106kbps.

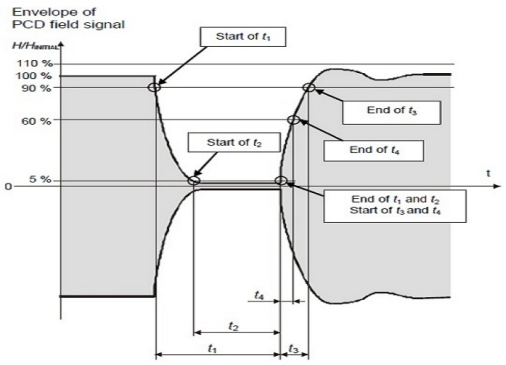

Figure 6.1: ISO/IEC 14443-A wave shape [12]

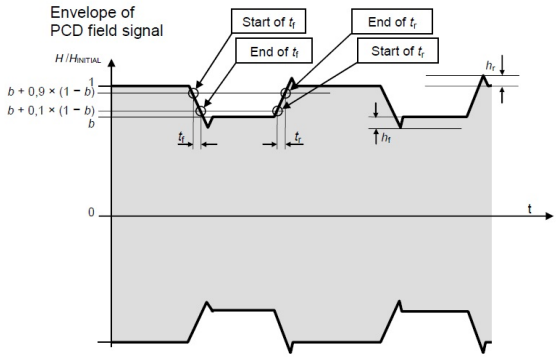

Figure 6.2: ISO/IEC 14443-B wave shape [12]

Wave shape characteristics for High Bit Rates (HBR) - up to 848kbps - are amended in the standard and are not described in detail in this thesis. The main difference to bit rate at 106kbps is a linear shrink of Elementary Timing Unit (ETU) and the corresponding shrink of modulated and unmodulated states. The unmodulated state is defined to be same in communication and non communication phases.

6.2 Definitions

The most important Laplace correspondences used in this chapter are listed in table 6.1

g(t)	G(s)
$\sin(\omega t)$	$\frac{\omega}{s^2+\omega^2}$
$\cos(\omega t)$	$\frac{s}{s^2+\omega^2}$
$e^{-\delta t} \cdot \sin(\omega t)$	$\frac{\omega}{(s+\delta)^2+\omega^2}$
$e^{-\delta t} \cdot \cos(\omega t)$	$\frac{s+\delta}{(s+\delta)^2+\omega^2}$

Table 6.1: Laplace tranform table [3]

Using definitions [10]

$$\omega_1^2 = \frac{1}{L_1 C_1}$$ is the angular frequency of Reader resonant circuit

$$\omega_2^2 = \frac{1}{L_2 C_2}$$ is the angular frequency of Card resonant circuit

$$Q_1 = \frac{1}{\omega_1 \cdot C_1 R_1}$$ is the quality factor of Reader resonant circuit

$$Q_{L_2} = \frac{\omega_1 \cdot L_1}{R_1}$$ is the quality factor of Card coil

$$Q_{IC} = \frac{1}{\omega_2 \cdot C_2 \cdot R_L}$$ is the quality factor of Card integrated circuit (IC)

$$Q_2 = \frac{1}{\frac{1}{Q_{L_2}} + \frac{1}{Q_{IC}}}$$ is the quality factor of Card resonant circuit

equations (5.2), (5.4) are giving

$$U_{L1}(s) = U_q(s) \cdot \frac{s^2}{s^2 + s \cdot \frac{\omega_1}{Q_1} + \omega_1^2}$$ Reader transfer function

$$U_L(s) = U_i(s) \cdot \frac{\omega_2^2}{s^2 + s \cdot \frac{\omega_2}{Q_2} + \omega_2^2 \cdot (\frac{R_2}{R_L} + 1)}$$ Card transfer function

6.3 Signal Generation

Contactless technology power and communication signal $U(t)$ in polar representation is depicted in equation (6.1)

$$U(t) = A_m \cdot \cos(\omega \cdot t + \varphi_m) \tag{6.1}$$

where

A_m	is the signal for ASK modulation
φ_m	is the signal for PSK modulation

Equation (6.1) can be noted in complex form as

$$U(t) = A_m \cdot \Re\left\{e^{j(\omega t + \varphi_m)}\right\} \tag{6.2}$$

$$\begin{aligned}
U(t) &= A_m \cdot \Re\left\{e^{j\omega t} \cdot e^{j\varphi_m}\right\} \\
U(t) &= A_m \cdot \Re\left\{[\cos(\omega t) + j\sin(\omega t)] \cdot [\cos(\varphi_m) + j\sin(\varphi_m)]\right\} \\
U(t) &= A_m \cdot \cos(\varphi_m) \cdot \cos(\omega t) - A_m \cdot \sin(\varphi_m) \cdot \sin(\omega t)
\end{aligned}$$

Introducing $I,\ Q$ gives the I/Q equation for $\cos(\omega t + \varphi)$

$$\begin{aligned}
I &= A_m \cdot \cos(\varphi_m) \\
Q &= A_m \cdot \sin(\varphi_m)
\end{aligned}$$

$$U(t) = I \cdot \cos(\omega t) - Q \cdot \sin(\omega t) \tag{6.3}$$

The Laplace correspondence is given as

$$\mathscr{L}\{U(t)\} = I \cdot \frac{s}{s^2 + \omega^2} - Q \cdot \frac{\omega}{s^2 + \omega^2} \tag{6.4}$$

6.4 Reader Signal Characteristics

Based on equations depicted in section 5.2, a time domain signal is derived by Laplace transformation. The transfer function $G_{L_1}(s)$ (5.2) is rearranged by inserting definitions ω_1, Q_1 and stimulated by generator signal $U_q(s)$ as denoted in equation (6.4). This results in

$$U_{L_1}(s) = \left(I \cdot \frac{s}{s^2 + \omega^2} - Q \cdot \frac{\omega}{s^2 + \omega^2} \right) \cdot \frac{s^2}{s^2 + s \cdot \frac{\omega_1}{Q_1} + \omega_1^2} \tag{6.5}$$

Splitting equation (6.5) into its $I\ [\cos(\omega \cdot t)]$ and $Q\ [\sin(\omega \cdot t)]$ channel components gives

$$I\_U_{L_1}(s) = I \cdot \frac{s}{s^2 + \omega^2} \cdot \frac{s^2}{s^2 + s \cdot \frac{\omega_1}{Q_1} + \omega_1^2}$$
$$Q\_U_{L_1}(s) = -Q \cdot \frac{\omega}{s^2 + \omega^2} \cdot \frac{s^2}{s^2 + s \cdot \frac{\omega_1}{Q_1} + \omega_1^2}$$

Expansion into partial fraction is used to split the nominator into fractions, which can be transformed from s-plane into time domain by using Laplace correspondence table 6.1.

6.4.1 Reader I-Channel Time Domain Signals

Expanding I-channel signal $I\_U_{L_1}(s)$ into partial fractions results in

$$\frac{A + sB}{s^2 + \omega^2} + \frac{C + sD}{s^2 + s \cdot \frac{\omega_1}{Q_1} + \omega_1^2} = \frac{s}{s^2 + \omega^2} \cdot \frac{s^2}{s^2 + s \cdot \frac{\omega_1}{Q_1} + \omega_1^2}$$

$$(A + sB) \cdot \left(s^2 + s \cdot \frac{\omega_1}{Q_1} + \omega_1^2 \right) + (C + sD) \cdot (s^2 + \omega^2) = s \cdot s^2 \tag{6.6}$$

The steady state part can be derived by

$$s = j\omega \qquad A = -\omega \cdot \Im\{G_{L_1}(j\omega)\}$$
$$B = \Re\{G_{L_1}(j\omega)\}$$

where

ω	is the angular frequency of generator $\cos(\omega \cdot t)$
$\Re\{G_{L_1}(j\omega)\}$	is the real part of reader transfer function at angular frequency ω
$\Im\{(G_{L_1}(j\omega)\}$	is the imaginary part of reader transfer function at angular frequency ω

Applying inverse Laplace operation results in

$$I_{AB\_}U_{L_1}(t) = I \cdot \mathscr{L}^{-1}\left\{-\Im\{G_{L_1}(j\omega)\} \cdot \frac{\omega}{s^2+\omega^2} + \Re\{G_{L_1}(j\omega)\} \cdot \frac{s}{s^2+\omega^2}\right\} \tag{6.7}$$

$$I_{AB\_}U_{L_1}(t) = I \cdot \Re\{G_{L_1}(j\omega)\} \cdot \cos(\omega \cdot t) - I \cdot \Im\{G_{L_1}(j\omega)\} \cdot \sin(\omega \cdot t) \tag{6.8}$$

Rearranging equation (6.8) gives

$$I_{AB\_}U_{L_1}(t) = I \cdot |G_{L_1}(j\omega)| \cdot \cos(\omega \cdot t + \arg(G_{L_1}(j\omega))) \tag{6.9}$$

which is derived from complex representation

$$\Re\{A \cdot e^{j(\omega t+\varphi)}\} = A \cdot \cos(\omega \cdot t + \varphi) = A \cdot \cos(\varphi) \cdot \cos(\omega \cdot t) - A \cdot \sin(\varphi) \cdot \sin(\omega \cdot t)$$

Equation (6.9) is representing the output signal of transfer function $G_{L_1}(s)$ which is stimulated by a cosine wave signal at angular frequency ω. Magnitude and phase are shaped by the transfer characteristic as expected for the steady state signal, which is depicted in figure 6.3.

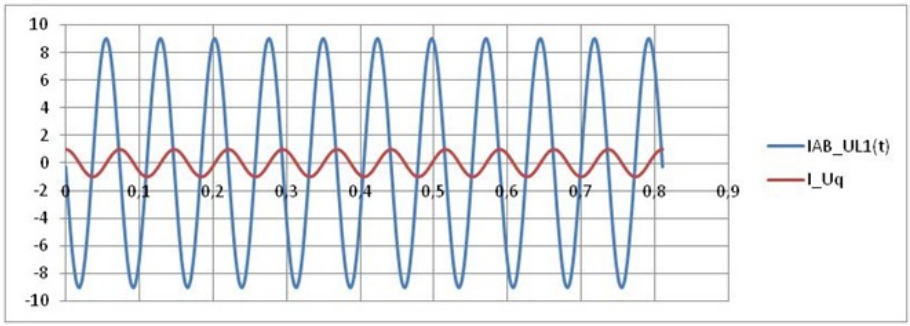

Figure 6.3: Steady state signal of Reader I-channel

The transient signal can be calculated by inserting a pole of transfer function $G_{L_1}(s)$ into equation (6.6).

$$(A + sB) \cdot \left(s^2 + s \cdot \frac{\omega_1}{Q_1} + \omega_1^2 \right) + (C + sD) \cdot (s^2 + \omega^2) = s \cdot s^2$$

$$\delta_1 = \frac{\omega_1}{2 \cdot Q_1} \qquad \Omega_1 = \omega_1 \cdot \sqrt{1 - \frac{1}{(2 \cdot Q_1)^2}}$$

$$s = s_1 = -\delta_1 + j\Omega_1 \qquad C = s_1^2 \cdot \Re\{G_{cos}(s_1)\} + \delta_1 \cdot B$$

$$D = s_1^2 \cdot \frac{\Im\{G_{cos}(s_1)\}}{\Omega_1}$$

where

δ_1	is the attenuation factor of reader resonant circuit
Ω_1	is the resonance frequency of reader resonant circuit
$\Re\{G_{cos}(s_1)\}$	is the real part of Laplace correspondence of $\cos(\omega \cdot t)$ at $s1$
$\Im\{G_{cos}(s_1)\}$	is the imaginary part of Laplace correspondence of $\cos(\omega \cdot t)$ at $s1$

$$I_{CD}\_U_{L_1}(t) = I \cdot \mathscr{L}^{-1} \left\{ \frac{C - \delta_1 \cdot D}{\Omega_1} \cdot \frac{\Omega_1}{(s + \delta_1)^2 + \Omega_1^2} + D \cdot \frac{s + \delta_1}{(s + \delta_1)^2 + \Omega_1^2} \right\} \tag{6.10}$$

$$I_{CD}\_U_{L_1}(t) = I \cdot e^{-\delta_1 \cdot t} \cdot \frac{|s_1^2 \cdot G_{cos}(s_1)|}{\Omega_1} \cdot \sin\left(\Omega_1 \cdot t + \arg\left(\frac{s_1^2 \cdot G_{cos}(s_1)}{\Omega_1} \right) \right) \tag{6.11}$$

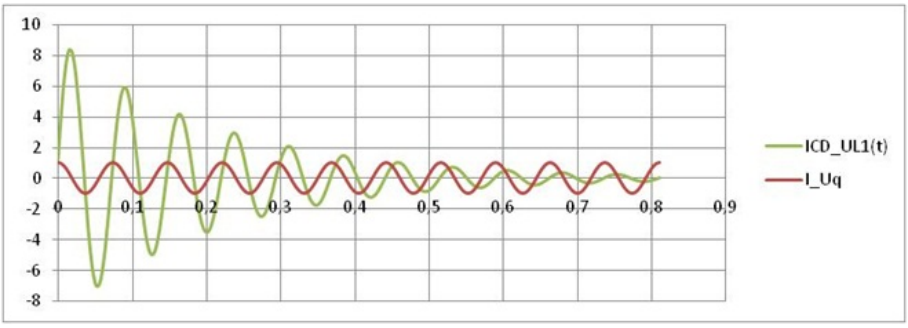

Figure 6.4: Transient signal of Reader I-channel

Step response of I-channel is derived by combining the steady state and transient signal.

$$\begin{aligned} I\_U_{L_1}(t) =& I \cdot |G_{L_1}(j\omega)| \cdot \cos(\omega \cdot t + \arg(G_{L_1}(j\omega))) + \\ & I \cdot e^{-\delta_1 \cdot t} \cdot \frac{|s_1^2 \cdot G_{cos}(s_1)|}{\Omega_1} \cdot \sin\left(\Omega_1 \cdot t + \arg\left(\frac{s_1^2 \cdot G_{cos}(s_1)}{\Omega_1}\right)\right) \end{aligned} \tag{6.12}$$

Figure 6.5 depicts the combined waveform which shows the exponential settling behavior of a resonance circuit. The voltage settles at approximately 9V which is defined by the quality factor G_1, which is approximately 9 in this example. The I-channel amplitude of generator signal is 1V.

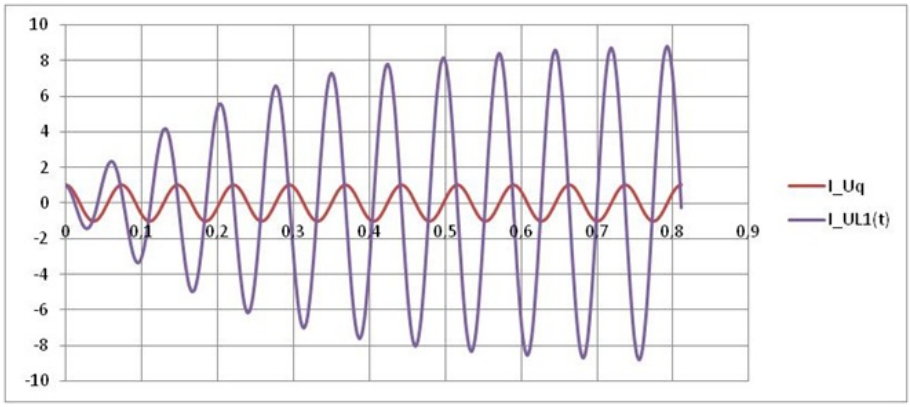

Figure 6.5: Step response signal of Reader I-channel

6.4.2 Reader Q-Channel Time Domain Signals

Q-channel Laplace transformation can be calculated accordingly by replacing $G_{cos}(s)$ by $G_{sin}(s)$ and I by -Q which gives

$$\frac{A + sB}{s^2 + \omega^2} + \frac{C + sD}{s^2 + s \cdot \frac{\omega_1}{Q_1} + \omega_1^2} = \frac{\omega}{s^2 + \omega^2} \cdot \frac{s^2}{s^2 + s \cdot \frac{\omega_1}{Q_1} + \omega_1^2}$$

$$(A + sB) \cdot \left(s^2 + s \cdot \frac{\omega_1}{Q_1} + \omega_1^2\right) + (C + sD) \cdot (s^2 + \omega^2) = \omega \cdot s^2 \tag{6.13}$$

$$\begin{aligned} s = j\omega \qquad & A = \omega \cdot \Re\{G_{L_1}(j\omega)\} \\ & B = \Im\{G_{L_1}(j\omega)\} \end{aligned}$$

$$Q_{AB}\_U_{L_1}(t) = -Q \cdot \mathscr{L}^{-1}\left\{\Re\{G_{L_1}(j\omega)\} \cdot \frac{\omega}{s^2 + \omega^2} + \Im\{G_{L_1}(j\omega)\} \cdot \frac{s}{s^2 + \omega^2}\right\} \tag{6.14}$$

$$Q_{AB}\_U_{L_1}(t) = -Q \cdot \Re\{G_{L_1}(j\omega)\} \cdot \sin(\omega \cdot t) - Q \cdot \Im\{G_{L_1}(j\omega)\} \cdot \cos(\omega \cdot t) \tag{6.15}$$

$$Q_{AB}\_U_{L_1}(t) = -Q \cdot |G_{L_1}(j\omega)| \cdot \cos(\omega \cdot t + \arg(G_{L_1}(j\omega))) \tag{6.16}$$

which is derived from complex representation

$$\Im\{A \cdot e^{j(\omega t+\varphi)}\} = A \cdot \sin(\omega \cdot t + \varphi) = A \cdot \sin(\varphi) \cdot \cos(\omega \cdot t) + A \cdot \cos(\varphi) \cdot \sin(\omega \cdot t)$$

Reader Q-channel steady state is displayed in figure 6.6. The generator signal is sine wave and the corresponding antenna signal which is shaped by $G_{L_1}(j\omega)$. Compared to I-channel waveform the only difference is the stimulus, which changes from cosine to sine wave.

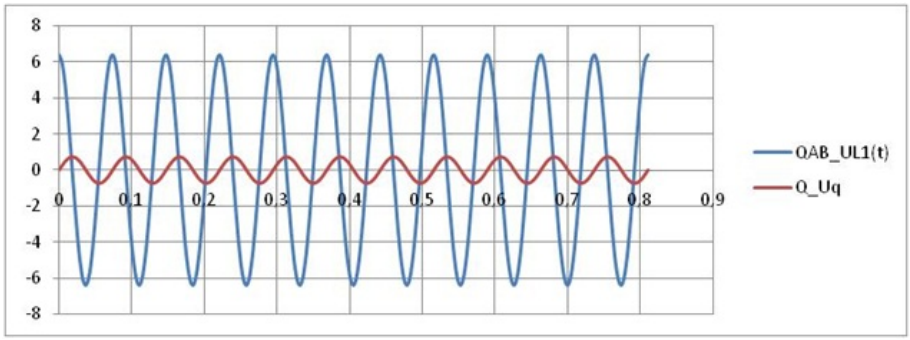

Figure 6.6: Steady state signal of Reader Q-channel

Transient signal of Q-channel is depicted consecutively. The pole of transfer function $G_{L_1}(s)$ is used to solve the transient part of equation (6.13).

$$\delta_1 = \frac{\omega_1}{2 \cdot Q_1} \qquad \Omega_1 = \omega_1 \cdot \sqrt{1 - \frac{1}{(2 \cdot Q_1)^2}}$$

$$s = s_1 = -\delta_1 + j\Omega_1 \qquad C = s_1^2 \cdot \Re\{G_{sin}(s_1)\} + \delta_1 \cdot D$$

$$D = s_1^2 \cdot \frac{\Im\{G_{sin}(s_1)\}}{\Omega_1}$$

$$Q_{CD}\_U_{L_1}(t) = -Q \cdot \mathscr{L}^{-1}\left\{\frac{C - \delta_1 \cdot D}{\Omega_1} \cdot \frac{\Omega_1}{(s+\delta_1)^2 + \Omega_1^2} + D \cdot \frac{s+\delta_1}{(s+\delta_1)^2 + \Omega_1^2}\right\} \tag{6.17}$$

$$Q_{CD}\_U_{L_1}(t) = -Q \cdot e^{-\delta_1 \cdot t} \cdot \frac{|s_1^2 \cdot G_{sin}(s_1)|}{\Omega_1} \cdot \sin\left(\Omega_1 \cdot t + \arg\left(\frac{s_1^2 \cdot G_{sin}(s_1)}{\Omega_1}\right)\right) \tag{6.18}$$

Figure 6.7 depicts the reader's transient Q-channel signal. The difference compared to the I-channel transient signal is the stimulation of sine wave transfer function $G_{sin}(s)$ by pole s_1 instead of stimulating $G_{cos}(s)$.

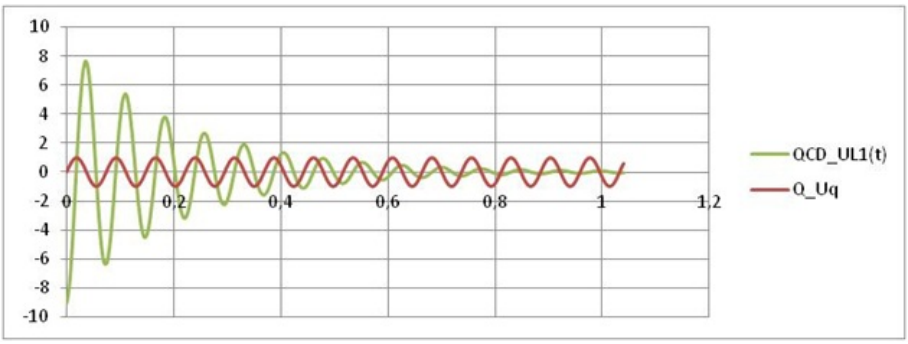

Figure 6.7: Transient signal of Reader Q-channel

Superposition of steady state and transient signals are resulting in reader Q-channel step response same as for the I-channel signal, which is shown figure 6.9.

$$\begin{aligned} Q\_U_{L_1}(t) = &-Q \cdot |G_{L_1}(j\omega)| \cdot \sin(\omega \cdot t + \arg(G_{L_1}(j\omega))) - \\ &Q \cdot e^{-\delta_1 \cdot t} \cdot \frac{|s_1^2 \cdot G_{sin}(s_1)|}{\Omega_1} \cdot \sin\left(\Omega_1 \cdot t + \arg\left(\frac{s_1^2 \cdot G_{sin}(s_1)}{\Omega_1}\right)\right) \end{aligned} \tag{6.19}$$

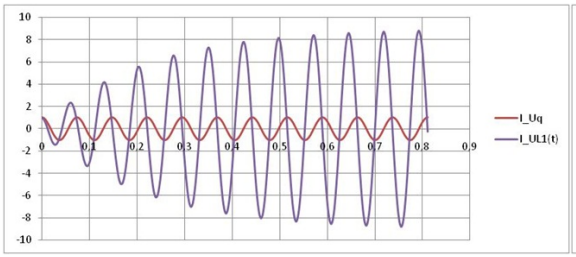

Figure 6.8: Reader I-channel

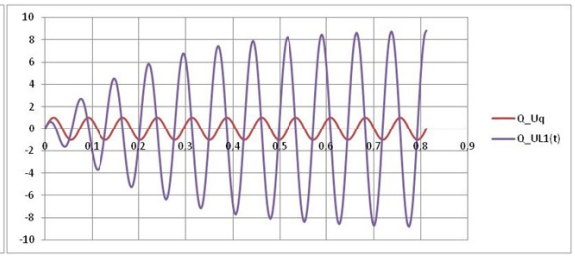

Figure 6.9: Reader Q-channel

6.5 Homogeneous H-field to Card-IC Input Voltage

Proximity Integrated Circuit Card (PICC) transient behavior can be analyzed by applying electromagnetic induction to a homogeneous H-field as source voltage.

$$\mathscr{L}\{U_i(t)\} = \omega \cdot \mu \cdot A_{mean} \cdot N \cdot \left(I \cdot \frac{s}{s^2 + \omega^2} - Q \cdot \frac{\omega}{s^2 + \omega^2}\right) \tag{6.20}$$

$$I_H = \omega \cdot \mu \cdot A_{mean} \cdot N \cdot I$$
$$Q_H = \omega \cdot \mu \cdot A_{mean} \cdot N \cdot Q$$

$$\mathscr{L}\{U_i(t)\} = I_H \cdot \frac{s}{s^2+\omega^2} - Q_H \cdot \frac{\omega}{s^2+\omega^2} \tag{6.21}$$

Transfer function (5.4) as depicted in section 5.3 is stimulated by H-field source.

$$U_L(s) = \left(I_H \cdot \frac{s}{s^2+\omega^2} - Q_H \cdot \frac{\omega}{s^2+\omega^2} \right) \cdot \frac{\omega_2^2}{s^2 + s \cdot \frac{\omega_2}{Q_2} + \omega_2^2 \cdot (\frac{R_2}{R_L}+1)}$$

$$I\_U_L(s) = I_H \cdot \frac{s}{s^2+\omega^2} \cdot \frac{\omega_2^2}{s^2 + s \cdot \frac{\omega_2}{Q_2} + \omega_2^2 \cdot (\frac{R_2}{R_L}+1)}$$
$$Q\_U_L(s) = -Q_H \cdot \frac{\omega}{s^2+\omega^2} \cdot \frac{\omega_2^2}{s^2 + s \cdot \frac{\omega_2}{Q_2} + \omega_2^2 \cdot (\frac{R_2}{R_L}+1)}$$

Using fractional expansion I/Q-channel signals are giving

$$\begin{aligned} I\_U_L(t) =& I \cdot |G_L(j\omega)| \cdot \cos(\omega \cdot t + \arg(G_L(j\omega))) + \\ & I \cdot e^{-\delta_2 \cdot t} \cdot \frac{\omega_2^2 \cdot |G_{cos}(s_2)|}{\Omega_2} \cdot \sin(\Omega_2 \cdot t + \arg(G_{cos}(s_2))) \end{aligned} \tag{6.22}$$

$$\begin{aligned} Q\_U_L(t) =& -Q \cdot |G_L(j\omega)| \cdot \sin(\omega \cdot t + \arg(G_L(j\omega))) - \\ & Q \cdot e^{-\delta_2 \cdot t} \cdot \frac{\omega_2^2 |G_{sin}(s_2)|}{\Omega_2} \cdot \sin(\Omega_2 \cdot t + \arg(G_{sin}(s_2))) \end{aligned} \tag{6.23}$$

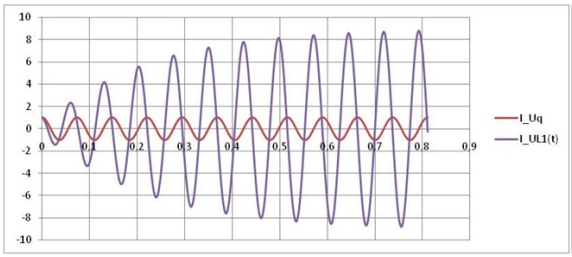

Figure 6.10: Card I-channel

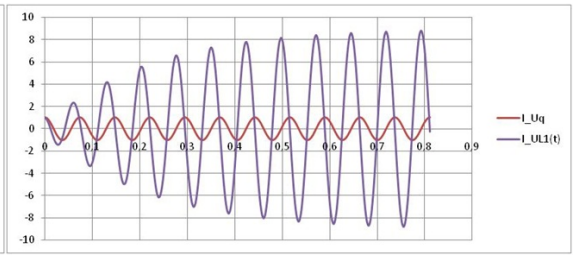

Figure 6.11: Card Q-channel

6.6 Reader to Card Signal Characteristics

Reader to card transient signal can be derived by using transfer function denoted in (5.15). For simplicity card feedback is omitted which is valid for cards at maximum operating distance. The impact of card feedback will be discussed in section 6.7. Equations (6.24), (6.25) denote the I/Q-channel transfer functions.

$$I\_U_L(s) = I \cdot \frac{s}{s^2+\omega^2} \cdot \frac{s^2}{s^2 + s \cdot \frac{\omega_1}{Q_1} + \omega_1^2} \cdot k \cdot \sqrt{\frac{L_2}{L_1}} \cdot \frac{\omega_2^2}{s^2 + s \cdot \frac{\omega_2}{Q_2} + \omega_2^2 \cdot (\frac{R_2}{R_L}+1)} \tag{6.24}$$

$$Q\_U_L(s) = -Q \cdot \frac{\omega}{s^2+\omega^2} \cdot \frac{s^2}{s^2 + s \cdot \frac{\omega_1}{Q_1} + \omega_1^2} \cdot k \cdot \sqrt{\frac{L_2}{L_1}} \cdot \frac{\omega_2^2}{s^2 + s \cdot \frac{\omega_2}{Q_2} + \omega_2^2 \cdot (\frac{R_2}{R_L}+1)} \tag{6.25}$$

Fractional expansion and inverse Laplace transformation $\mathscr{L}^{-1}$ by using the poles of transfer functions are resulting in equations (6.26) and (6.27).

$$\delta_1 = \frac{\omega_1}{2 \cdot Q_1} \qquad \Omega_1 = \omega_1 \cdot \sqrt{1 - \frac{1}{(2 \cdot Q_1)^2}}$$

$$\delta_2 = \frac{\omega_2}{2 \cdot Q_2} \qquad \Omega_2 = \omega_2 \cdot \sqrt{\frac{R_2}{R_L} + 1 - \frac{1}{(2 \cdot Q_2)^2}}$$

the three poles are

$s_0 = j\omega$

$s_1 = -\delta_1 + j\Omega_1$

$s_2 = -\delta_2 + j\Omega_2$

$$\begin{aligned} I\_U_{L_{tot}}(t) =& I \cdot |G_{L_1}(j\omega)| \cdot |G_L(j\omega)| \cdot \cos(\omega \cdot t + \arg(G_{L_1}(j\omega) \cdot G_L(j\omega))) + \\ & I \cdot e^{-\delta_1 \cdot t} \cdot \frac{|s_1^2 \cdot G_{cos}(s_1) \cdot G_L(s_1)|}{\Omega_1} \cdot \sin(\Omega_1 \cdot t + \arg(s_1^2 \cdot G_{cos}(s_1) \cdot G_L(s_1))) + \\ & I \cdot e^{-\delta_2 \cdot t} \cdot \frac{|\omega_2^2 \cdot G_{cos}(s_2) \cdot G_{L_1}(s_2)|}{\Omega_2} \cdot \sin(\Omega_2 \cdot t + \arg(\omega_2^2 \cdot G_{cos}(s_2) \cdot G_{L_1}(s_2))) \end{aligned} \tag{6.26}$$

$$\begin{aligned} Q\_U_{L_{tot}}(t) = & -Q \cdot |G_{L_1}(j\omega)| \cdot |G_L(j\omega)| \cdot \sin(\omega \cdot t + \arg(G_{L_1}(j\omega) \cdot G_L(j\omega))) - \\ & Q \cdot e^{-\delta_1 \cdot t} \cdot \frac{|s_1^2 \cdot G_{sin}(s_1) \cdot G_L(s_1)|}{\Omega_1} \cdot \sin(\Omega_1 \cdot t + \arg(s_1^2 \cdot G_{sin}(s_1) \cdot G_L(s_1))) - \\ & Q \cdot e^{-\delta_2 \cdot t} \cdot \frac{|\omega_2^2 \cdot G_{sin}(s_2) \cdot G_{L_1}(s_2)|}{\Omega_2} \cdot \sin(\Omega_2 \cdot t + \arg(\omega_2^2 \cdot G_{sin}(s_2) \cdot G_{L_1}(s_2))) \end{aligned}$$

(6.27)

The steady state signal is defined in magnitude and phase by the transfer function $G_e(s)$. The transient signal is a superposition of the self-oscillation frequencies determined by the individual resonance circuits of reader and card.

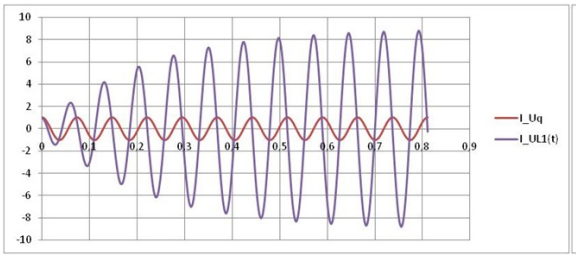

Figure 6.12: Reader, Card I-channel

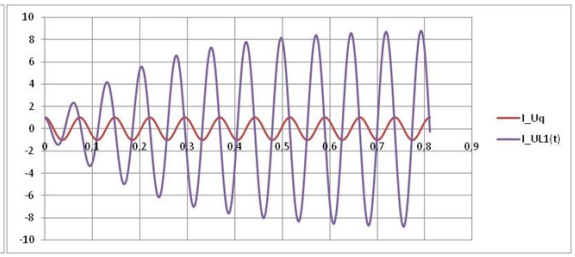

Figure 6.13: Reader, Card Q-channel

6.7 Antenna Tuning Impact

In previous sections time domain signals are derived for I- and Q-channel. Individual figures for steady state and transient characteristics are depicted where the resonance frequencies of the two antenna circuits are tuned to the system frequency 13.56MHz. A contactless card is typically detuned to higher resonance frequencies - e.g. 16.50MHz, whereas the reader circuit is tuned to system frequency to obtain best power transfer. Manufacturing tolerances, temperature behavior and card loading are resulting in detuning a tuned reader resonant circuit as well.

6.7.1 Bidding Frequency

Step response of a detuned LC tank results in an oscillation of the resonant circuit at a frequency different to the system frequency. This is depicted in equation (6.12), which is the I-channel representation of reader antenna signal stimulated by a cosine generator voltage.

$$\begin{aligned} I\_U_{L_1}(t) =& I \cdot |G_{L_1}(j\omega)| \cdot \cos(\omega \cdot t + \arg(G_{L_1}(j\omega))) + \\ & I \cdot e^{-\delta_1 \cdot t} \cdot \frac{|s_1^2 \cdot G_{cos}(s_1)|}{\Omega_1} \cdot \sin\left(\Omega_1 \cdot t + \arg\left(\frac{s_1^2 \cdot G_{cos}(s_1)}{\Omega_1}\right)\right) \end{aligned}$$

where

δ_1	is the attenuation factor
Ω_1	is oscillation frequency of reader resonant circuit
ω	is the system frequency - 13.56MHz
$G_{cos}(s)$	is the Laplace representation of cos(ωt)
$G_{L_1}(s)$	is the reader transfer function

The oscillation frequency of reader resonant circuit is denoted as

$$\Omega_1 = \sqrt{\frac{1}{L_1 \cdot C_1} \cdot \left(1 - \frac{1}{(2 \cdot Q_1)^2}\right)}$$

which is mainly defined by L_1, C_1. Figure 6.14 shows the step response characteristic of a antenna circuit tuned to 15.5MHz with an antenna quality factor Q_1 of 9. A low frequency bidding characteristic can be observed at the signal envelope.

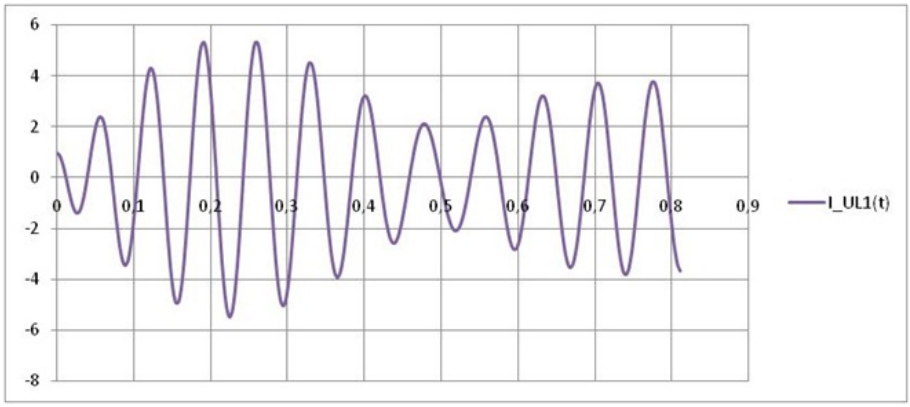

Figure 6.14: Bidding frequency characteristics of I-channel

Figure 6.14 is plotted with following parameter set

Q_1	≈ 9
Ω_1	$\approx 2 \cdot \pi \cdot 15.5MHz$
ω	$2 \cdot \pi \cdot 13.56MHz$

The bidding frequency can be seen best in the magnitude. It is necessary to introduce the imaginary part of the signal to be able to calculate phase and magnitude. This is corresponding to an I/Q-plot, where I represents the real part and Q the imaginary. A -π/2 phase shift is the way to generate the imaginary signal. A cosine signal is used to depict this method.

$\cos(\omega \cdot t)$	represents the time domain signal
$\cos(\omega \cdot t - \frac{\pi}{2})$	is the corresponding imaginary part
$\cos(\omega \cdot t - \frac{\pi}{2})$	$\sin(\omega \cdot t)$
Magnitude	$\sqrt{\cos^2 + \sin^2} = 1$

Applying the -π/2 phase shift to I-channel signal, equation (6.24) gives

$$\begin{aligned} I\_U_{L_1}\_90(t) =& I \cdot |G_{L_1}(j\omega)| \cdot \cos\left(\omega \cdot t + \arg(G_{L_1}(j\omega)) - \frac{\pi}{2}\right) + \\ & I \cdot e^{-\delta_1 \cdot t} \cdot \frac{|s_1^2 \cdot G_{cos}(s_1)|}{\Omega_1} \cdot \sin\left(\Omega_1 \cdot t + \arg\left(\frac{s_1^2 \cdot G_{cos}(s_1)}{\Omega_1}\right) - \frac{\pi}{2}\right) \end{aligned} \tag{6.28}$$

Figure 6.15 is depicting the envelope characteristic of signal $I\_U_{L_1}$ by calculating the magnitude according to equation

$$\sqrt{I\_U_{L_1}(t)^2 + I\_U_{L_1}\_90(t)^2}$$

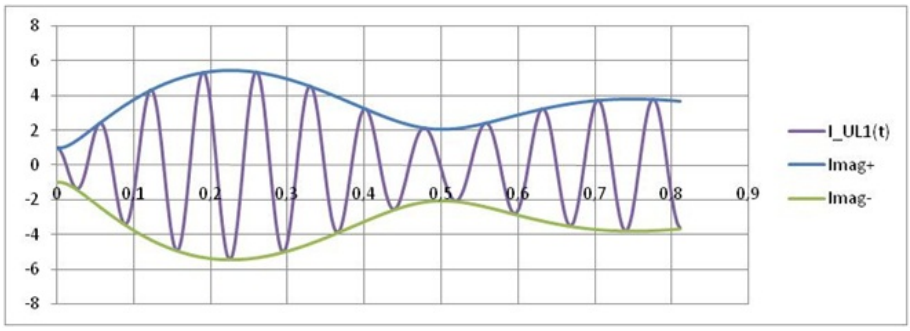

Figure 6.15: Bidding frequency envelope of I-channel

The bidding frequency is calculated by the difference of the carrier frequency of 13.56MHz and the frequency defined by the resonance circuit. To be able to calculate the phase of the bidding signal, it is necessary to suppress the high frequency components of signals $I\_U_{L_1}(t)$, $I\_U_{L_1}\_90(t)$. The low frequency (LF) signal can be obtained by subtracting the system frequency, which results in

$$\begin{aligned} I\_LF\_U_{L_1}(t) =& I \cdot |G_{L_1}(j\omega)| \cdot \cos(\arg(G_{L_1}(j\omega))) + \\ & I \cdot e^{-\delta_1 \cdot t} \cdot \frac{|s_1^2 \cdot G_{cos}(s_1)|}{\Omega_1} \cdot \sin\left((\Omega_1 - \omega) \cdot t + \arg\left(\frac{s_1^2 \cdot G_{cos}(s_1)}{\Omega_1}\right)\right) \end{aligned} \tag{6.29}$$

$$\begin{aligned} I\_LF\_U_{L_1}\_90(t) =& I \cdot |G_{L_1}(j\omega)| \cdot \cos\left(\arg(G_{L_1}(j\omega)) - \frac{\pi}{2}\right) + \\ & I \cdot e^{-\delta_1 \cdot t} \cdot \frac{|s_1^2 \cdot G_{cos}(s_1)|}{\Omega_1} \cdot \sin\left((\Omega_1 - \omega) \cdot t + \arg\left(\frac{s_1^2 \cdot G_{cos}(s_1)}{\Omega_1}\right) - \frac{\pi}{2}\right) \end{aligned} \tag{6.30}$$

Phase and magnitude of bidding frequency can be derived by

$$I\_Magnitude(t) = \sqrt{I\_LF\_U_{L_1}(t)^2 + I\_LF\_U_{L_1}\_90(t)(t)^2}$$

$$I\_Phase(t) = \arctan\left(\frac{I\_LF\_U_{L_1}(t)}{I\_LF\_U_{L_1}\_90(t)}\right)$$

Figure 6.16, 6.17 show the full step response of Reader I-channel and its corresponding phase and magnitude of the low frequency (LF) bidding signal.
Parameters are defined as

Q_1	is approximately 9
Ω_1	is approximately $2 \cdot \pi \cdot$ 15.5 MHz
ω	is the system angular frequency $2 \cdot \pi \cdot$ 13.56 MHz
Bidding Frequency	is approximately 2MHz

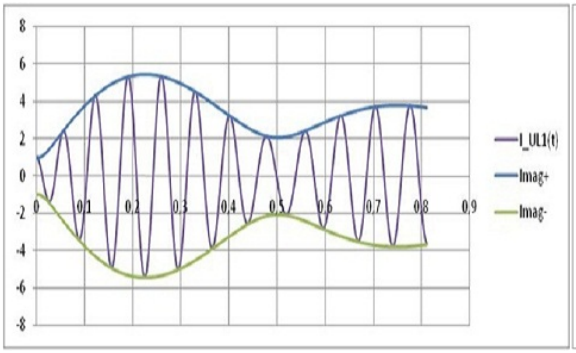

Figure 6.16: Bidding Signal

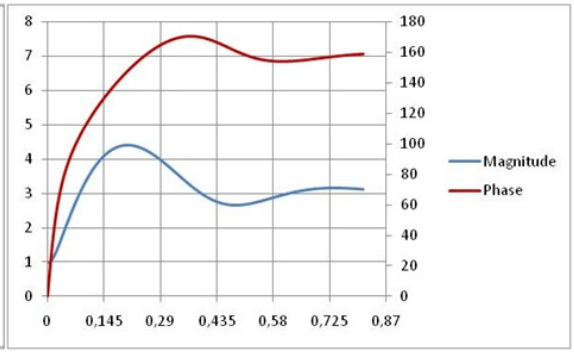

Figure 6.17: Phase and Magnitude

6.7.2 Detuning by Card Loading

In section 6.6 the step response signal for a coupled reader to card operation without feedback loop is analyzed. In that case the coupling factor is negligible because the card is operated at a 'far' distance to the reader. The card quality factor Q_2 is in the range of 5. When the card is approaching the reader antenna the coupling factor increases. As an increased coupling factor is also increasing energy transferred to the card the regulation of the card-IC starts to lower the card quality factor. This reduces the influence of bidding signal generated by the card resonance circuit as the bidding signal strength decreases with decreased quality factor. On the other hand card feedback starts to influence the reader resonance circuit.

Equation (5.15) depicts the transfer function of reader to card with feedback.

$$G_e(s) = G_{L1}(s) \cdot \frac{k \cdot \sqrt{\frac{L_2}{L_1}}}{1 + G_{L1}(s) \cdot G_{L2}(s) \cdot k^2} \cdot G_L(s) \tag{6.31}$$

Rearranging (6.31) using definitions of section 6.2 gives

$$G_e(s) = \frac{s^2 \cdot \omega_2^2 \cdot k \cdot \sqrt{\frac{L_2}{L_1}}}{\left(s^2 + s \cdot \frac{\omega_1}{Q_1} + \omega_1^2\right) \cdot \left(s^2 + s \cdot \frac{\omega_2}{Q_2} + \omega_2^2 \cdot \left(\frac{R_2}{R_L} + 1\right)\right) - k^2 \cdot \left(s^4 + s^3 \frac{\omega_2}{Q_{IC}}\right)} \tag{6.32}$$

Nominator of equation (6.32) is denoting a 4th degree polynom. In the case of a contactless system typically two conjugate-complex poles can be derived by solving this equation. If the card feedback is negligible, the poles are same as denoted in sections 6.4 and 6.5 derived from reader and card transfer functions. To take card feedback into account, it is necessary to solve the 4th degree equation using the appropriate dynamic card load which has to be calculated additionally.

6.7.3 Summary Detuned Resonant Circuits

In section 6.7 it is shown that antenna tuning frequency is impacting data communication a lot. The behavior of a low frequency bidding signal can disturb data signals. The quality factor of antenna tuning circuit influences the bidding signal strength. The higher the quality factor the higher the signal strength. The difference between resonance and system frequency defines the bidding frequency. The higher the deviation the faster is the bidding interference. In previous sections step response signals for reader, card and a contactless system were given. Detuning of cards to 16.5MHz is a typical case for an ID1 form factor. The resonance capacitor is integrated in silicon and therefore has tolerances up to $\pm$ 10%. The tolerance of resonance frequency can be approximated by the sum of capacitor and inductor tolerance divided by two. An inductor typically has tolerances of $\approx \pm$ 2% which yields a $\pm$ 6% resonance frequency deviation. In case of a nominal frequency of 16.5MHz this leads to a worst case detuning of $\approx$ 17.5MHz. Calculated bidding frequency is $\approx$ 4MHz which is in the range of a communication signal of 3.4Mbps. Reader to card transfer function even includes two resonance circuits which are oscillating on their self resonance frequency in case of a step response which is applied during Amplitude or Phase Shift Keying (ASK, PSK) modulation.

7 Dual Antenna Architecture

Chapter Time Domain Analysis and Transient Settling 6 accomplishes settling behavior of a contactless system. Step response characteristics for Amplitude and Phase Shift Keying (ASK, PSK) are analyzed in detail. Both schemes are modulated by digital amplitude or phase changes, which generate step responses in time domain. Very high bit rates (VHBR) are limited by resonant circuit characteristics of Proximity Coupling Device (PCD) and Proximity Integrated Circuit Cards (PICC). The quality factor of the individual tuning circuits are shaping the settling envelope. Increasing power loss of the resonant circuit is - to date - the way of handling bandwidth limitations for High and Very High Bit Rates (HBR, VHBR) - i.e. reducing quality factor. This strategy is sufficient for High Bit Rates (HBR) but already challenging for Very High Bit Rates (VHBR) up to 6.8Mbps. Transient behavior of low quality factor Amplitude and Phase Shift Keying (ASK, PSK) is depicted in Infineon's ISO/IEC 14443 TF2 contribution in Berlin, April 2010 meeting [21]. This contribution considers resonant and detuned case. Figures 7.1, 7 are depicting tuned case settling characteristics of Amplitude and Phase Shift Keying (ASK, PSK) signals [21].

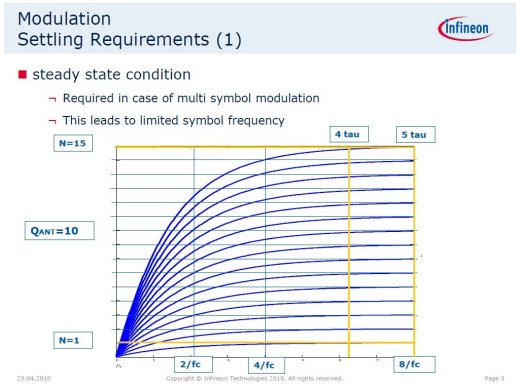

Figure 7.1: M Symbol settling [21]

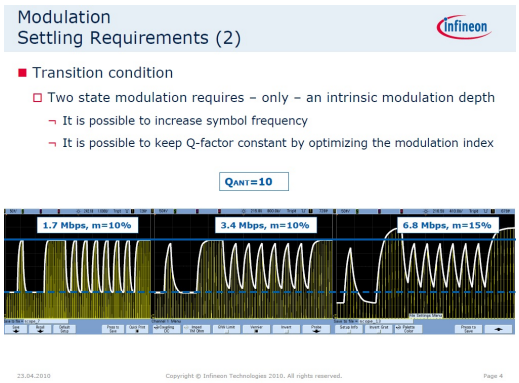

Two state settling [21]

Bidding frequency, which is elaborated in chapter Time Domain Analysis and Transient Settling 6, is depicted in measurement results for Amplitude and Phase Shift Keying (ASK, PSK) signal shapes. Although the antenna Q-factor is already limited to 10 which gives an operating Q-factor of 5, it is hard to discriminate a sixteen symbol Phase Shift Keying (PSK) modulated data stream. Sixteen symbols are necessary to achieve a 6.8Mbps bit rate based on a symbol frequency of 1.7MHz. Multi-symbol modulation has to evaluate the symbol at an almost settled state. Transient rising and falling edges are giving too weak signals to distinguish reliably between the individual symbols. Bidding frequency makes symbol detection worse. Even the settled symbol states become complex to be detected correctly. A learning pattern with ninety predefined symbols is proposed to circumvent these issues. A two state modulation - Amplitude or Phase Shift Key-

ing (ASK, PSK) - is easier to handle. Two states can be discriminated in the transient phase of rising and falling edges. In that case a reduction of Elementary Timing Unit (ETU) is necessary to speed up communication. This limits a reasonable bit rate to 6.8Mbps. Further increase of bit rate up to 13.56 Mbps can be hardly realized for both, two state Amplitude and Multi-symbol Phase Shift Keying (ASK, MPSK).

Before mentioned limitations concerning power dissipation and bandwidth raise the question: Is contactless technology already at its limit to increase bit rates beyond 6.8Mbps? Is it reasonable to further increase Very High Bit Rates (VHBR) by a factor of eight to 54Mbps? This chapter is placing emphasis on novel transmit and receive architectures to break restrictions, given by existing state of the art circuits. Bandwidth constraints can be solved by a broadband antenna circuit. A digital modulation of antenna voltage can be realized by reducing the quality factor or even omitting the resonant capacitor - i.e. no self resonant circuit is built. The resonant circuit is necessary to be able to power a Proximity Integrated Circuit Card (PICC). Assuming a quality factor of ten for a conventional Proximity Coupling Device (PCD) the voltage, which has to be supplied by the driver circuit, has to be eleven times higher with a non resonant antenna structure for the same field strength. A conventional driver uses a push pull output stage with a 3V to 5V power supply a 30V to 50V output stage would be necessary for a direct driven antenna to generate the same H-field strength. Figure 7.2 depicts a novel RX-path antenna architecture, which is discussed in detail in sections below [7] .

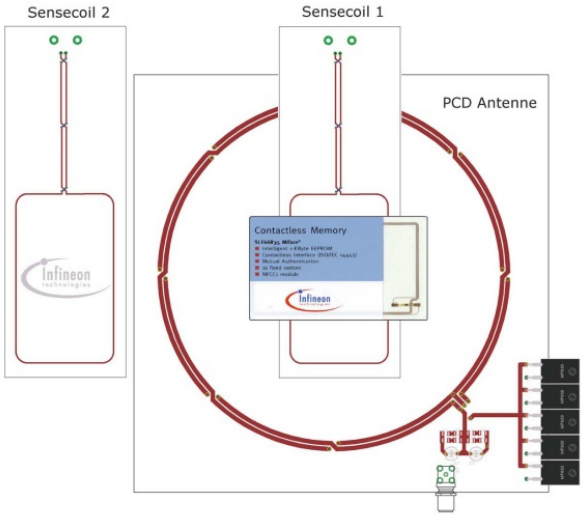

Figure 7.2: Novel Antenna Architecture [7]

7.1 Novel Receive Path Architecture

A novel receive path architecture is introduced. Power and receive path is split into two separate structures. One is optimized for powering a Proximity Integrated Circuit Cards (PICC). The second one is used to receive Load Modulation Amplitude (LMA) generated by a Proximity Integrated Circuit Card (PICC). Receiver path is built as independent sensing antenna circuit. This antenna

is located in the same plane as the standard reader antenna which is used for power transfer. The receive antenna is used to sense the H-field, which is generated by a Proximity Integrated Circuit Card (PICC), without shaping the signals by a resonant circuit. This is achieved by a high ohmic voltage sensing circuit. The basic concept is used in the ISO10373-6 test standard for measuring Load Modulation Amplitude (LMA). Matthias Emsenhuber did his master thesis [7] on the novel receive architecture. A comparison overview presented in this thesis will be shown afterwards.

7.2 Receive Path Equivalent Circuit

Figure 7.3 depicts the novel receive path architecture.

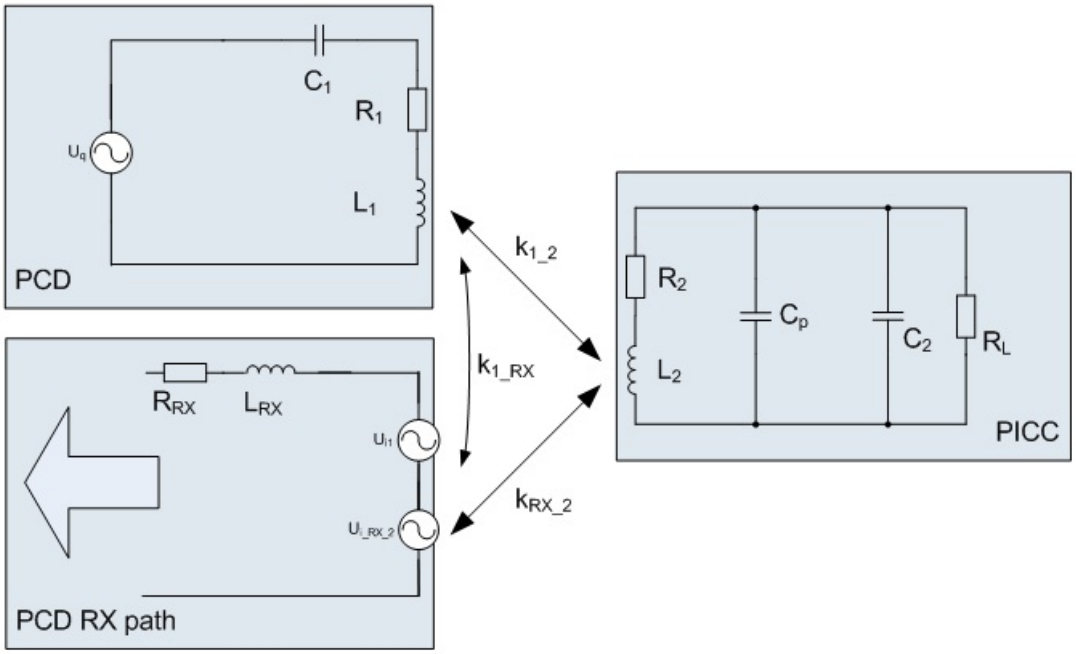

Figure 7.3: Receive Path Equivalent Circuit

L_1	is the inductance of reader energy antenna
L_{RX}	is the inductance of reader receive antenna
L_2	is the inductance of the card coil
k_{1_2}	is the coupling coefficient between reader antenna and card coil
k_{RX_2}	is the coupling coefficient between receive antenna and card coil
k_{1_RX}	is the coupling coefficient between reader and receive antenna
C_1	is the tuning capacitance of reader antenna
C_2	is the tuning capacitance of card coil

Coupling between Proximity Integrated Circuit card (PICC) and sense antenna is already mentioned. A second voltage is induced in the receiver antenna which is generated by the conventional Proximity Coupling Device (PCD) power antenna. This additional induced voltage is an unwanted signal for the receiver of a Proximity Coupling Device (PCD) receiver circuit as described in section 5.8.

7.3 Receive Antenna Signal Optimization

US Patent Application 20100243737 [18] is depicting methods to minimize receive signal disturbance. A signal cancellation circuit is used to optimize receive path quality. Both induced voltages - U_{i1} and $U_{i\_RX\_2}$ - are generated by their corresponding antenna currents as denoted in equations (4.1) and (4.8). The Proximity Coupling Device (PCD) antenna current is generating the disturb signal at the receiver input. Mutual induction - as presented in section 4.4 - and antenna current are giving basic information to compensate the unwanted signal at receiver antenna.

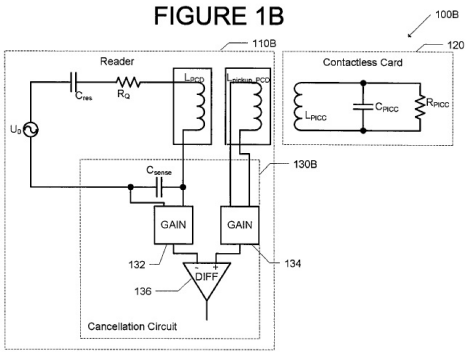

Figure 7.4: Current sensing method [18]

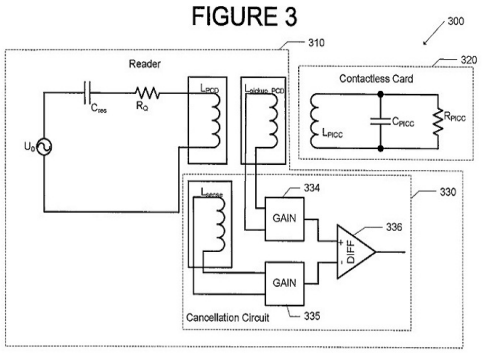

Figure 7.5: H-field sensing method [18]

Figures 7.4 and 7.5 are depicting two compensation options disclosed in US Patent Application 20100243737 [18]. Current compensation method is advantageous over antenna compensation as there is no mutual coupling influence between a Proximity Integrated Circuit Card (PICC) coil and the compensation antenna. It is the objective not to couple signals between the two inductances.

Voltage sensing is a good option to realize the right phase between the induced voltage and the compensation signal as the induced voltage is in-phase with the Proximity Coupling Device (PCD) antenna voltage. Same is valid for an antenna compensation. Current sensing with a resistor is giving a 90° shift due to the inductive behavior of the antenna. Therefore it is recommended to us a capacitor as current sensing device which then gives a 180° shift with reference to the antenna voltage. An inductor is also an option which typically is much more expensive. The sensing capacitor can be a part of the tuning circuit which further saves cost.

Figure 7.6 shows simulation results of novel compensation methods [7] .

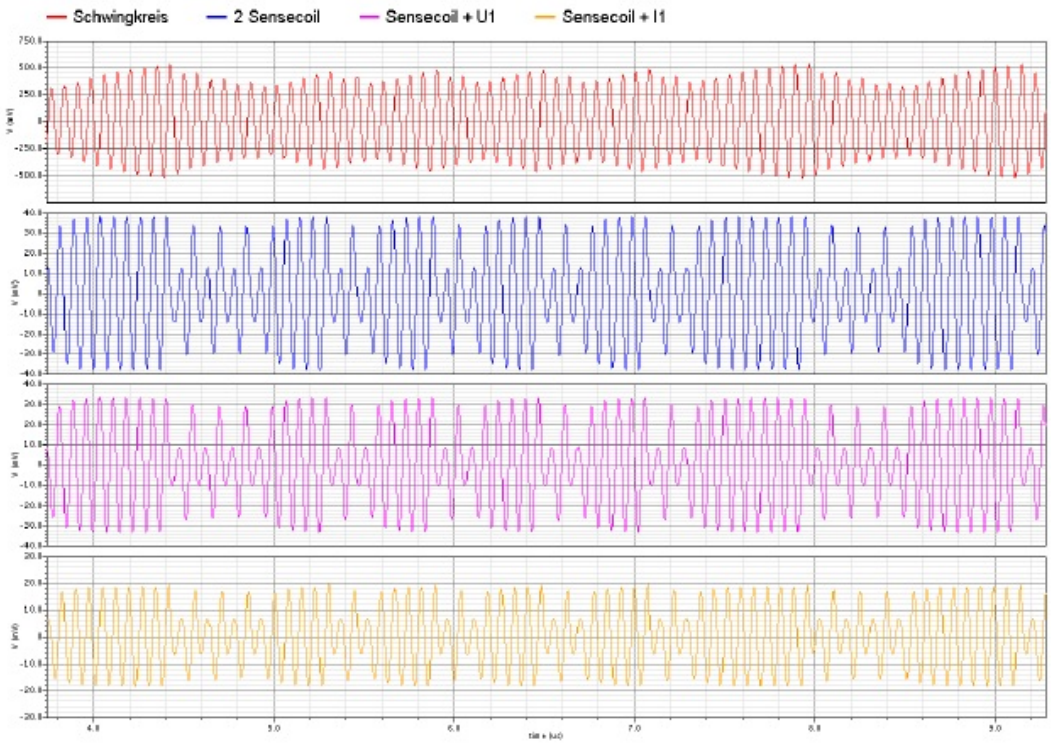

Figure 7.6: Receive Path Comparison [7]

An antenna quality factor of fifteen and a bit rate of 6.8Mbps is used in this simulation.

Figure 7.6 depicts different receive path solutions which are described bellow.

- Red line graph represents the signal wave shape of a conventional receiver architecture.
- Blue line graph is based on antenna compensation method
- Magenta line graph depicts a voltage compensation
- Yellow line graph shows the current compensation

The wave shapes of the novel compensation methods are superior over the conventional receiver signals. It can be seen that a 6.8Mbps signal based on 6.8MHz subcarrier frequency cannot be discriminated by a conventional receiver architecture. This is caused by signal shaping of the reader antenna circuit with a high quality factor. This is described in chapter Transfer Functions 5. Card feedback can be represented by an induced voltage source which is shaped by the reader transfer function $G_{L1}(s)$. This is omitted in the novel receiver architecture by the use of a high impedance antenna. This high impedance circuit does not form a resonant circuit and therefore does not influence the wave shape negatively.

7.4 Novel Transmit Path Architecture

A novel transmit path architecture is introduced. Power and communication path is split into two separate power lines. One is optimized for powering a Proximity Integrated Circuit Card (PICC). The second one is designed to modulate communication signals.

The power path is based on a high quality factor resonant circuit tuned to 13.56MHz. No bandwidth constraints are given as the data signal path is not incorporated. Antenna circuit design can be focused on power transfer with no regard to communication circuit requirements. Power can be increased as long as emission limits and maximum H-field constraints - as depicted in chapter Regulation and Standards 3 - are regarded.

Communication path is built as independent second antenna circuit. Amplitude and/or Phase Shift Keying (ASK, PSK) signals can be modulated best on a broad band antenna. Inter Symbol Interference (ISI), bidding frequency characteristics, time constant and settling behavior can be optimized. Data signal strength is constraint by emission sideband limitations presented in chapter 3.

7.5 Dual Antenna Transmit Path Equivalent Circuit

To introduce the dual antenna architecture an equivalent circuit is used. The Proximity Integrated Circuit Card (PICC) representation stays same as depicted in figure 5.1. The difference is built in a novel resonant circuit architecture of a Proximity Coupling Device (PCD). Figure 7.7 presents the novel circuit.

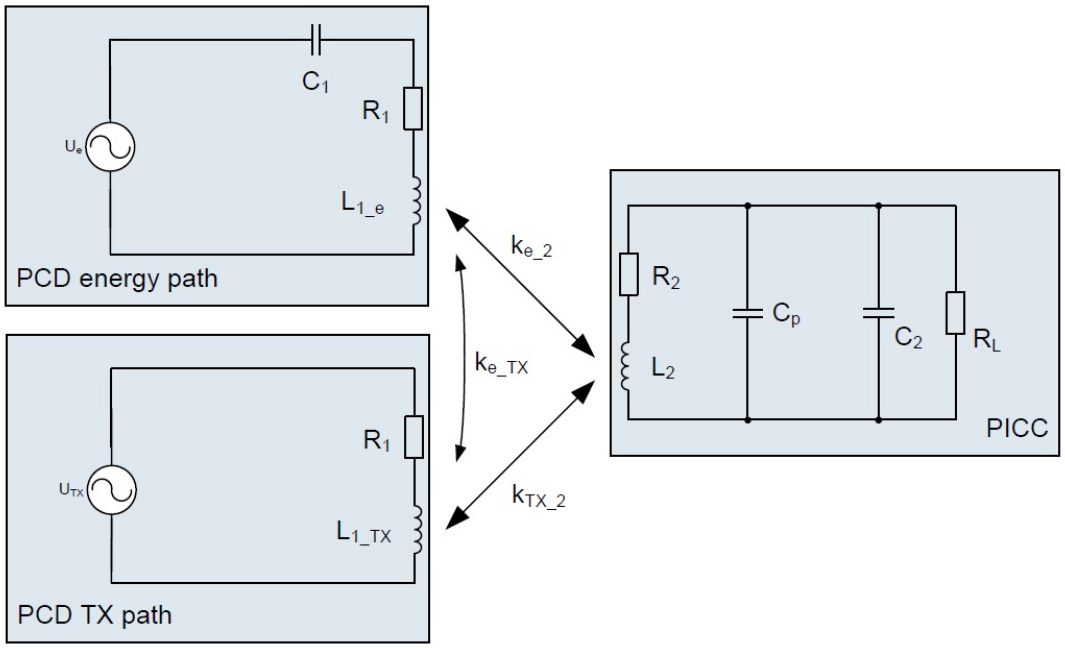

Figure 7.7: Dual Antenna Equivalent Circuit

The dual antenna architecture introduces to inductors L_{1e}, L_{1TX} compared to L_1 in a conventional Proximity Coupling Device (PCD). Individual coupling coefficients k_{e_2}, k_{TX_2} and k_{e_TX}.

L_{1e}	is the inductance of reader energy antenna
L_{1TX}	is the inductance of reader transmit antenna
L_2	is the inductance of the card coil
k_{e_2}	is the coupling coefficient between energy antenna and card coil
k_{TX_2}	is the coupling coefficient between transmit antenna and card coil
k_{e_TX}	is the coupling coefficient between energy and transmit antenna
C_1	is the tuning capacitance of reader energy antenna
C_2	is the tuning capacitance of card coil

The energy antenna is built as tuned resonant circuit which can be optimized to transfer power to the Proximity Integrated Circuit Card (PICC). The transmit antenna is denoted as direct driven antenna, which is a broadband antenna type to be able to transmit very high bit rates (VHBR) and even higher.

7.6 Dual Antenna Transmit Path Coupling Compensation

Mutual interaction of reader's energy and transmit antennas are represented by coupling coefficient k_{e_TX} is a parasitic effect of the novel architecture. As the two antennas are located in the same plain - i.e. placed on the same Printed Circuit Board (PCB) - the coupling is defined by geometric parameters of the individual antenna turns and the relative position of their centers.It is the objective to reduce the parasitic coupling effect to a minimum. This guarantees a proper energy and data transfer without influencing each other. The combination of energy and transmit signals is done in the H-field domain. The superimposed transmit and energy H-fields are picked up by the Proximity Integrated Circuit Card (PICC) coil.

Two compensation strategies are depicted in more detail. As the mutual interaction can be described by induced voltages according to equations (5.8), (5.12) an appropriate compensation voltage can be applied at the driver of the individual antenna circuit. Figure 7.8 represents a circuit implementation using the voltage method which is disclosed in US Patent Application 20100311328 [19].

$-U_{i_{TX\_e}}$ is the compensation signal for induced voltage $k_{e\_TX} \cdot \sqrt{\frac{L_{1_e}}{L_{1_{TX}}}} \cdot U_{L_{1_{TX}}}$

$-U_{i_{e\_TX}}$ is the compensation signal for induced voltage $k_{e\_TX} \cdot \sqrt{\frac{L_{1_{TX}}}{L_{1_e}}} \cdot U_{L_{1_e}}$

Compensation voltages $-U_{i_{TX\_e}}$, $-U_{i_{e\_TX}}$ are introduced in the individual antenna circuits to compensate for the mutualy induced voltages generated by coupling coefficient k_{e_TX}. A voltage

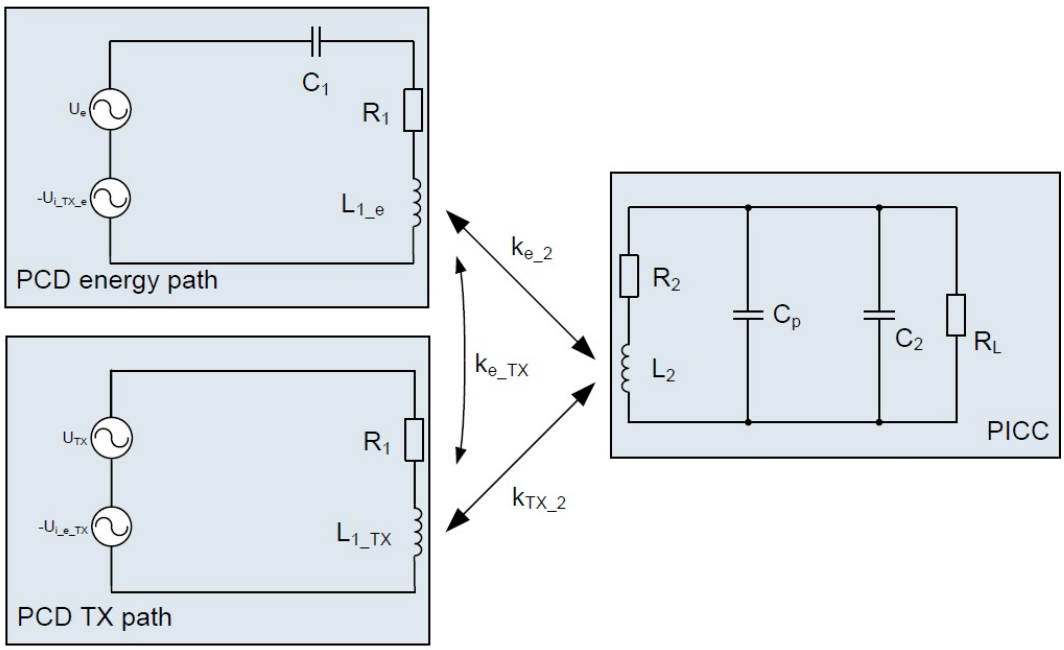

Figure 7.8: Dual Antenna Compensation Method Equivalent Circuit

compensation method is reasonable, if the coupling factor between the two Proximity Coupling Device (PCD) antennas is not too good. As the powering antenna is generating a high voltage at inductor L_{1e} a high voltage is also induced at transmit antenna. Peak voltages of 50V at the energy antenna are typical in an unloaded tuned state. A compensation of a high induced voltage can be hardly realized in modern short channel technologies.

Reducing the mutual coupling to a minimum is the second method which is presented in this section. As the two Proximity Coupling Device (PCD) antennas are located in the same plane different strategies are possible to minimize mutual inductance. The H-field characteristic depicted in chapter Contactless Technology Air Interface 4 gives a guideline how to reduce the coupling coefficient. The H-field at the antenna plane is positive inside an antenna turn and negative outside [10]. This property is used to built two antennas at the same plane - i.e. the same Printed Circuit Board (PCB) - which are not mutually coupled. The calculation of a mutual inductance is presented in section Self and Mutual Induction 4.4. Assuming a rectangular shape for energy and transmit antenna the mutual induction can be calculated based on equation (7.1).

$$M_{eTX}(0) = \frac{X_1 \cdot X_2}{N_1 \cdot N_2} \cdot \sum_{i=0}^{N_1-1} \sum_{j=0}^{N_2-1} M_{rect}(X_2 - \frac{\Delta w}{2} \cdot (1+2i), Y_2 - \frac{\Delta w}{2} \cdot (1+2i), 0, X_1 - \frac{\Delta w}{2} \cdot (1+2j), Y_1 - \frac{\Delta w}{2} \cdot (1+2j)) \tag{7.1}$$

The z-component is set to zero as the two antennas are at the same plane. The geometric difference can be designed by different centers and/or different xy-dimensions. The objective is to minimize coupling and keep the coupling coefficients to a Proximity Integrated Circuit Card

(PICC) at a level close to a single Proximity Coupling Device (PCD) antenna structure. A simple approach is to bring the two antennas out of center. The centers of the two antennas are positioned that the integral over the individual H-field of the mutual inductance is zero. A basic drawing of this concept is disclosed in US Patent Application 20100311328 [19]. Many other geometric options can be used to gain the same effect.

Design constraints for the two antennas are

- Minimize coupling coefficient between antennas L_{1e} and L_{1TX}
- Minimize Proximity Coupling Device (PCD) antenna size
- Maximize coupling between Proximity Coupling Device (PCD) energy antenna and Proximity Integrated Circuit Card (PICC)
- Maximize coupling between Proximity Coupling Device (PCD) transmit antenna and Proximity Integrated Circuit Card (PICC)

Equations - presented in chapter Contactless Technology Air Interface 4 - support the design process of involved antenna and coil shapes.

7.7 Dual Antenna Transmit Path Modulation Signals

This section presents a comparison of conventional single antenna structure and the novel dual antenna transmit architecture. New modulation schemes are going to be presented to address the architecture's potential to increase bit rates beyond 13.56Mbps. Proximity Coupling Device (PCD) transmit path communication is already running at 27.12Mbps in lab environment.

As a starting point two signal wave shapes are depicted in figure Comparison of dual and single antenna structure at 848kbps.

Figure 7.9 is a 10% modulation Amplitude Shift Keying (ASK) signal as specified in the ISO/IEC 14443 Type B standard. One wave shape is generated by a conventional Proximity Coupling Device (PCD) antenna circuit. The second one is modulated with the novel dual antenna architecture. The settling characteristic of single antenna structure is shaped by the resonant circuit quality factor - which is 10 in this case. The settling of the novel antenna structure is almost rectangular. This is achieved by the broadband transmit antenna. The high Q of energy path antenna is not influencing the communication wave shape at all. The new architecture is superior even at High Bit Rate (HBR) communication speed compared to a conventional single antenna structure. The novel transmit path architecture is almost mandatory for Very High Bit Rates (VHBR) if the quality factor of reader resonant circuit stays the same.

Figure 7.10 depicts the wave shapes for a 3.4Mbps Very High Bit Rate (VHBR) communication speed. A reader resonant circuit with a quality factor of 10 attenuates an Amplitude Shift Keying

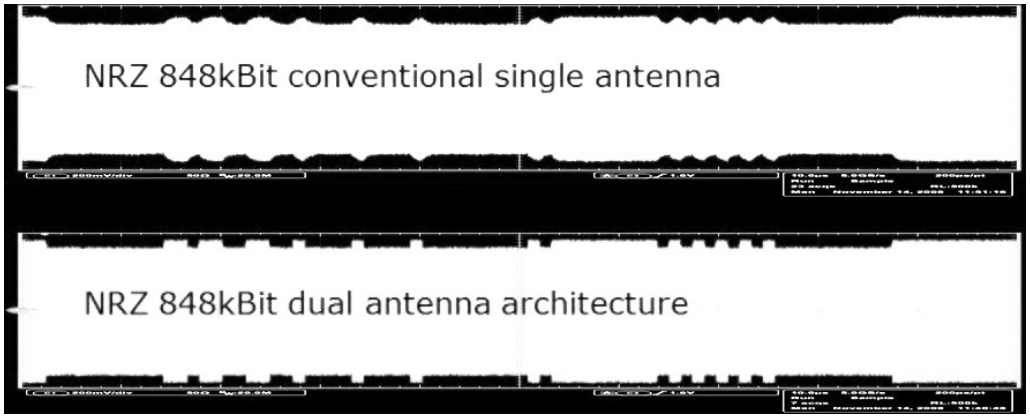

Figure 7.9: Comparison of dual and single antenna structure at 848kbps

(ASK) signal at this high speed that it hardly can be discriminated by a Proximity Integrated Circuit Card (PICC) receiver.

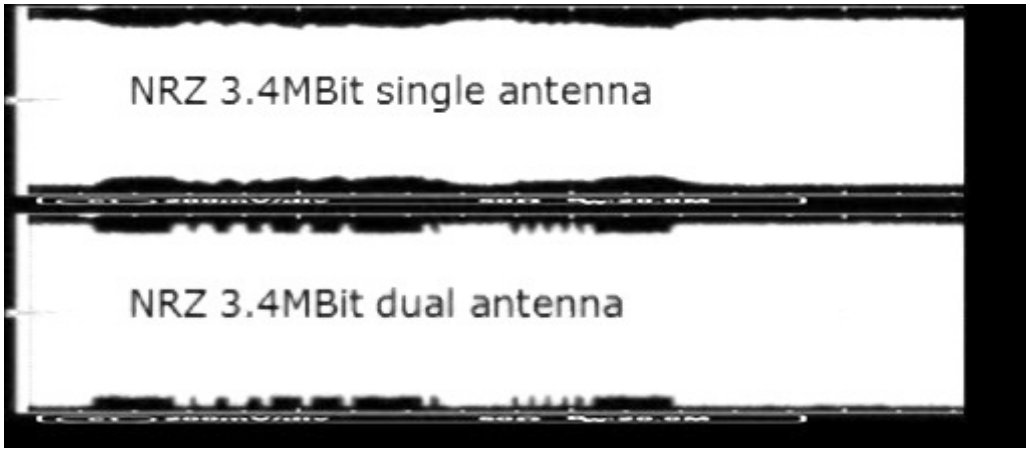

Figure 7.10: Comparison of dual and single antenna structure at 3.4Mbps

A reader with the novel dual antenna configuration is able to modulate the 3.4Mbps signal without almost no attenuation of data signals whereas the energy path is built with a high quality factor. The signal characteristic can be shown best with Amplitude Shift Keying (ASK) modulation. Phase Shift Modulation (PSK) or other modulation concept - e.g. Quadrature Amplitude Modulation (QAM) - can be realized.

Elementary Timing Unit (ETU) reduction is a reasonable approach for a dual antenna system to step up bit rates, as the data shaping is not influenced by resonant circuit characteristics. A linear increase of communication speed is a clear advantage compared to a binary logarithm characteristic of a symbol modulation. A Phase Shift Keying (PSK) symbol modulation with up to sixteen symbols at an Elementary Timing Unit (ETU) of eight carrier cycles is proposed by

companies NXP and Gemalto. A single antenna circuit does not allow bit time reduction as Inter Symbol Interference (ISI)- forced by the antenna quality factor - handicaps correct signal detection at the Proximity Integrated Circuit Card (PICC) receiver.

7.8 Dual Antenna Modulation Vectors

A transmit antenna modulation signal superimposes the energy carrier signal of the Proximity Coupling Device (PCD). This results in one H-field component which is received by a Proximity Integrated Circuit Card (PICC). Figures 7.11, 7.12 represent an Amplitude and Phase Shift Keying (ASK, PSK) modulated H-field. The carrier vector $\vec{H}_c$ is superimposed by the individual data vectors $\vec{H}_{ASK}$, and $\vec{H}_{PSK}$.

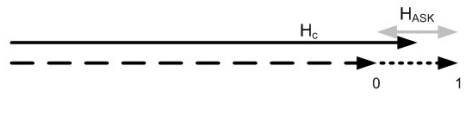

Figure 7.11: ASK vector diagram

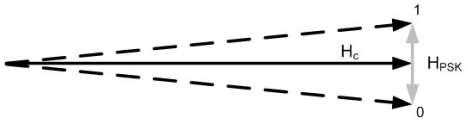

Figure 7.12: PSK vector diagram

Transmit vectors in figures 7.11, 7.12 are both phase modulated - for Amplitude Shift Keying (ASK) as well as for Phase Shift Keying (PSK) - with respect to the energy carrier. The Amplitude Shift Keying (ASK) is generated by a (0°, 180°) phase modulated transmit signal, whereas Phase Shift Keying (PSK) is modulated by (+90°, -90°). The superimposed signal for Amplitude Shift Keying (ASK) results in an amplitude modulated vector whereas the Phase Shift Keying (PSK) signal is phase and at a small amount amplitude modulated. A modulation state (1, 0) can be defined as the unmodulated condition to omit amplitude modulation for the phase modulated signal. Alternatively a 100% Amplitude Modulation (AM) can be applied for Amplitude and Phase Shift Keying (ASK, PSK) where the 180° signal represents amplitude modulation and 90° signal the phase modulation.

A novel Proximity Integrated Circuit Card (PICC) receiver is presented in [2]. The phase receiver is based on a Phase Locked Loop (PLL) together with a novel two state detector, which is able to demodulate phase changes at very high speed up to Elementary Timing Unit (ETU) of one carrier cycle. A detailed description of the two state phase detector is disclosed in US Patent Application 'CIRCUIT FOR DEMODULATING A PHASE MODULATED SIGNAL' [22]. Markus Auer focused his research on a high speed Proximity Integrated Circuit Card (PICC) receiver [1].

Amplitude receivers are more common for contactless technologies. Phase Jitter Modulation invented by Megallan Pty is the only standardized phase modulation technology in the frequency band of 13.56MHz. All other types are Amplitude Modulated (AM). Lab measurement results of an improved ISO14443 compliant Proximity Integrated Circuit Card (PICC) receiver are available, which proof a 13.56Mbps communication speed for Amplitude Shift Keying (ASK).

7.9 Dual Antenna Architecture at 27.12Mbps Communication Speed

A 13.56Mbps communication speed with an Elementary Timing Unit (ETU) of one carrier cycle is feasible for both Amplitude and Phase Shift Keying (ASK, PSK) signals. A doubling of 13.56Mbps is obvious by combining both signals in a Quadrature Amplitude Modulation (QAM). Figure 7.13 depicts the vector diagram of a Quadrature Amplitude Modulation (QAM) which is represented by a Quadrature Phase Shift Keying (QPSK) transmit vector $\vec{H}_{QAM}$.

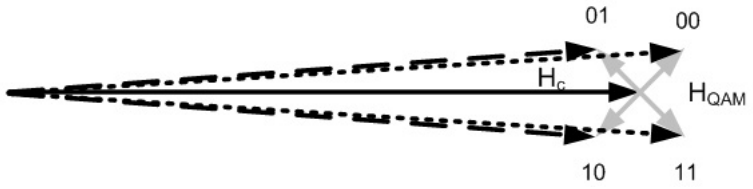

Figure 7.13: QAM vector diagram

First tests in a lab environment are proofing the feasibility of a 27.12Mbps communication speed from Proximity Coupling Device (PCD) to Proximity Integrated Circuit Card (PICC). A dual antenna transmit architecture has the potential to further increase bit rates to 54.24Mbps. It is a break through compared to the possibilities of a conventional - band width limited - single antenna structure. Modern signal techniques like Discrete Multi Tone (DMT) modulation as used in Very High Speed Digital Subscriber Line (VDSL) technology can be implemented. The novel dual antenna structure separates energy and data transfer which allows an independent usage for both - data and energy - channels. An increase up to 54.24Mbps is possible in the near future, which is a factor of eight compared to actual Very High Bit Rate (VHBR) proposals and a factor of sixty four compared to the existing standard.

7.10 Dual Antenna Transient Settling Characteristics

Chapter Time Domain Analysis and Transient Settling 6 explains the tuning impact and quality factor dependency of a conventional single antenna Proximity Coupling Device (PCD). Two characteristics - settling time constant and bidding frequency - are depicted in detail. For a Very High Bit Rate (VHBR) implementation both properties limit a bit rate increase. A dual antenna architecture does not have these limitations as the data transmit path is a low Q or even a non resonance resonant circuit. Bidding frequency is a result of superimposing the carrier frequency with the self resonance frequency of a resonant circuit as denoted in equation (6.12). The settling behavior of a conventional antenna system is worst, if the resonance frequency is the same as the system frequency which can be seen in figure 6.5.

8 Research Summary, Conclusion and Outlook

The funding project ReadRF addressed three research fields to increase communication speed in a contactless proximity system. This thesis focused on the air interface properties. A set of equations was elaborated in chapter 4, Contactless Technology Air Interface and chapter 5, Energy Transfer Functions which are used to calculate H-fields, inductances and transfer functions of a contactless channel. In chapter 6, Time Domain Analysis and Transient Settling a special emphasis was given to the time domain behavior of communication signals and channel characteristics. This chapter depicts the challenges of bidding frequencies and high quality factor settling of resonant circuits.

A significant increase of communication speed compared to actual standardized 848kbps can be achieved by the introduction of a novel dual antenna architecture. This concept allows mixing of a high quality energy path with an broad band optimized communication antenna. A 13.56Mbps data speed is proven for both communication directions. For communication from Proximity Coupling Device (PCD) to Proximity Integrated Circuit Card (PICC) a data rate of 27.12Mbps is already tested in a lab environment.

8.1 Conclusion

An increase of bit rates beyond 6.8Mbps requires a change of channel architecture to the novel dual antenna structure. This is necessary to handle resonant circuit limitations of conventional reader circuits.

Restrictions are

- Energy transfer with optimized quality factor
- Settling characteristic of resonant circuits
- Bidding frequency due to detuned resonant circuits

A dual antenna architecture gives significant advantages in communication stability and Inter Symbol Interference (ISI), which is already an added value at standard bit rates. A reasonable effort has to be spent in antenna design and alignment of the two paths - energy and transmit/receive path. A significant cost increase is not expected due to the implementation of a dual antenna architecture in Proximity Coupling Device (PCD). The novel structure can be used for receive path only or both transmit and receive path. The implementation for receive path only is increasing communication stability for standard bit rate of 106kbps. Payment applications are typically run at 106kbps speed but with a high quality factor. As the subcarrier frequency of standard bit rates is 848kHz, signal distortion and Inter Symbol Interference (ISI) is already a Proximity Coupling Device (PCD) design topic and a challenge for a reader receiver circuit.

8.1.1 Key Facts

A novel Proximity Integrated Circuit Card (PICC) coding scheme to achieve

- Bit rate increase of a factor of sixteen (up to 13.56Mbps) [16]
- Base band modulation - i.e. no subcarrier - with special run in pattern [16]
- Elementary Timing Unit (ETU) of one carrier cycle and None Return to Zero (NRZ) bit coding [16]

A novel dual antenna architecture for Proximity Coupling Device (PCD) receive path to achieve

- Bit rate increase of a factor of eight (up to 6.8Mbps) based on subcarrier technology [18]
- A data reception up to 13.56Mbps load modulated PICC data [18, 16]

A novel dual antenna architecture for Proximity Coupling Device (PCD) transmit path to achieve

- Bit rate increase by a factor of sixteen (13.56Mbps) [19]
- A Potential increase up to 54.24Mbps [19]

8.1.2 Figure of Merit

Figure 8.1 depicts the dependency of bit rate over symbol complexity. Symbol frequencies from 1.695MHz up to 27.12MHz are compared. An exponential increase of number symbols over a linear increase of bit rate can be observed at constant symbol frequencies.

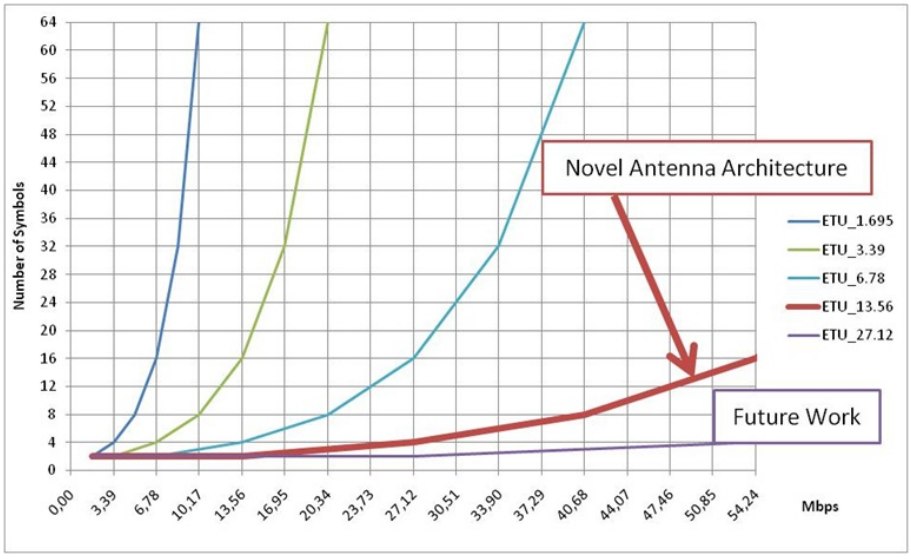

Figure 8.1: Symbol complexity over bit rate

An increase of Elementary Timing Unit (ETU) is a clear advantage for increasing bit rates. A 1.7MHz Symbol frequency requires sixteen (16) symbols to achieve a bit rate of 6.78Mbps and two hundred fifty six (256) symbols for 13.56Mbps. A bit time reduction to one carrier cycle realizes the same communication speed at a number of symbols of two (2).

Proposal	**Bit Rate**	**Symbol Rate**	**Number of Symbols**	**Antenna Quality Factor**
NXP	1.695Mbps	1.695MHz	2	9
	3.39Mbps	1.695MHz	4	9
	6.78Mbps	1.695MHz	16	9
	(13.56Mbps)	(1.695MHz)	(256)	(9)
	13.56Mbps	3.39MHz	16	4.5
Gemalto	1.695Mbps	1.695MHz	2	9
	3.39Mbps	1.695MHz	4	9
	6.78Mbps	1.695MHz	16	9
	(13.56Mbps)	(1.695MHz)	(256)	(9)
Infineon	1.695Mbps	1.695MHz	2	9
	3.39Mbps	3.39MHz	2	9
	6.78Mbps	6.78MHz	2	9
Novel architecture	1.695Mbps	1.695MHz	2	9
	3.39Mbps	3.39MHz	2	9
	6.78Mbps	6.78MHz	2	9
	13.56Mbps	13.56MHz	2	9
	27.12Mbps	13.56MHz	4	9
	54.24Mbps	13.56MHz	16	9

Table 8.1: Figure of Merit

Table 8.1 depicts a comparison of individual ISO/IEC 14443 contributions with the novel dual antenna architecture potential. Options in braces are known to be hardly implemented. A reasonable number of symbols is known to be sixteen (16). Higher number of symbols can be hardly realized in a stable high quality implementation.

8.2 Outlook

Communication speed from Proximity Coupling Device (PCD) to Proximity Integrated Circuit Card (PICC) has the potential to be increased up to 54.24Mbps in the next years. First successful tests were performed at 27.12Mbps. Research studies will be started to assess modulation techniques - e.g. Discrete Multi Tone (DMT), Orthogonal Frequency Division Multiplexing(OFDM). An optimization of Proximity Integrated Circuit Card (PICC) will be necessary to prevent data signal distortion which is inherently generated by superpostion of the two antenna signals. A carrier cancellation method is under evaluation, which is replicating the unmodulated carrier. The replica is used to notch out the unmodulated signal. Therefore data signals can be received without any influence by the energy carrier. This will further improve communication signal quality. This step will speed up communication beyond 54.24Mbps.

Communication direction from Proximity Integrated Circuit Card (PICC) to Proximity Coupling Device (PCD) is limited to 13.56Mbps at this time. Load modulation technology cannot easily increase the bit rate beyond 13.56Mbps, as a symbol modulation can be hardly implemented. Coupling dynamic and resonance frequency are changing signal characteristics of Load Modulation Amplitude (LMA), which is described in detail in chapter Transfer Functions 5. A Proximity Integrated Circuit Card (PICC) dual antenna architecture is anlayzed to overcome these limitations. This will introduce an active modulation scheme which has similar properties as the transmit path of a Proximity Coupling Device (PCD).

Own Publications

Paper

- Markus Auer, Edmund Ehrlich, Albert Missoni, Walter Kargl, Gerald Holweg and Wolfgang Pribyl. Design and development of a mixed signal prototyping system to achieve very high data rates for contactless applications. Wien, New York: Springer, e&i March 2008
- Christian Klapf, Albert Missoni, Wolfgang Pribyl, Graz University of Technology; Günter Hofer, Gerald Holweg, Walter Kargl Infineon Tech. Graz. Improvements in Operational Distance in Passive HF RFID Transponder Systems. IEEE RFID 2008, April 2008
- Holger Bock, Michael Braun, Markus Dichtl, Johann Heyszl, Erwin Hess, Walter Kargl, Helmut Koroschetz, Bernd Meyer, and Hermann Seuschek. A milestone towards RFID products offering asymmetric authentication based on elliptic curve cryptography. In RFIDSec2008 - Proceedings of the 4th Workshop on RFID Security, July 9-11, 2008, Budapest, Hungary, July 2008.
- Markus Auer, Edmund Ehrlich, Albert Missoni, Walter Kargl, Gerald Holweg and Wolfgang Pribyl. Analoge Eingangsstufe mit ADC-basierendem Demodulator für HF-Transponder zur Verarbeitung hoher Datenraten. Wien, New York: Springer, e&i August 2009
- Markus Auer, Edmund Ehrlich, Wolfgang Pribyl, Albert Missoni and Walter Kargl. Design und Entwicklung eines Mixed Signal Prototyping Systems für RFID Applikationen mit Datenraten größer 848 kbit/s. Workshop on Microelectronics, Austrochip 2009, October 2009
- Markus Auer, Albert Missoni and Walter Kargl. HF RFID Transponder with Phase Demodulator for Very High Bit-Rates up to 13.56 Mbit/s. RFID conference, IEEE RFID 2010, April 2010

Project Related Invention Disclosures and Patent Applications

- Walter Kargl, Edmund Ehrlich, Matthias Emsenhuber. CONTACTLESS DATA RECEPTION. United States Patent Application 20100243737
- Walter Kargl, Edmund Ehrlich, Matthias Emsenhuber. CONTACTLESS DATA TRANSMISSION. United States Patent Application 20100311328
- Walter Kargl, Markus Auer, Albert Missoni, Circuit for demodulating a phase modulated signal. United States Patent Application 20100303173
- Walter Kargl, Edmund Ehrlich. Coding method for very high data rates in contactless applications. Invention Disclosure, 2009. Infineon Reference No.: 2009E51126 AT
- Walter Kargl, Edmund Ehrlich. Digital demodulation method for a contactless receiver. Invention Disclosure, 2009. Infineon Reference No.: 2009E50041 AT

Patents and Patent Applications not Related to this Thesis

- Eleven granted patent families
- More than twenty Patent Applications

Supervised Diploma Thesis and Research Cooperations in the Field of this Thesis

- Thomas Leutgeb. Entwicklung eines automatisierten Meßplatzes zur Qualifikation kontaktloser Chipkarten. Diploma Thesis, Graz, University of Technology, Institute of Electronics, 1999
- Günter Stromberger. Meßtechnik für kontaktlose induktive Chipkartenschnittstellen. Diploma Thesis, Graz, University of Technology, Institute of Electronics, 2000
- Alois Danninger. MATLAB Modell eines kontaktlosen Systems. Diploma Thesis, Graz, University of Technology, Institut für Regelungstechnik, 2002
- Richard Mayer. Design of a discrete analogue Interface for Proximity Systems. Master Thesis, Kapfenberg, FH-Joanneum, Electronic Engineering, 2003
- Simon Pilz. Contact-Less Emulation System Hardware Add-on for a Spea Mixed Signal Tester. Diploma Thesis, Kapfenberg, FH-Joanneum, Electronic Engineering, 2006
- Martin Erler. A configurable power source for contactless smart cards. Diploma Thesis, Graz, University of Technology, Institute of Electronics, 2009
- Matthias Emsenhuber. Development of an analog frontend for an RFID reader for high datarate. Diploma thesis, Graz, University of Technology, Institute of Electronics, 2008
- Matthias Pichler. Implementation of a digital demodulator to process high data rates in contactless applications (13.56MHz). Diploma Thesis, Graz, University of Technology, Institute of Electronics, 2009
- Matthias Pichler. Verification of a contactless transponder test chip. IT electronic project, Graz, University of Technology, Institute of Electronics, 2008

- Dipl.-Ing. Edmund Ehrlich. Digital Demodulator Architecture of a Contactless Reader System for HF RFID Applications Supporting Data Rates up to 13.56Mbit/sec. PhD, Graz, University of Technology, Institute of Electronics, 2010
- Dipl.-Ing. Markus Auer. Design and Development of an HF-RFID Transponder to Achieve Very High Data Rates for Contactless Applications. PhD, Graz, University of Technology, Institute of Electronics, 2010

Bibliography

[1] Markus Auer. *Design and Development of an HF-RFID Transponder to Achieve Very High Data Rates for Contactless Applications*. PhD, Graz, University of Technology, Institute of Electronics, 2011.

[2] Markus Auer, Edmund Ehrlich, Albert Missoni, Walter Kargl, Gerald Holweg, and Wolfgang Pribyl. *Design und Entwicklung eines Mixed Signal Prototyping Systems für RFID Applikationen mit Datenraten größer 848 kbit/s*. Austrochip, 2009.

[3] Hans-Jochen Bartsch. *Taschenbuch Mathematischer Formeln*. Verlag Harri Deutsch Thun und Frankfurt/Main, 7. bis 10. edition, 1987.

[4] CEPT/ERC. *ERC Recommendation 70-03 relating to the use of short range devices (SRD), Including Appendixes and Annexes*. European Radiocommunications Committee (ERC), 2004.

[5] Christoph Schenk, Ulrich Tietze. *Halbleiter-Schaltungstechnik*. Springer, Berlin, 12. edition, 2002.

[6] Edmund Ehrlich. *Digital Demodulator Architecture of a Contactless Reader System for HF RFID Applications Supporting Data Rates up to 13.56Mbit/sec*. PhD, Graz, University of Technology, Institute of Electronics, 2011.

[7] Matthias Emsenhuber. *Development of an analog frontend for an RFID reader for high datarate*. Diploma thesis, Graz, University of Technology, Institute of Electronics, 2008.

[8] ETSI. *EN 300 330-2 Part 1: Electromagnetic compatibility and Radio spectrum Matters (ERM); Short Range Devices(SDR); Radio equipment in the frequency range 9 kHz to 25 MHz and inductive loop systems in the frequency range 9 kHz to 30 MHz. Part-1: Technical characteristics and test methods*. European Telecommunications Standards Institute, 2006.

[9] Klaus Finkenzeller. *RFID HANDBUCH, Grundlagen und praktische Anwendungen induktiver Funkanlagen, Transponder und kontaktloser Chipkarten*. Hanser Fachbuchverlag, 4th edition, 2006.

[10] Heinrich Frohne Paul Vaske Franz Moeller, Hans Fricke. *Grundlagen der Elektrotechnik*. B.G. Teubner Stuttgart, 17th edition, 1986.

[11] Michael Gebhart. *Vorlesung RFID Systems*. Graz, University of Technology, 2009.

[12] ISO/IEC. *International Standard ISO/IEC 14443 (Part 1 to 4), Identification Cards - Contactless integrated circuit(s) cards - Proximity cards*. ISO copyright office, 2000.

[13] ISO/IEC. *International Standard ISO/IEC 10373 (Part 6), Identification Cards - Test methods - Proximity cards*. ISO copyright office, 2001.

[14] Walter Kargl. *Proact Summer school on RFID - RF Frontend Design*. Graz, University of Technology, 2006, 2007.

[15] Walter Kargl and Edmund Ehrlich. *DEMODULATOR AND METHOD FOR DEMODULATING A MODULATED CARRIER SIGNAL. Invention Disclosure, United States Patent Application*.

[16] Walter Kargl and Edmund Ehrlich. *Coding method for very high data rates in contactless applications. Invention Disclosure, 2009. Reference No.: 2009E51126 AT,DE102010002584*. Infineon, 2009.

[17] Walter Kargl and Edmund Ehrlich. *Digital demodulation method for a contactless receiver. Invention Disclosure, 2009. Reference No.: 2009E50041 AT*. Infineon, 2009.

[18] Walter Kargl, Edmund Ehrlich, and Matthias Emsenhuber. *CONTACTLESS DATA RECEPTION. United States Patent Application 20100243737*. USPTO, 2010.

[19] Walter Kargl, Edmund Ehrlich, and Matthias Emsenhuber. *CONTACTLESS DATA TRANSMISSION. United States Patent Application 20100311328*. USPTO, 2010.

[20] Thomas Leutgeb. *Entwicklung eines automatisierten Meßplatzes zur Qualifikation kontaktloser Chipkarten*. Diploma thesis, Graz, University of Technology, Institute of Electronics, 1999.

[21] Infineon Technologies. *Phase/Amplitude Modulation, ISO/IEC 14443 tf2n660*. ISO/IEC SC17/WG8/TF2, 2010.

[22] Walter Kargl and Markus Auer and Albert Missoni. *CIRCUIT FOR DEMODULATING A PHASE MODULATED SIGNAL. United States Patent Application 20100303173*. USPTO, 2010.

[23] Harald Witschnig. *Selected Topics of Advanced Analog Chip Design - Architectures in RFID*. Lecture, Graz, University of Technology, Institute of Electronics, 2009.

[24] Hubert Zangl and Thomas Bretterklieber. *Limitations of Range of Operation and Data Rate for 13.56 MHZ Load-Modulation Systems*. Institute of Electrical Measurement and Measurement Signal Processing, Graz University of Technology, Austria.